

https://dspace.org/

# The influence of Ru additions on the corrosion behaviour of WC-Co cemented carbide in corrosive media

**Thanjekwayo, Nompumelelo Pretty**

**2010-09-07**
http://hdl.handle.net/10539/8625

Downloaded from a DSpace repository. https://dspace.org/

# The influence of Ru additions on the corrosion behaviour of WC-Co cemented carbide in corrosive media

**Nompumelelo Pretty Thanjekwayo**

A dissertation submitted to the faculty of Engineering and the Built Environment, University of the Witwatersrand, Johannesburg, in fulfilment of the requirements for the degree of Masters of Science in Engineering.

Johannesburg, June, 2009

## *DECLARATION*

I (Nompumelelo Pretty Thanjekwayo) declare that the dissertation is my own unaided work except where references were made and were properly acknowledged. It is being submitted for the degree of Masters of Science in Engineering in the University of the Witwatersrand, Johannesburg. It has not been submitted previously at this or any other university for any degree or examination.

_____

Nompumelelo Pretty Thanjekwayo

At _____ Date: _____

## *ABSTRACT*

The aim of the study is to investigate the influence of Ru additions on the corrosion behaviour of WC-Co cemented carbides when exposed in corrosive media. The study involved the characterisation of the microstructures, morphologies and phases present by using the optical microscopy, SEM, XRD and Raman spectroscopy before and after corrosion. The corrosion behaviour was investigated using the electrochemical polarization tests in 1M hydrochloric acid, 1M sodium chloride and synthetic mine water solutions. Three types of corrosion tests were done on the samples by electrochemical techniques: potential versus time test, potentiodynamic polarisation scans and chronoamperometry.

Ruthenium affects $\beta_c$ in 1M $H_2SO_4$ and synthetic mine water, but not really in NaCl solution. It was also observed that the passivity range and corrosion resistance decreases in order of synthetic mine water> sodium chloride> sulphuric acid. It also appears that Ru is more effective in improving corrosion resistance in all the solutions than a small vanadium carbide addition. Therefore, ruthenium additions of up to 3 wt% Ru of the WC-10%Co alloy increased the corrosion resistance of the WC-Co alloys. This is attributed to the stabilization of the cobalt fcc phase due to ruthenium additions while hcp phase is obtained when there is no ruthenium additions.

*DEDICATIONS*

In memory of my grandfather

**Kinki Johannes Thanjekwayo**

He has always been there for me as a grandfather and as a father, guiding me through life and teaching me things that have brought me this far. To be hardworking, brave, confident, courageous and independent. I will forever be thankful to you for being my dad and my superman.

**Rest in peace Daddy, May God be with you.**

## *ACKNOWLEDGEMENTS*

I wish to thank the following people that have the invaluable contribution in the completion of this project:

**Professor J.H. Potgieter:** For the best supervision, constructive criticism, guidance and also moral and financial support. Thank you for the opportunities you have given me throughout this journey.

**Mr. J. Van der Merwe:** For the supervision and support in my work especially laboratory work. Thank you for being there when I was in difficult situations.

**Dr. P.A. Olubambi:** For teaching me corrosion techniques and the reading and give positive attribution to my written work. Thank you for teaching me writing skills.

**Professor S. Potgieter-Vermaak, Nthabiseng Maledi and Vongani Shabalala**: For supervising and helping with the Raman Spectroscopy.

**Mr. A. Xoseka (laboratory technician):** For helping with the metallographic preparation of the samples and transport.

I wish to thank all the **staff members** of the School of Chemical and Metallurgical Engineering Wits University for helping and supporting me during this study.

I wish to acknowledge the financial support for funding this study received from The DST\NRF Centre of Excellence in Strong Materials, The Davidson Educational Trust and Corrosion Institute of Southern Africa (The Ivan Ogilvie Research Scholarship). I am gratefully thankful.

I would like to express my sincere appreciation to my **family (Thanjekwayo)** for the prayers, love and support received thoughout my studies. Thanks to my mother **(Nomthandazo Thanjekwayo)** and my grandmother **(Mrs. K Thanjekwayo)** for

believing in me and also the support. I wish to appreciate my special friend (Mthokozisi) for being a shoulder to cry on and being my best friend and my friends for their support, encouragement and belief in me.

Lastly, My **God and Saviour**, for giving me the strength and empowerment. Thank you Heavenly Father!

# *TABLE OF CONTENTS*

*DECLARATION* ..... i
*ABSTRACT* ..... ii
*ACKNOWLEDGEMENTS* ..... iv
*TABLE OF CONTENTS* ..... vi
*LIST OF FIGURES* ..... ix
*LIST OF TABLES* ..... xiv
*CHAPTER 1* ..... 1
1.0 INTRODUCTION ..... 1
1.1 Background and motivation ..... 1
1.2 Problem Statement ..... 2
1.3 Objectives of the study ..... 4
1.4 Hypotheses ..... 4
1.5 General layout ..... 5
*CHAPTER 2* ..... 6
2.0 LITERATURE REVIEW ..... 6
2.1 Introduction to hardmetals ..... 6
2.2 History of hardmetals ..... 6
2.3 The Tungsten Carbide-Cobalt System ..... 7
2.4 WC – Co manufacture ..... 9
2.5 Uses of WC-Co ..... 9
2.6 Limitations ..... 10
2.7 Corrosion behaviour ..... 10
2.7.1 WC–Co corrosion products in the different electrolytes ..... 12
2.7.2 The effect of the grain size on corrosion ..... 14
2.7.3 WC – Co corrosion: effect of other carbides ..... 15
2.7.4 Chemical modification of W-Co with metal carbides ..... 18
2.8. Ruthenium additions to WC-Co ..... 21
2.8.1 Uses of ruthenium ..... 22
2.8.2 The effect of ruthenium on Co or WC-Co ..... 23
2.8.3 Influence of ruthenium on corrosion behaviour ..... 24
2.8.4 Effects of ruthenium on cemented carbides corrosion ..... 25

*CHAPTER 3* ..... 27
3.0 EXPERIMENTAL PROCEDURE ..... 27
3.1 Characterisation of the samples ..... 27
3.2 Sample compositions ..... 28
3.3 WC-Co-Ru manufacture ..... 28
3.4 Sample preparation ..... 29
3.5 Microstructural observation ..... 30
3.6 Scanning Electron Microscopy (SEM) ..... 30
3.7 X-ray Diffractrometry (XRD) ..... 30
3.8 Raman Spectrocopy ..... 31
3.9 Corrosion Tests ..... 31
3.10 Surface analysis after electrochemical tests ..... 33
*CHAPTER 4* ..... 34
4.0 RESULTS AND DISCUSSIONS ..... 34
4.1 Characterisation of the materials ..... 34
4.2 Corrosion tests (Electrochemical tests) ..... 45
4.2.1 Sulphuric acid (1M $H_2SO_4$) electrolyte ..... 45
4.2.2 Sodium chloride (1M NaCl) electrolyte ..... 51
4.3.2 Synthetic mine water electrolyte ..... 56
4.3 Surface analysis after electrochemical tests ..... 61
4.3.1 Sulphuric acid environment ..... 61
4.3.2 Sodium chloride environment ..... 71
4.3.3 Synthetic Mine Water environment ..... 82
4.4 GENERAL DISCUSSIONS ..... 91
4.4.1 Comparisons of the electrochemical behaviour of WC-Co with the additions of ruthenium ..... 91
4.4.2 Comparisons of sulphuric acid, sodium chloride and synthetic mine water ..... 91
4.4.3 The corrosion products formed on the surface ..... 95
4.4.4 Effects of ruthenium on binding effects of cobalt on the WC-Co cemented carbide and hypotheses validation ..... 96
*CHAPTER 5* ..... ……99
5.0 CONCLUSIONS AND RECOMMENDATIONS ..... 99
5.1 Conclusions ..... 99
5.1.1 Effect of ruthenium additions on WC-Co alloys ..... 99

5.1.2 Corrosion behaviour of WC-Co-Ru ..... 99
5.1.3 Validation of Claims..... 100
5.1.4 Validation of the hypothesis ..... 100
5.2 Recommendations ..... 101
*REFERENCES*..... 102

## *LIST OF FIGURES*

Figure 3.1: Manufacturing process of WC-Co-Ru samples. ..... **Error! Bookmark not defined.**

Figure 3.2: The electrochemical measurements experimental set-up... **Error! Bookmark not defined.**

Figure 4.1.1: Optical micrographs of the cemented carbide alloys samples in the as-received samples..... **Error! Bookmark not defined.**

Figure 4.1.2: SEM micrograph of WC-10%Co alloy..... **Error! Bookmark not defined.**

Figure 4.1.3: SEM micrograph of WC-10%Co-0.4% Ru alloy..... **Error! Bookmark not defined.**

Figure 4.1.4: SEM micrograph of WC-10%Co-1.0% Ru alloy..... **Error! Bookmark not defined.**

Figure 4.1.5: SEM micrograph of WC-10%Co-1.5% Ru alloy..... **Error! Bookmark not defined.**

Figure 4.1.6: SEM micrograph of WC-10%Co-2.0% Ru alloy..... **Error! Bookmark not defined.**

Figure 4.1.7: SEM micrograph of WC-10%Co-3.0% Ru alloy..... **Error! Bookmark not defined.**

Figure 4.1.8: EDX spectra analyses of the polished surface of the alloys used in the investigation..... **Error! Bookmark not defined.**

Figure 4.1.9: XRD patterns for WC-10%Co alloy ..... **Error! Bookmark not defined.**

Figure 4.1.10: XRD patterns for WC-10%Co-0.4%Ru alloy..... **Error! Bookmark not defined.**

Figure 4.1.11: XRD patterns for WC-10%Co-1.0%Ru alloy..... **Error! Bookmark not defined.**

Figure 4.1.12: XRD patterns for WC-10%Co-1.5%Ru alloy..... **Error! Bookmark not defined.**

Figure 4.1.13: XRD patterns for WC-10%Co-2.0%Ru alloy..... **Error! Bookmark not defined.**

Figure 4.1.14:XRD patterns for WC-10%Co-3.0%Ru alloy..... **Error! Bookmark not defined.**

Figure 4.1.15: Raman spectra from the polished alloys .. **Error! Bookmark not defined.**

Figure 4.2.1: Open Circuit Potential results of the samples exposure to 1M $H_2SO_4$…..46
Figure 4.2.2: Comparative behaviour of WC-Co in 1 M $H_2SO_4$ with increasing additions of Ru……47
Figure 4.2.3: The effect of ruthenium additions on corrosion rate of the alloys in 1M $H_2SO_4$ .……48
Figure 4.2.4: Current-Time results of the samples exposure to 1M $H_2SO_4$ at 0.6V……49
Figure 4.2.5: The effect of ruthenium addition on passivation range of the alloys 1M $H_2SO_4$……...…50
Figure 4.2.6: Open Circuit Potential versus time for the samples exposed to 1M NaCl.51
Figure 4.2.7: Comparative behaviour of WC-Co with increasing additions of Ru in 1M NaCl……...…..52
Figure 4.2.8: The effect of ruthenium additions on corrosion rate of the various WC-Co alloys in 1M NaCl……53
Figure 4.2.9: Current- Time response of the samples exposure to 1M NaCl at 0.6V…54
Figure 4.2.10: The effect of ruthenium on passivation on the WC-Co in 1M NaCl...…55
Figure 4.2.11: Open Circuit Potential results of the WC-Co-Ru samples exposed to synthetic mine water……56
Figure 4.2.12: Comparative potentiodynamic behaviour of WC-Co in synthetic mine water with increasing additions of Ru…….58
Figure 4.2.13: The effect of ruthenium additions on corrosion rate of the alloys in synthetic mine water……59
Figure 4.2.14: Current -Time results of the samples exposure to synthetic mine water at 0.6V…….59
Figure 4.2.15: The effect of ruthenium on passivation on the WC-Co in synthetic mine water ……...60
Figure 4.3.1: SEM micrograph of the WC-10%Co alloy after exposure to 1M $H_2SO_4$ solution with corresponding EDX spectra analyses ..... 62
Figure 4.3.2: SEM micrograph of the 0.4 wt% Ru containing alloy after exposure to 1M $H_2SO_4$ solution with corresponding EDX spectra analyses. ..... 63
Figure 4.3.3: SEM micrograph of the 1.0 wt% Ru containing alloy after exposure to 1M $H_2SO_4$ solution with corresponding EDX spectra analyses. ..... 63
Figure 4.3.4: SEM micrograph of the 1.5 wt% Ru containing alloy after exposure to 1M $H_2SO_4$ solution with corresponding EDX spectra analyses. ..... 64
Figure 4.3.5: SEM micrograph of the 2.0 wt% Ru containing alloy after exposure to 1M

$H_2SO_4$ solution with corresponding EDX spectra analyses ..... 64
Figure 4.3.6: SEM micrograph of the 3.0 wt% Ru containing alloy after exposure to 1M $H_2SO_4$ solution with corresponding EDX spectra analyses ..... 65
Figure 4.3.7: XRD patterns for alloy containing 0 wt% Ru after exposure to 1M $H_2SO_4$ .....**Error! Bookmark not defined.**
Figure 4.3.8: XRD patterns for alloy containing 0.4 wt% Ru after exposure to 1M $H_2SO_4$.....**Error! Bookmark not defined.**
Figure 4.3.9: XRD patterns for alloy containing 1.0 wt% Ru after exposure to 1M $H_2SO_4$..... 67
Figure 4.3.10: XRD patterns for alloy containing 1.5 wt% Ru after exposure to 1M $H_2SO_4$..... 68
Figure 4.3.11: XRD patterns for alloy containing 2.0 wt% Ru after exposure to 1M $H_2SO_4$..... 68
Figure 4.3.12: XRD patterns for alloy containing 3.0 wt% Ru after exposure to 1M $H_2SO_4$..... 69
Figure 4.3.13: Raman spectra of the WC-Co-Ru after exposure to 1M sulphuric acid .....**Error! Bookmark not defined.**
Figure 4.3.14: SEM micrograph of the 0.0 wt% Ru containing alloy after exposure to 1M NaCl solution with corresponding EDX spectra analyses ..... **Error! Bookmark not defined.**
Figure 4.3.15: SEM micrograph of the 0.4 wt% Ru containing alloy after exposure to 1M NaCl solution with corresponding EDX spectra analyses..... **Error! Bookmark not defined.**
Figure 4.3.16: SEM micrograph of the 1.0 wt% Ru containing alloy after exposure to 1M NaCl solution with corresponding EDX spectra analyses. .... **Error! Bookmark not defined.**
Figure 4.3.17: SEM micrograph of the 1.5 wt% Ru containing alloy after exposure to 1M NaCl solution with corresponding EDX spectra analyses. ..... **Error! Bookmark not defined.**
Figure 4.3.18: SEM micrograph of the 2.0 wt% Ru containing alloy after exposure to 1M NaCl solution with corresponding EDX spectra analyses..... **Error! Bookmark not defined.**
Figure 4.3.19: SEM micrograph of the 3.0 wt% Ru containing alloy after exposure to 1M NaCl solution with corresponding EDX spectra analyses . .... **Error! Bookmark not**

**defined.**

Figure 4.3.20: XRD patterns for 0.0 wt% Ru after exposure to 1M NaCl ..... 77

Figure 4.3.21: XRD patterns for 0.4 wt% Ru after exposure to 1M NaCl ..... 78

Figure 4.3.22: XRD patterns for 1.0 wt% Ru after exposure to 1M NaCl ..... 78

Figure 4.3.23: XRD patterns for 1.5 wt% Ru after exposure to 1M NaCl ..... 79

Figure 4.3.24: XRD patterns for 2.0 wt% Ru after exposure to 1M NaCl ..... **Error! Bookmark not defined.**

Figure 4.3.25: XRD patterns for 3.0 wt% Ru after exposure to 1M NaCl ..... **Error! Bookmark not defined.**

Figure 4.3.26: Raman spectra from the alloys after exposure to 1M NaCl ..... **Error! Bookmark not defined.**

Figure 4.3.27: SEM micrograph of the WC-10%Co alloy after exposure to synthetic mine water solution with corresponding EDX spectra analyses ... **Error! Bookmark not defined.**

Figure 4.3.28: SEM micrograph of the 0.4 wt% Ru containing alloy after exposure to synthetic mine water solution with corresponding EDX spectra analyses. ..... **Error! Bookmark not defined.**

Figure 4.3.29: SEM micrograph of the 1.0 wt% Ru containing alloy after exposure to synthetic mine water solution with corresponding EDX spectra analyses . ..... **Error! Bookmark not defined.**

Figure 4.3.30: SEM micrograph of the 1.5 wt% Ru containing alloy after exposure to synthetic mine water solution with corresponding EDX spectra analyses ..... **Error! Bookmark not defined.**

Figure 4.3.31: SEM micrograph of the 2.0 wt% Ru containing alloy after exposure to synthetic mine water solution with corresponding EDX spectra analyses ..... **Error! Bookmark not defined.**

Figure 4.3.32: SEM micrograph of the 3.0 wt% Ru containing alloy after exposure to synthetic mine water solution with corresponding EDX spectra analyses ..... **Error! Bookmark not defined.**

Figure 4.3.33: XRD patterns for 0 wt% Ru after exposure to synthetic mine water..... 86

Figure 4.3.34: XRD patterns for 0.4 wt% Ru after exposure to synthetic mine water.. 87

Figure 4.3.35: XRD patterns for 1.0 wt% Ru after exposure to synthetic mine water.. 87

Figure 4.3.36: XRD patterns for 1.5 wt% Ru after exposure to synthetic mine water.. 88

Figure 4.3.37: XRD patterns for 2.0 wt% Ru after exposure to synthetic mine water.. 88

Figure 4.3.38: XRD patterns for 3.0 wt% Ru after exposure to synthetic mine water.. 89
Figure 4.3.39: Raman spectra from the alloys after exposure to synthetic mine water solution .....**Error! Bookmark not defined.**
Figure 4.4.1: Polarization curves showing the influence of ruthenium on the corrosion behaviour of the WC-Co alloys in 1M NaCl and 1M $H_2SO_4$ solutions. .....**Error! Bookmark not defined.**

## *LIST OF TABLES*

Table 3.1: The chemical composition of the samples ..... 28
Table 3.2: The chemical composition of synthetic mine water..... 32
Table 4.1.1: Raman peak positions ($cm^{-1}$) of the polished sample WC-10%Co-Ru alloys ..... 45
Table 4.2.1: Electrochemical parameters for the samples in 1M sulphuric acid..... 48
Table 4.2.2: Electrochemical parameters for the samples in 1M sulphuric acid..... 48
Table 4.2.3: Electrochemical parameters for the samples in synthetic mine water..... 54
Table 4.3.1: Peak positions ($cm^{-1}$) found on the surface of WC-Co-Ru alloys after exposure in 1M sulphuric acid solution..... 70
Table 4.3.2: Raman peak positions ($cm^{-1}$) found on the surface of WC-Co-Ru alloys after exposure in 1M sulphuric acid solution ..... 81
Table 4.3.3: Raman peak positions ($cm^{-1}$) found on the surface of WC-Co-Ru alloys after exposure in synthetic mine water solution ..... 90
Table 4.4.1: Electrochemical parameters for the samples in 1M sulphuric acid and 1M NaCl and synthetic mine water solutions ..... 93
Table 4.4.2: Effect of ruthenium in the crystallographic structure of WC-Co..... 98

# *CHAPTER 1*

## 1.0 INTRODUCTION

### 1.1 Background and motivation

Conventional tungsten carbide hardmetals are composed of hard tungsten carbide particles embedded in a tough metallic matrix of cobalt, which are produced during a liquid phase sintering process that embedded the tungsten carbide in a ductile binder phase (Guilemany *et al*., 1993-1994). The common purpose of the metal matrix composites such as a tungsten carbide is to develop a material with superior mechanical properties that has increased toughness, stiffness and wear resistance (Trueman et *al*., 1999). Tungsten carbide is widely used as a coating material for protection against wear, erosion, and high-temperature oxidation due to its high-hardness and excellent thermal stability (Human and Exner, 1997). The tungsten alloys are composed mainly of tungsten (88–95%) with various combinations of carbon and nickel, cobalt, iron or copper as binders usually making up the remaining fraction (Aw et *al*., 2007).

In order to meet the requirements of specific applications, WC hardmetals may contain small amounts of binding elements such as cobalt, nickel or iron. The use of Ni instead of Co as binder material or alloying $Cr_3C_2$ into the binder phase could lead to a higher corrosion resistance (Hochstrasser-Kurz) *et al*., 2007). However, the mechanical properties of the WC composite containing nickel could be deteriorated since the hardmetals based on WC-Co usually have a better combination of mechanical properties compared to WC-Ni grades (Kny *et al*., 1986). According to Almond and Roebuck (1988), the compressive properties of the WC-Co hardmetals are usually superior to those of WC-(Co-Ni) hardmetals. In most cases cobalt has been used as the tough metal binder phase, due to its excellent wetting, adhesion and adequate mechanical properties (Wentzel and Allen, 1997).

The cobalt phase is a solid solution with a face centred cubic (FCC) lattice (Lisovsky *et al*., 1991). During cooling after sintering, the carbon and tungsten elements precipitate on neighboring carbide grains; as a result there is a gradient of tungsten concentration in the binder phase. The cobalt binder has amounts of tungsten and carbon in solid solution. High contents of tungsten in the binder phase give improved performance, for instance in milling operations. It is known that a high concentration of tungsten and carbon atoms in cobalt can increase its martensite transforming temperature from fcc to hcp to about 750°C from 417°C. This avoids the formation and expansion of the brittle hexagonal close-packed cobalt at low temperature, increases the Co content and improves the transverse rupture strength and toughness of the cemented carbides (Jia *et al*., 1998).

The exceptional wear resistance of cemented carbides, owing to the combination of a tough metal binder with a hard carbide, has resulted in their applications in many engineering fields. In addition to their good performance in mining and cutting tool applications, cemented carbides are increasingly used in a variety of other industrial applications, such as seal rings, linings, valves, jet nozzles, saw blades, fluid mixers and conveyor belt scrapers. These applications differ from the traditional uses in that significantly longer lifetimes are demanded and components may be expected to remain in service for several years. If components are not only subjected to wear processes but are also in contact with chemically aggressive environments, corrosion can play a major role in the degradation of the surface and can significantly accelerate wear (Human and Exner, 1996; Wentzel and Allen, 1997; Hochstrasser -Kurz) *et al*., 2007).

## 1.2 Problem Statement

The corrosion resistance of the conventional tungsten carbide-cobalt hardmetals is most of the time less than satisfactory in certain applications in the chemical and food industries (Guilemany, *et al*., 1993 &1994). Since the cobalt binder phase is most susceptible to corrosion an improvement of the corrosion resistance of the binder will have a major influence on the overall corrosion resistance of cemented carbide, thus influencing the overall performance in long-life applications (Human and Exner, 1996). Cobalt has low corrosion resistance and thus to improve the wear resistance in

aggressive environments, several metallic alloy compositions, including VC, $Cr_3C_2$, TiC and TaC have been formulated and used (Tomlinson and Linzell, 1988; Lisovsky *et al*., 1991; Wentzel and Allen, 1997; Sutthiruangwong and Mori, 2003; Sutthiruangwong *et al*., 2005).

The corrosion susceptibility of the WC composite is influenced by microstructural parameters such as the microstructure and binder phase composition. Due to the heterogeneous microstructural nature and binder phase composition of WC–Co, their corrosion mechanisms are very complex and little is known about the exact corrosion processes taking place (Hochstrasser -Kurz *et al*., 2007). Tungsten carbide is chemically more stable than cobalt in acidic media and corrosion progresses by oxidation of the binder, leaving only a WC skeleton which is easily broken down by mechanical action (Human and Exner, 1996; Sutthiruangwong and Mori, 2003). Aggressive media preferably attack the binder while the tungsten carbide itself remains immune (Sutthiruangwong and Mori, 2003). This is because of a higher reduction potential of tungsten carbide when compared to the binder.

Studies have revealed that not the whole WC–Co surface behaves equally active, but the corrosion attack proceeds predominantly at locations where the WC phase has fallen out after localized initiation of corrosion has taken place (Hochstrasser -Kurz) *et al*., 2007). Due to a galvanic coupling, WC–Co hardmetals have poor corrosion resistance in aqueous solutions. Synergistic effects due to galvanic coupling between the Co binder and WC are accelerating Co dissolution and hindering WC dissolution in the hardmetals compared to the pure compounds (Sutthiruangwong and Mori, 2003; Hochstrasser – Kurz *et al*., 2007).

The structure and properties of the Co phase can be modified through the alloying of the WC-Co cemented carbides with effective alloying elements. According to Lisovsky *et al*. (1991), the addition of some alloying elements changes the qualitative and quantitative compositions of the binder and thus may change the corrosion behaviour of the binder. A number of research studies have been reported on alternative binders with cobalt, such as nickel, nickel-chromium, nickel-chromium-molybdenum (Human and Exner, 1997) and iron, cobalt (Scholl *et al.,* 1991). Recently, it has been shown that the addition of Ru as a binder had stabilizing properties in the WC-Co composite (Bonjour,

2004).

A considerable amount of research (Shing *et al.,* 2001; Shing *et al.,* 2002; Bonjour, 2004; Bonjour and Actis-Data, 2004) has been focused on the change of the mechanical properties of cemented carbides when the Ru is added. Shing *et al.* (2001) observed that the toughness of cemented carbides decrease with an increasing amount of ruthenium content. It was suggested that the decrease in toughness may be due to the hardening of the binder, which results from ruthenium remaining in solution in the cobalt. However, limited work has been done to study corrosion behaviour and the comparisons of corrosion rates in different solutions.

## 1.3 Objectives of the study

The main purpose of the research is to investigate the influence of Ru additions on the corrosion behaviour of a WC-Co composite. The research aims to attain the following objective:

- To study and compare the electrochemical behavior of WC-Co cemented carbide containing a varying amount of Ru, and compare it to WC-Co without any Ru.

## 1.4 Hypotheses

Two hypotheses were formulated. The first hypothesis was formulated based on the theory that ruthenium is a nobler metal than cobalt; a tungsten carbide containing cobalt will therefore be less noble than the one containing ruthenium. This then means that the noble alloy should be more thermodynamically stable and therefore more corrosion resistant than the one without Ru. The second hypothesis was formulated based on the crystal structure of the cobalt phase. Human *et al.* (1998); Broccardo (2003); Srivastava *et al.,* (2006) reported that the cubic Co is more corrosion resistant than the hexagonal cobalt. Ruthenium stabilises the cobalt binder, thus retaining its fcc crystal structure which will result in better corrosion resistance compared to the hcp crystal structure.

## 1.5 General layout

The dissertation has been presented by dividing the work into five chapters. The current chapter has provided the motivation of the work. Chapter 2 gives the literature review, a background description of WC-Co-Ru hardmetals and corrosion behaviour of the available knowledge. The detailed methodology of the experimental procedures and the equipment used in this study is provided by chapter 3. The results and discussion are presented in Chapter 4. Chapter 5 provides the conclusions of this study and recommendations that could be used for future research.

# *CHAPTER 2*

## 2.0 LITERATURE REVIEW

### 2.1 Introduction to hardmetals

Hardmetals are sintered composites of metal-ceramic powders (Schnyder *et al*., 2004). They consist of mixtures of one or more finely divided hard carbides particles, such as tungsten, titanium, tantalum and vanadium embedded in a matrix of soft and ductile binding materials such as cobalt, iron or nickel. These materials are very hard and possess excellent wear-resistance, and have been the most widely used super-hard tool materials. The most often used hardmetals in industry is tungsten carbide (Ringas et *al*., 1990; Schnyder *et al*., 2004; Ogundipe *et al*., 2006). The commercial hardmetals of the type [(WC, M); where M = Fe, Ni or Co], or their mixtures are normally prepared in a way that they have different desired properties, such as surface phase characteristics, corrosion resistance and electrolytic properties (Scholl *et al*., 1992). The tungsten heavy alloys are composed mainly of 88–95% tungsten by weight with the rest usually made up of Ni, Co or Fe binders in different combinations and proportions (Ogundipe *et al*., 2006).

### 2.2 History of hardmetals

The beginning of tungsten carbide-cobalt alloy production may be traced to the years 1920–1930 when they were introduced into the European market (Krakhmalev *et al.,* 2007a). This alloy was produced for various applications, due to its high wear resistance which was particularly important, as well as the favorable combination of high hardness and reasonable fracture toughness (Spriggs, 1995; Krakhmalev *et al.,* 2007a). The early

alloys were made in the laboratory of Osram (German electrical bulb company) as well as the associate firms of AEG and Siemens. Osram in the years 1923-1924 produced the tungsten wire up to a diameter of 0.3 mm as an alternative to the expensive diamond drawing dies. The earliest commercial grade of hardmetal which was a tungsten carbide-6% cobalt alloy was manufactured by Krupp after having acquired the early patents of Osram at the end of 1925. The first tungsten carbide-cobalt grades were soon successfully applied in the cutting and milling of cast iron (Spriggs, 1995; Brookes, 2001).

In 1939, small amounts of a second and third carbide, namely vanadium carbide and tantalum carbide were added to the WC-Co alloy. The addition of the vanadium carbide was 0.6% by weight and the tantalum carbide was l% by weight. This was specifically aimed to prevent discontinuous/general grain growth during sintering. Thus, the first use of grain growth inhibitors can be attributed to the Krupp workers (Spriggs, 1995).

The ultra high strength material known commercially as 'Baxtron' was developed in 1967 to 1968 by DuPont de Nemoirs in the USA. Baxtron was based on a heterogeneous mixture of low carbon and high carbon tungsten carbides resulting in up to 2.5 wt% tungsten in the solution of the cobalt binder. Corresponding values for dissolved carbon were 0.5 and 0-2 wt%, respectively. The data from these experiments show that tungsten, di-tungsten carbide (WC), mono-tungsten carbide (WC) and tungsten-titanium (50/50) carbide acted as strengtheners by solution in cobalt. Carbon on the other hand, does not act as a strengthener, but past the solubility limit degrades properties (Penrice, 1997). From 1981 to 1992, the greatest activity was the development of both very high quality submicron tungsten carbide powder and submicron hardmetal alloys. Virtually every manufacturer of both products devoted a considerable amount of research and effort to the production of genuine submicron material with a narrow particle/grain size range (Spriggs, 1995).

## 2.3 The Tungsten Carbide-Cobalt System

The tungsten carbide-cobalt hardmetals are composed of hard WC particles in a tough metallic cobalt matrix produced during a liquid phase sintering process (Hochstrasser-Kurz *et al.,* 2007). The material is also called "cemented carbide". They are one of the

most frequently used hardmetals in industry (Ringas *et al*., 1990; Schnyder *et al*., 2004; Ogundipe *et al*., 2006). According to Hochstrasser-Kurz *et al*. (2007), the WC–Co hardmetals are used for their combined high hardness and toughness.

The cobalt phase is a solid solution of tungsten and carbon with a face centred cubic (fcc) lattice and is designated as ß-Co. At 690K, ß-Co modification becomes unstable and transforms to ε-Co modification with a hexagonal close-packed (hcp) lattice. This phase transformation process was identified during the deformation of WC-Co cemented carbides. The Co phase transformation (fcc to hcp), is realized by a martensitic transformation mechanism and results in ß-Co phase strengthening with thin ε-Co layers. This mechanism is due to lower stacking fault energy in cobalt (Lisovsky *et al.*, 1991).

Generally, the mechanical properties of hardmetals are improved if there are fewer fracture pathways within its matrix. In order to reduce fracture pathways, a major requirement is that the binder should possess very good wettability so that the fracture path could pass through the binder phase rather WC-binder phase interface. The fracture could also be controlled by the strength and ductility of the binder phase rather than by the cohesive strength of the interface (Almond and Roebuck, 1988). In most cases cobalt has been used as a very tough metal binder phase, because of its excellent wetting and adhesion properties (Wentzel and Allen, 1997), together with its good mechanical properties, which has improved the mechanical properties of the cemented carbides.

The properties of WC-Co hardmetals such as hardness, toughness, strength, abrasion resistance and thermal conductivity can be widely improved by means of varying the grain sizes of both the binder and the carbide. According to Beste *et al*. (2001), a broad range of combinations of hardness and toughness can be achieved by varying the WC grain size and the Co content. The material can hence be optimized for different applications (Exner, 1979). The abrasive wear of WC–Co hardmetals has been reported to be largely improved by decreasing WC grain size, and that submicron size grades could result in double the wear resistance compared to the conventional grades (Krakhmalev *et al.,* 2007a). However, the influence of the WC grain size and Co content on the edge wear mechanisms is still under intense study (Krakhmalev *et al.,* 2007b).

## 2.4 WC – Co manufacture

Tungsten carbide-cobalt-alloys are traditionally made by powder metallurgy techniques involving liquid phase sintering that helps to achieve maximum densification. (Ogundipe *et al.,* 1996; Hochstrasser -Kurz *et al.,* 2007). The powders of tungsten carbide and the cobalt are milled to the required size and then mixed and compacted. After the compaction, the WC-Co alloys are vacuum sintered for 1 hour at about 1430°C (Penrice, 1997). Vacuum sintering is normally carried out in a batch type furnace**.** There has been continuous improvement of vacuum sintering technology, which started from the late 1980s, e.g. hot isostatic pressure sintering. This improvement has led to new standards in hardmetal quality.

Sintering or hot isostatic pressing (HIP) is the process of combining tungsten carbide with cobalt. During this process cobalt eventually enters the liquid stage and WC grains (with higher melting point) remain in the solid stage. As a result of this process, cobalt will embed/cement the WC grains and thereby create the metal matrix composite with its distinct material properties. The high carbon level tungsten carbide is improved by vacuum annealing whereas there is no need to improve low carbon material (Penrice, 1997).

## 2.5 Uses of WC-Co

Tungsten carbide is a widely used as coating material for protection against wear, erosion, and high-temperature oxidation due to its high hardness and excellent thermal stability. Cobalt is used for the fabrication of cutting tools as it combines hardness with ductility (Trueman *et al.,* 1999). The rationale for metal-matrix composites such as a tungsten carbide-cobalt is to develop a material with superior mechanical properties such as increased toughness, stiffness and hardness (Trueman *et al.,* 1999; Pugsley and Sockel, 2004). WC-Co combines these superior properties with exceptional wear resistance. These properties made them suitable alloys in many engineering fields as well as several industrial applications, such as cutting-tools or seal-rings, linings, valves, jet nozzles, saw blades, fluid mixers and conveyor belt scrapers (Wentzel and Allen, 1997; Human and Exner, 1996; Hochstrasser-Kurz *et al.,* 2007).

## 2.6 Limitations

The various applications demanded that WC-Co materials remain in service for several years. Since these materials are not only subjected to wear processes, but are also in contact with chemically aggressive environments, corrosion can play a major role in the degradation of the surface and can significantly accelerate wear (Human and Exner, 1996; Pugsley and Sockel, 2004). In long-life applications, the corrosion properties of cemented carbides can have a large influence on overall performance. Although corrosion resistance is not a prime requirement of hardmetals, nevertheless, this property is very important in its industrial uses (Scholl *et al.,* 1992). Since the cobalt binder phase is the most susceptible to corrosion in acidic and neutral media, it follows that improvement of the corrosion resistance of the binder will have a major influence on the overall corrosion resistance (Tomlinson and Ayerst, 1989; Human and Exner, 1997; Wentzel and Allen, 1997). The understanding of corrosion kinetics and thermodynamics is therefore necessary for improvement of cemented carbides in corrosive environments (Sutthiruangwong and Mori, 2003).

## 2.7 Corrosion behaviour

Corrosion is the typical mechanism of release of metals from their elemental forms or alloys to the environment (Ogundipe *et al.,* 2006; Aw *et al.,* 2007). Sutthiruangwong *et al.,* (2005) reported that cemented carbides are often confronted with deterioration problems in corrosive solutions via dissolution of the binder. However, their poor corrosion resistance in aqueous solutions reduces the spectrum of their applications (Hochstrasser-Kurz *et al.,* 2007; Guilemany *et al.,* 1993-1994). In principle Co-based cemented carbides do not passivate. Tungsten in the alloys shifts the corrosion potential to more noble values (Schnyder *et al.,* 2004). This is firstly due to the diffusion limitation of cobalt ions throughout the rest of the WC skeleton. Secondly, in the cemented carbide with high content of W in the binder, the corrosion products (such as tungsten oxides) can be formed on the surface of the binder and thus decrease the dissolution rate by inhibiting further dissolution of the binder. Tungsten oxide precipitates are formed in cemented carbides with high tungsten contents in the binder

phase, leading to a decreased dissolution rate in the pseudopassive region (Sutthiruangwong *et al.,* 2005).

Aggressive media preferably attack the binder while the tungsten carbide itself remains immune (Sutthiruangwong and Mori, 2003). This is because of a higher reduction potential of tungsten carbide when compared to the binder. After dissolution of the binder, skeleton of tungsten carbide at the surface remains (Sutthiruangwong and Mori, 2003). Corrosion attack proceeds predominantly at locations where the WC phase has fallen out after localized initiation of corrosion has taken place (Hochstrasser (-Kurz) *et al*., 2007).

Cemented carbides or hardmetals are heterogeneous materials, which basically suffer galvanic corrosion (Bozzini *et al.,* 2003; Sutthiruangwong and Mori, 2003; Schnyder *et al.,* 2004; Hochstrasser (-Kurz) *et al*., 2007). The synergistic effects of galvanic coupling between the WC phase (cathodically active) and the metallic matrix (anodically active) (Bozzini *et al.,* 2002; Hochstrasser-Kurz *et al.,* 2007), could accelerate Co dissolution and hinder WC dissolution in the hardmetals compared to the pure compounds. This is due to the fact that the Co binder phase contains W and C, making it more corrosion resistant than pure Co (Sutthiruangwong and Mori, 2003; Hochstrasser(Kurz *et al.,* 2007).

There is a certain amount of W and C that could be dissolved in the Co binder during sintering. However, a direct correlation of the corrosion behaviour of Co (W, C) and industrial hardmetals is not very straightforward as the exact concentrations of dissolved W and C strongly depend on the sintering conditions. The lower corrosion susceptibility of the binder phase of WC–Co compared to metallic Co is claimed to result from a stabilization of the FCC phase due to the dissolved W and C amounts (Human *et al.,* 1998; Hochstrasser-Kurz *et al.,* 2007). Thus, industry obtains reproducibility in properties of hardmetals based on cobalt by controlling the total carbon content and by keeping the magnetic saturation constant. These measures ensure that the carbon content of the binder phase is repeatable and the tungsten (or non-magnetic) content does not alter hardmetals toughness and strength properties (Almond and Roebuck, 1988).

### 2.7.1 WC–Co corrosion products in the different electrolytes

The few investigations (Tomlinson and Linzell, 1988; Tomlison and Ayerst, 1989; Hochstrasser -Kurz *et al*., 2007) comparing WC–Co hardmetals in acidic, neutral and alkaline solutions revealed a steady corrosion rate decrease with increasing solution pH. The presence of aggressive chloride ions in electrolyte solution could cause increasing corrosion rates. At room temperature, cemented carbides show an excellent resistance in basic and neutral aqueous solutions. However, strong acid solutions such as hydrochloric and sulfuric acid can cause severe corrosion and material degradation. It is known that sea water and acids are corrosive environments for cemented carbide corrosion (Sutthiruangwong and Mori, 2003; Sutthiruangwong *et al.,* 2005).

#### *2.7.1.1 Dissolution of Tungsten Carbide (WC)*

The dissolution of WC has been widely studied by several authors (Tomlinson and Linzell, 1988; Tomlinson and Ayerst, 1989; Human and Exner, 1996; Human and Exner, 1997). Generally, the corrosion of cemented carbides could be determined by studying the dissolution of the binder in acid and neutral solution. In alkaline solution, WC might dissolve at higher potentials (Mori *et al.,* 2001). Increasing the pH value can also shift corrosion potential to the more negative direction (Hochstrasser (-Kurz) *et al*., 2007). In acidic and neutral solutions, pure WC-Co alloys could show pseudopassivity (Mori *et al.,* 2001).

In sulphuric acid media, there could be formation of the oxide $WO_3$ at the surface as shown in equation (1). This oxide film could thus be responsible for the pseudopassive region.

$$WC + 5H_2O \rightarrow WO_3 + CO_2 + 10H^+ + 10e^- \quad \text{..... (1)}$$

Tungsten passivates readily and the electronic conductivity of the oxide film could be sufficiently low to prevent oxidation. The solid state properties of the growing film and the electrolyte composition determine the current distribution. The grown films of $WO_3$

may undergo different types of breakdown (mechanical or electrical) in different electrolytes. After the anodic pre-polarization of the metal/oxide/electrolyte systems, the breakdown determines the upper limit of the thickness reached by the oxide during growth (Tomlinson and Linzell, 1988; Scholl *et al.,* 1992; Bozzini *et al.,* 2002). Oxidation of WC with formation of $WO_3.xH_2O$ species might relate to the passivation of the hardmetals with formation of a continuous layer of oxides inhibiting the reaction of the binder phase (Bozzini *et al.,* 2003).

#### *2.7.1.2 Dissolution of Cobalt (Co)*

The electrochemical behaviour of the WC–Co hardmetal strongly resembles the behaviour of pure Co. In a neutral solution, selective dissolution of the less noble component Co can be expected. After exposure to an aqueous solution and the transfer in air, the cobalt seems to form an oxide layer (Schnyder *et al.,* 2004). Cobalt is a member of the transition metals with main oxidation states $Co^{2+}$ and $Co^{3+}$ as shown in equation (2) and (3).

$$Co \rightarrow Co^{2+} + 2e^{-} \quad \ldots\ldots\ldots\ldots\ldots\ldots\ldots\ldots \quad (2)$$

$$Co^{2+} \rightarrow Co^{3+} + e^{-} \quad \ldots\ldots\ldots\ldots\ldots\ldots\ldots\ldots \quad (3)$$

The $Co^{3+}$ ion is unstable and readily reduces to $Co^{2+}$. Consequently, $Co^{3+}$ can be disregarded for the consideration of the corrosion behaviour in acid solutions. Cobalt corrodes actively in acidic media and oxide formation occurs at pH levels around 7 in oxygenated environments. Numerous cobalt oxides are thermodynamically possible and stepwise oxidation of oxide layers is probable. In the absence of oxygen, cobalt is immune at pH levels above 7. In oxidising electrolytes, cobalt may be in the active or passive state depending on the type and concentration of electrolyte, the current density and temperature. The increasing polarization causes $Co(OH)_2$ to initially form on the metal surface as shown in equation (4).

$$Co + 2H_2O \rightarrow Co(OH)_2 + 2H^{+} + 2e^{-} \quad \ldots\ldots\ldots\ldots\ldots\ldots \quad (4)$$

At some potential, cobalt is oxidised to form $Co_3O_4$, and with a further increase in the potential $Co_3O_4$ becomes unstable and is reduced to form $Co(OH)_2$ or CoO. Pure cobalt has been found to exhibit no active to passive transition in different acid solutions with

sulphate ions at a pH of around 2.55 (Human *et al.,* 1998).

The corrosion susceptibility of the WC composite is influenced by microstructural parameters such as the microstructure and binder phase composition. Due to the heterogeneous microstructural nature and binder phase composition of WC–Co, their corrosion mechanisms are very complex and very little is known about the exact corrosion processes taking place (Hochstrasser-Kurz *et al*., 2007). Corrosion resistance of cemented carbides strongly depends on binder composition. WC dissolution during the sintering process leads to alteration of corrosion properties (Sutthiruangwong and Mori, 2003).

### 2.7.2 The effect of the grain size on corrosion

Corrosion of WC-Co hardmetal results mainly in the dissolution of the cobalt based binder phase. Different WC grain sizes could exhibit different corrosion behaviour. However, it has not been established whether the cobalt mean free path affects the corrosion resistance, i.e. whether grades of the equal cobalt content with different grain sizes could exhibit different corrosion behaviour (Fernandes *et al.,* 1992). Milman *et al.* (1999) quantified the influence of hardness, grain size and cobalt content on the behaviour of WC-10vol%Co alloys. The grain sizes ranged from 0.5 – 2.3μm. It was concluded that the hardness of WC-Co decreased with increasing WC grain size. Although the corrosion behaviour was not investigated, it was concluded that finer grained size alloys could preserve their hardness at higher temperatures than coarser grained size alloys.

Fernandes *et al.* (1992) observed that the corrosion rate of the WC-6%Co with 2μm mean WC grain size in a concentrated HCl solution is one order of magnitude higher than that of WC-6%Co with 3-4 μm mean WC grain size. By contrast, Tomlison and Ayerst (1989) concluded that the corrosion rate of a 3μm WC-6%Co is higher than that of 1.4 μm WC-6%Co in a 0.01M $H_2SO_4$+ 0.99 M $Na_2SO_4$ solution. Human and Exner, (1997) and Hochstrasser-Kurz *et al.* (2007), on the other hand, concluded that there is no effect of the WC grain size on WC-Co corrosion behaviour and only the amount of tungsten dissolved in the cobalt binder was expected to affect the corrosion resistance.

Fernandes *et al.* (1992) investigated whether the cobalt mean free path could affect the corrosion behaviour of WC-Co. The results were observed to be very inconsistent. It was suggested that the inconsistencies of the results were attributed to the fact that there is a large scatter in the results obtained from both immersion and electrochemical tests. The scatter in the results could be due mainly to differences in the amounts of tungsten dissolved in the cobalt or to different amounts of WC grains dislodged during total immersion tests and to extrapolations involved in the determination of corrosion current density from electrochemical tests. This could also be the reason for the reported (Tomlison and Ayerst (1989); Human and Exner, 1997; Hochstrasser-Kurz- *et al.,* 2007) inconsistencies.

### 2.7.3 WC – Co corrosion: effect of other carbides

The influence of the binder phase fraction induces a strong debate in the literature. Sutthiruangwong and Mori (2003) studied the corrosion properties of Co-based cemented carbides in acidic solutions and investigated the effect of the Co binder content on corrosion of WC-Co. It was concluded that the lower the cobalt content, the better the corrosion resistance. Conversely, Human and Exner (1997) studied the effect of binder content and WC grain size on the electrochemical behaviour of cemented carbides. The effect of binder content was examined by varying the binder content between 6 to 17wt% with a constant average grain size of about 2µm. The material was exposed to sulphuric acid and synthetic mine water environments. It was reported that no significant change occurred in the corrosion rate of the binder phase with varying binder content. The rate of material loss could increase with increasing binder content because the fraction of corroding phase could be increased. The kinetics of the binder phase corrosion rate was observed not to be measurably altered.

The cobalt binder may be partly replaced by noble metals such as platinum group metals. The high costs of noble metals and alloys have led to the development of various base-alloy materials, which are more economical. The most important components of these alloys are nickel, cobalt, copper and iron. The main difference between the noble and non-noble alloys is that the latter are less thermodynamically stable, and therefore their corrosion resistance may depend greatly on the formation of a

thin, protective oxide film (passive film) on the surface of the material. If the oxide film could be disrupted, then the metal or alloy must repassivate in order for the materials to be protected (Nascimentoa *et al.,* 2007).

The substitution of part or all of the cobalt by nickel or nickel and iron has been investigated in recent years in an attempt mainly to improve the properties of the binder and at the same time to reduce costs associated with the short supply and prevailing high market price of cobalt powder (Scholl *et al.,* 1992; Guilemany *et al.,* 1993-1994). The cobalt can also be partly replaced by nickel-chromium or nickel-chromium-molybdenum (Human and Exner, 1997). The effect of each binder alternative is briefly discussed below.

#### *2.7.3.1 Nickel*

Different authors (Tomlinson and Linzell, 1988; Tomlinson and Ayerst, 1989; Ringas *et al*., 1990 Wentzel and Allen, 1995; Bozzini *et al.,* 2002; Bozzini *et al.,* 2003; Aw *et al.,* 2007) have studied the effect of partly or fully replacing cobalt with a nickel binder on the electrochemical behaviour of cemented carbides in different corrosive media. It was reported that the binders containing nickel showed a significantly improved corrosion resistance in the studied systems. The amount of the nickel in the binder could be the most important factor that affects corrosion performance. Lisovsky *et al.* (1991) investigated the structure of a binding cemented carbide phase in re-alloyed WC-Co to show that the alloying process was the most efficient for influencing both the stacking fault energy in the Co phase and the mechanism of its polymorphic transformation. It was observed that the nickel-alloying of a binder in WC-Co cemented carbide results in changes in the Co phase transformation mechanism from fcc to hcp.

Penrice (1997) studied the characteristics of the binder phase in cemented carbides by fully replacing the cobalt with larger contents of nickel in some samples. It was reported that nickel could be solution strengthened by tungsten but it has intrinsically lower strength and higher ductility than cobalt. It also appeared to have a greater solubility for carbon. Although the corrosion-resistance of hardmetals could be considerably improved by substituting cobalt partially or completely by nickel, it was found that using nickel instead of cobalt as a binder material or into the binder phase leads to

deteriorated mechanical properties, (Tomlinson and Linzell, 1988; Scholl *et al.,* 1992; Human and Exner, 1997; Bozzini *et al.,* 2002).

#### *2.7.3.2 Nickel-chromium*

Wentzel and Allen (1997) investigated the polarization behaviour of different grades of cobalt, nickel, nickel-chromium and nickel-chromium–cobalt binders. It was observed that the Ni-Cr and Ni-Cr-Co alloys are more corrosion resistant than the pure metal binder grades of nickel and cobalt. The variation in the corrosion behaviour of the pure binder grades as compared with the alloyed binder grades can be attributed to the inclusion of chromium in the composition. It appeared that the chromium could serve to retard the corrosion process and also increase the hardness of the hardmetals which in turn improved its corrosion resistance. The addition of chromium to the pure cobalt binder could also serve to retard WC grain growth during the manufacturing process. Nevertheless, the nickel-chromium and nickel-chromium-cobalt systems had far better corrosion resistance than the pure binder of Co. Therefore, it was concluded that the additions of chromium in the binder phase improved the corrosion resistance of WC-Co cemented carbides.

#### *2.7.3.3 Nickel-chromium-molybdenum*

Tomlinson and Ayerst (1989) investigated the anodic polarization and corrosion behaviour of WC-Co hardmetals containing small amounts of $Cr_3C_2$ and/or VC. Some of the samples contained molybdenum and were exposed to chloride and mine water environments. It was observed that the molybdenum decreased the corrosion rate. The molybdenum alloyed material could withstand pitting corrosion over a wider range of potentials than the un-alloyed binder. This was manifested by an increase in pitting potential, corresponding to an increase in the passive range. It was concluded that pitting resistance of cemented carbides could markedly be improved by alloying with molybdenum. Since cemented carbides are often used in waters such as mine waters, where pitting corrosion due to chloride ions can be a problem, improvements in pitting resistance could be highly desirable.

Human and Exner (1997) investigated the relationship between electrochemical behaviour and in-service corrosion of WC based cemented carbides. Cobalt binder was substituted with nickel-chromium-molybdenum. The electrochemical experiments were conducted in both 1M $H_2SO_4$ and a synthetic mine water solution. It was observed that when comparing WC-Co with WC-Ni (Cr,Mo) in both normal sulphuric acid and a synthetic mine water, the behaviour of the two grades was markedly different. WC-Co could exhibit a 'pseudo-passivity' during electromechanical tests, but corrode actively in industrial applications. In contrast, WC-Ni (Cr,Mo) could passivate and the rate of corrosion can be several orders of magnitude lower than that of WC-Co.

#### *2.7.3.4 Iron*

The presence of iron in the alloy formulation could increase the susceptibility to galvanic corrosion (Ogundipe *et al.*, 2006). This could be due to the fact that tungsten solubility in nickel and cobalt is about 45% (wt/wt) at 1480$^{o}$C, whilst solubility in iron at this temperature is about 30% (wt/wt). The inclusion of iron however could lead to a reduction in the overall solubility of tungsten in the binder. This thus led to a greater difference in electrode potential between the two phases and consequently, a greater susceptibility to galvanic corrosion might result. Scholl *et al.* (1992) studied the anodic polarization of WC with different binders of Co, Ni and Fe. It was observed from the results that the values of current density indicated poor corrosion resistance of the (WC, Fe) materials as compared to the (WC, Ni) materials. The passivation and corrosion resistance of the pure metals can be judged as being excellent (Ni), good (Co, W) and weak (Fe). The following sequence of corrosion resistance was then established for the cemented tungsten carbide electrodes in most sulphuric acid solutions: (WC, Ni) > (WC, Co) >(WC, Fe).

### 2.7.4 Chemical modification of W-Co with metal carbides

The structure and properties of the cobalt phase can be modified through the alloying of the WC-Co cemented carbides with effective alloying elements. According to Lisovsky

*et al*. (1991), the addition of some alloying elements changes the qualitative and quantitative compositions of the binder and thus may change the corrosion behaviour of the binder. The presence of a relatively small amount of a substance added to the cemented carbide to improve the fabrication or mechanical properties also changes the corrosion properties. The binder composition is a key parameter to compare corrosion properties of both straight grade and alloyed grade cemented carbide (Sutthiruangwong *et al.,* 2005).

Several metallic alloy compositions, including ruthenium and the additions of the refractory metal carbides such as vanadium carbide (VC), chromium carbide ($Cr_3C_2$), titanium carbide (TiC) and tantalum carbide (TaC) increase corrosion resistance (Tomlinson and Linzell, 1988; Lisovsky *et al.,* 1991; Ringas *et al.,* 1990;Wentzel and Allen, 1997; Sutthiruangwong and Mori, 2003; Sutthiruangwong *et al.,* 2005). The effect of these metals and carbide additions is discussed in the following sections.

#### *2.7.4.1 Vanadium carbide (VC)*

Sutthiruangwong *et al*. (2005) studied the effect of different binder compositions on corrosion behavior cemented carbides. It was observed that the addition of VC could have a marginal effect on the corrosion resistance of cemented carbide. Vanadium carbide has been known as a grain growth inhibitor (Shing *et al.,* 2001; Shing *et al.,* 2002; Bonjour, 2004; Bonjour and Actis-Data, 2004). As a grain growth inhibitor the metal added might not be all dissolved in the binder but precipitate as carbide between growing WC grains preventing WC grain agglomeration.

Vanadium can also dissolve in the binder and influence the corrosion resistance of cemented carbides. The vanadium outside of the binder presents as a VC pocket. The solubility of vanadium in the cobalt binder is very low according to V/Co ratios. Moreover, vanadium carbide had been found to segregate as a thin layer between WC grains in addition to precipitating as a VC pocket. A thin VC layer less than 1 nm thick is deposited on the surfaces of WC grains. The layer could act as a liner and separate binder from WC grains. The layer would thus result in VC/Co instead of WC/Co galvanic coupling. Sutthiruangwong *et al*. (2005) concluded that the dissolved

vanadium in the binder increases corrosion resistance.

### *2.7.4.3 Chromium Carbide ($Cr_3C_2$)*

The corrosion behaviour of hardmetals containing chromium carbide has been widely studied. Tomlinson and Ayerst (1989) investigated the anodic polarization and corrosion properties of WC-Co containing $Cr_3C_2$. It was observed that the small additions of $Cr_3C_2$ to WC-Co could substantially increase the corrosion resistance. Sutthiruangwong *et al.* (2005) studied the effect of different binder compositions on corrosion behaviour. It was observed that chromium distributed together with cobalt which indicated that the chromium dissolved in the binder. The ratios suggested that about 89% of the added $Cr_3C_2$ was dissolved in the binder during fabrication. The rest (about 11%) of it precipitated as carbide which is well known as a grain growth inhibitor. It was further observed that chromium could significantly reduce corrosion current density, critical current density, and pseudopassive current density. Chromium shifted the corrosion potential to more noble values, while the critical potential was shifted towards the anodic region indicating that chromium could increase the polarization resistance of cobalt based binder. Chromium in the binder was reported to increase the corrosion resistance by stabilizing the cobalt-based passive oxide layer.

Mori *et al.* (2001) investigated the influence of additions of $Cr_3C_2$ on corrosion resistance. It was concluded that chromium carbide could act as a grain growth inhibitor. $Cr_3C_2$ additions have been found to significantly improve the corrosion resistance of Co-based cemented carbide in acid solution (Tomlinson and Ayerst, 1989; Mori *et al.,* 2001; Bozzini *et al.,* 2002 and Sutthiruangwong *et al.,* 2005).

### *2.7.4.4 Titanium Carbide (TiC) and Tantalum Carbide (TaC)*

High amounts of titanium carbides and tantalum carbides additions (approximately 4%TiC + 8%TaC) could improve the corrosion resistance of cemented WC-carbides (Tomlinson and Ayerst, 1989; Sutthiruangwong *et al,.* 2005). Bozzini *et al*. (2003) studied the anodic behaviour of WC-Co hardmetals and observed that the additions of titanium carbides and tantalum carbides to WC-Co brought about pseudopassive

behaviour in both acidic and alkaline de-aerated environments.

Tomlinson and Linzell (1988) and Mori *et al.* (2001) observed that the additions of small amounts (some tenth of a percent) of titanium carbides and tantalum carbides do not influence corrosion resistance of WC cemented carbides in acidic, alkaline and neutral solutions. It was further observed that increasing the amounts of titanium carbides and tantalum carbides to the cemented carbides could have a slight decrease in corrosion rate in both acidic and neutral solutions, although in alkaline media there was no significant change in the corrosion when comparing it with pure WC-Co cemented carbides.

## 2.8. Ruthenium additions to WC-Co

An additive component of a binder can comprise one or more metals from the platinum group metals, preferably one or more of ruthenium, rhodium, palladium, osmium, iridium, platinum or their mixtures and their alloys. Amongst the Platinum Group Metala, ruthenium or ruthenium alloy additions have been observed to be very effective. Bonjour (2004) has shown that the addition of Ru into a cobalt binder had stabilizing properties in the WC-Co composite. A considerable amount of research (Shing *et al.,* 2001; Shing *et al.,* 2002; Bonjour, 2004; Bonjour and Actis-Data, 2004) has been focused on the change of the mechanical properties of cemented carbides when Ru is added. However, limited work has been done to study corrosion behaviour and the comparisons of corrosion rates in different solutions.

Ruthenium (Ru) has been found to be a key chemical element in the cobalt-based binder phase of the tungsten carbide hardmetals (Festeau *et al.,* 2007). Ruthenium is a noble metal of the platinum group. It is a by-product of the development of nickel, copper and platinum. Ruthenium is hard, lustrous and a white metal that does not tarnish at room temperatures. The principal characteristics of ruthenium are its melting point which is around 2410$^{o}$C, the density of 2.45g/cm$^{3}$, a high Young's Modulus of 420GPa and the compact hexagonal structure (Bonjour, 2004; Bonjour and Actis-Data, 2004). Presently, a very limited amount of cemented carbide cutting tools have been prepared with ruthenium added to the cobalt binder.

Stellram, an Allegheny Technologies Company in the USA has found that adding an amount of ruthenium into the cobalt binder continuous phase of a tungsten carbide substrate could result in a cemented carbide cutting insert with improved resistance to thermal cracking and significant reduction of the propagation of cracks along and beyond the cutting insert edges and propagation of cracks into the substrate during use in machining processes. The amount of ruthenium used is normally varied depending on the application. The typical commercially available products include a concentration of ruthenium in the binder phase of cemented carbide substrates in the ranges of approximately 5% to 25%, by weight (Festeau *et al.,* 2007).

Bonjour (2004) studied the effects of ruthenium additions on the properties and machining behaviour of WC-Co hardmetals. It was observed that the addition of ruthenium increase the hardness and mechanical resistance compared to standard cemented carbides. The grade containing ruthenium had a very good resistance to thermal shock and to thermal fatigue. It had high resistance to strong cutting stresses and a good resistance to mechanical impacts and to wear. This improvement could be ascribed to the stabilization of the cobalt phase and to the improvement of the characteristics of the binding phase. This improvement is mainly due to the stabilization of the ε phase of the cobalt. A Co-Ru alloy has better stabilization and inhibition of grain growth, probably due to a lower viscosity which causes less porosity during the sintering process.

### 2.8.1 Uses of ruthenium

The advantages offered by the ruthenium additions in hardmetals are that of grain growth refinement, an increase in resistance to chemical attack and a strengthening of the binder phase without significantly affecting the edge toughness (Festeau *et al.,* 2007). Ruthenium can also increase both the hardness and flexural strength of WC-Co cemented carbides (Technical trends, 2004). Ruthenium-based electrocatalytic electrodes are widely used commercially, for example in the chloro-alkali industry, and their electrochemical and structural properties have been studied extensively (Walker *et al.,* 1998). Festeau *et al.* (2007) observed that ruthenium could increase the force of

cohesion between the carbide grains and the binder. A grade containing ruthenium could have a higher tenacity characterised by better edge and wear resistance. Ruthenium may also be used as an effective hardener, producing alloys that are extremely wear resistant.

### 2.8.2 The effect of ruthenium on Co or WC-Co

#### *2.8.2.1 Ruthenium with other alloys*

A report on (Technical Trends, 2004) the effect of ruthenium on the WC-Co hardmetals reported that the presence of titanium and niobium carbides do not have any influence in WC-Co. On the other hand, it was observed that an addition of ruthenium alone to the cobalt binder (with which it forms a solid solution), has a measurable but not outstanding action as a grain-growth inhibitor. It does indeed have a synergistic effect in conjunction with chromium or vanadium carbides. It was concluded that the major effect of the ruthenium appeared to be in grain refining during sintering, particularly when it was combined with chromium and vanadium carbides and the binder content was relatively high. Bonjour and Actis-Data, (2004) corroborated these results.

*Ruthenium is an inhibitor of grain growth particularly when it is used:*

- With chromium and vanadium carbides;
- For grades with high cobalt content; and
- For grades with CoFeNi binder (Technical trends, 2004)

#### *2.8.2.2 Effects of Ru in a binder*

Ruthenium could inhibit the formation of eta phase in substoichiometric WC-Co and normally only a minimum amount of Ru is required (Shing *et al.,* 2002; Bonjour and Actis-Data, 2004).

*By its action on the binder, ruthenium improves:*

- The toughness of hardmetal grades;
- Their hardness;
- Corrosion behaviour;
- Wear resistance as well as impact strength;

• Machining performance in general; and
• Higher density of grades with ruthenium (Technical trends, 2004)

However, contrary to previously described observations (Technical trends, 2004), Shing *et al.* (2001) found that the toughness could decrease with an increasing amount of ruthenium content. Shing *et al.* (2001) suggested that the decrease in toughness may be due to the hardening of the binder, which results from ruthenium remaining in solution in the cobalt.

### 2.8.3 Influence of ruthenium on corrosion behaviour

The use of ruthenium in sintered carbides was very much a development of the 1970s (Technical trends, 2004). Previously a group of Russian researchers showed that the additions of platinum group metals (PGM) to chromium-based alloys cause a spontaneous shift of corrosion potential towards more noble values, a phenomenon generally known as cathodic modification (Potgieter *et al.,* 1993). The passivity of the stainless steels usually relies on its chromium content, which may provide a protective film on the surface to prevent corrosion. Early work by Mintek focused on Ru additions of up to 0.2wt% to ferritic stainless steels. The remarkable effectiveness of these small ruthenium additions led Mintek to commercialize variants of these cathodically modified stainless steels. The first of these appeared under the trade name Ruthalloy, and was based on a Fe-29%Cr-4%Mo-0.2%Ru composition (Wolff, 1999).

In the 1990's work by Mintek expanded earlier investigations to show that a RuAl intermetallic compound could withstand attack in very aggressive media ranging from hydrofluoric acid, mixed acids, and aqua regia, and even through hot chloride environments. According to Wolff (1999), the remarkable passivity of ruthenium aluminide renders RuAl suitable for application as protective coatings, both for aqueous as well as high temperature oxidation and corrosion environments. In the short term, it was found that the small additions of ruthenium could enhance the oxidation resistance of the alloys based on Fe-Cr-Al, which find its application as substrates for autocatalytic converters.

In the 1990s the main efforts have been directed at understanding the kinetics and

mechanisms of oxygen and chlorine evolution reactions at the electrodes. Mixed $RuO_2/TiO_2$ anodes are remarkably stable, whereas bulk $RuO_2$ electrodes corrode rapidly during oxygen or chlorine evolution. It is reasonable to assume that the redox chemistry of ruthenium is relevant to electro-catalysis as well as to electrode stability, and several ex-situ XPS and Auger studies have been directed at identifying the oxidation state(s) of ruthenium surfaces formed during oxygen or chlorine evolution (Walker *et al.* (1998).

Llopis *et al.* (1966) studied the anodic corrosion of ruthenium in hydrochloric acid solution. It was observed that the electrochemical corrosion of ruthenium in HCl solution both by the action of direct current and alternating current leads to the formation of chloro-complexes of Ru (III) and/or Ru (IV), depending on the potential. With solutions of HClO, anodic corrosion by direct current may occur with formation of RuO, which partially dissolves in the electrolyte. In HCl solution anodic corrosion by direct current could lead to the formation of as yet undefined chloro-complexes. The superimposition of square-wave alternating current could notably increase the attack if the frequency is below 4 Hz. Under these conditions the complexes [RuCl]* were formed in proportions depending on the experimental conditions. It was concluded that the corrosion resistance of ruthenium in HCl solution was higher than that of rhodium and platinum and of the same order as that of iridium.

### 2.8.4 Effects of ruthenium on cemented carbides corrosion

A high-volume fraction of hard tungsten carbide particles in a ductile cobalt matrix provides industry with a material that could exhibit the best combination of strength and toughness available. The arduous requirements for these material, usually embracing high temperatures, thermal and mechanical stresses, and corrosivity, led manufacturers to identify new grades containing ruthenium in the 1970s. As little as 15wt% of ruthenium in the cobalt binder phase was found to address the problem experience with thermal fatigue, providing a greater hardness and wear resistance, and maintaining good toughness (Wolff, 1999).

Previous studies on ruthenium additions have focused on its effects on the corrosion behaviour of stainless steels alloys (Potgieter, 1991; Potgieter, 1993; Potgieter *et al.,* 1990; Potgieter *et al.,* 1993; Wolff, 1999; Wolff *et al.,* 1998; Myburg *et al.,* 1998). The

few related studies on hardmetals (Shing *et al.,* 2001; Shing *et al.,* 2002; Bonjour, 2004; Bonjour and Actis-Data, 2004) were mostly focused on improving mechanical properties, without much attention to studying the effects of ruthenium on the corrosion behaviour of WC-Co hardmetals. There is therefore scope to expand previous investigations to include research on the corrosion behaviour of WC-Co-Ru hardmetals in various corrosion media and environments. The current study will address this lack of data and knowledge in the field of hardmetals.

# *CHAPTER 3*

## 3.0 EXPERIMENTAL PROCEDURE

The changes in properties (microstructural) of the samples were assessed through optical microscopy, scanning electron microscopy (SEM) equipped with energy dispersive X-ray spectroscopy (EDX) for morphological and qualitative analyses of the samples, X-ray diffractometry (XRD) to identify the mineral phases within the samples and Raman spectroscopy before and after corrosion to determine the formation of any oxide films and compounds. Corrosion behaviour was investigated using the electrochemical polarization techniques.

### 3.1 Characterisation of the samples

The samples were characterised in the as received state to determine their morphologies and elemental compositions. Chemical characterisation of the samples was done using a scanning electron microscope (SEM) coupled with an energy dispersive x-ray spectroscopy (EDX) to determine the elemental composition of the samples. The samples were then analysed using the X-ray diffractrometry (XRD) to identify the mineral phases present in each sample. The corrosion behaviour of WC-Co alloys with and without Ru were investigated using three different electrochemical techniques, namely open circuit potential (OCP), potentiodynamic polarisation measurements and chronoamperometry measurements. Chemical characterisation of the corrosion products was performed by using Raman spectroscopy, SEM/EDX and XRD. The techniques used are described briefly in the next sections.

## 3.2 Sample compositions

The starting material was obtained from previously manufactured samples (collection of Prof. Luyckx from the University of the Witwatersrand (Wits) Johannesburg). The samples were obtained in a tablet form and their chemical compositions are shown in Table 3.1. The compositions of the samples were verified by EDX.

**Table 3.1: The chemical composition of the samples**

| **Sample Identity** | | **Ru additions** | |
|---|---|---|---|
| S1 | WC | 10 wt% Co | 0.0 wt% Ru |
| S2 | WC | 10 wt% Co | 0.4 wt% Ru |
| S3 | WC | 10 wt% Co | 1.0 wt% Ru |
| S4 | WC | 10 wt% Co | 1.5 wt% Ru |
| S5 | WC | 10 wt% Co | 2.0 wt% Ru |
| S6 | WC | 10 wt% Co | 3.0 wt% Ru |

## 3.3 WC-Co-Ru manufacture

The samples manufacturing was described by Bonjour *et al.* (2004). WC-Co-Ru was usually made by compacting together a layer of Ru powder (in the range of 17 μm mean particle sizes) and a layer of WC-10% Co (normally in the range of 1 μm Co and 1 μm mean particle size) at the applied pressure of about 1.5 MPa. The sample is then heated to temperatures of about 1000ºC in a tube furnace and kept at the temperature for 24 hours in argon flowing at a rate of $3.33\times10^{-5}m^3s^{-1}$. The sample is then sintered in vacuum at about 1410ºC for one hour. Ruthenium powder is usually dry milled with the x wt.%WC- y wt.% Co powder for 24hrs before heat treatment, following an industrial standard procedure, in order to reduce the Ru powder particle size and to thoroughly mix the two powders. The sintered samples were sectioned at the WC-Co-Ru interface by means of a diamond wafer blade. The process of the production of WC-Co-Ru is shown in Figure 3.1.

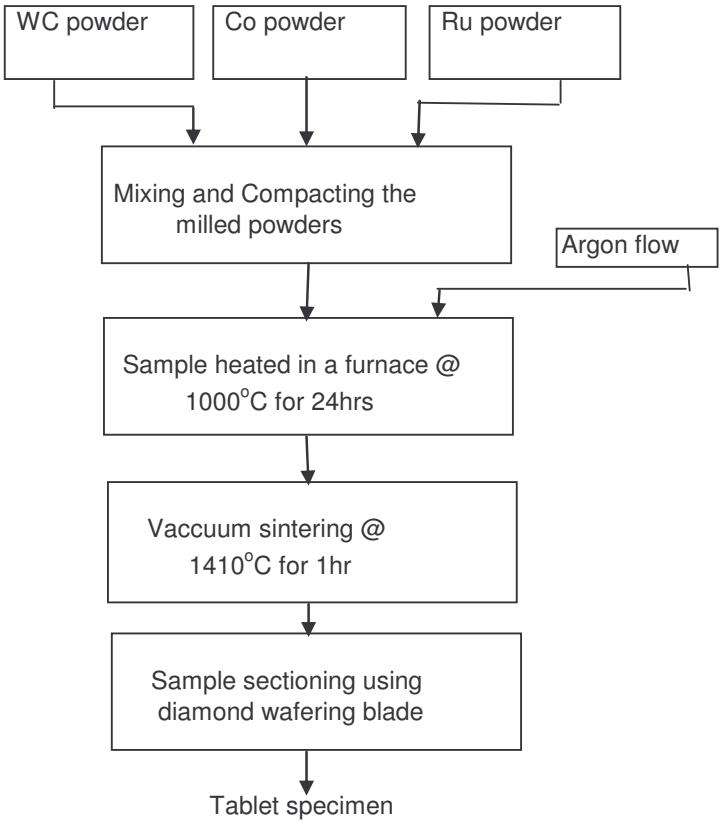



**Figure 3.1:** Manufacturing process of WC-Co-Ru samples.

### 3.4 Sample preparation

The samples were prepared by attaching an insulated copper wire to one face of the sample using an aluminum conducting tape, and the samples with the insulated copper wire were cold mounted in resin. The samples were wet ground using coarse plate of MD- Allegro with 80 μm grit to achieve a top flat polished surface, then successively on 120, 220, 1200 μm of fine plate of MD-Allegro with 1200 μm grit to achieve the smooth surface. Wet grinding was done by using fast-running water in order to prevent excessive build up of heat. The top surface was polished with a pan cloth with 3 μm diamond paste followed by a 1 μm diamond spray with an extender to obtain a mirror-like surface. The polished surfaces were cleansed in distilled water and etched using Murakami's reagent (10g $K_3[Fe(CN)_6]$ + 10g KOH + 100ml water) at room temperature for 2-3 minutes followed by a rinse with distilled water (Polini *et al.,* 2006) to reveal the details of their microstructures. Light pressure was applied throughout all the

surface preparation to prevent grain fallout.

### 3.5 Microstructural observation

The etched surface was analysed for microstructural features to obtain optical micrographs using an Axiotech microscope (Carl Zeiss AG, Oberkochen, Germany) equipped with an AxioCam MRc digital camera.

### 3.6 Scanning Electron Microscopy (SEM)

Morphological and qualitative analyses of the samples were performed using Scanning Electron Microscopy (SEM) equipped with Energy Dispersive X-ray Spectroscopy (EDX) analyzer. The SEM provided information on the physical properties of minerals, while EDX provided information on their chemistry. The JEOL JSM-5700 SEM was used and operated at 20kV. Scanning electron microscopy was undertaken on polished samples in order to determine the microstructures of the as-received samples.

### 3.7 X-ray Diffractrometry (XRD)

X-ray diffraction (XRD) analyses were conducted for the qualitative and quantitative analyses (phase identification) of the minerals within the sample. Phase identification of the sample constituents were carried out by X-ray diffractometry using a Philips PW1710 X-ray diffractometer control set at the voltage of 40kV and a current of 20mA. Standard Bragg–Brentano $\theta$ –$2\theta$ scans were made from a $2\theta$ angle of 20° to 80° using nickel filtered copper radiation. The measurements were performed over the diffraction angle range $2\theta$=20° to 80° using a step size of 0.02° $2\theta$ with a time per step of 1 second. The difficulty with the XRD techniques is that some phases are isostructural or have almost similar unit cells which result in almost identical Bragg diffraction peak positions almost throughout the $2\theta$ range. The semi-quantitative analyses of the samples were carried out using X //Pert PRO Diffractometer by PANanalytical, operated at

40kV and 40mA for 30s. High Score Plus software was used for quantification of the constituent phases.

## 3.8 Raman Spectrocopy

In order to identify the thin surface films (corrosion products) at high resolution, Raman spectroscopy was used. A laser source of $Ar^+$ was capture, with the scan patterns at room temperature, whereas to capture the image on the surface of the alloy, a light microscope was used. The spectrum was collected by directing a continuous laser of $Ar^+$ (514.5nm) on the alloy surface. The samples were scanned from 100 to 2500 $cm^{-1}$ wavenumbers.

## 3.9 Corrosion Tests

### 3.9.1 *Electrochemical tests*

Electrochemical measurements were carried out in a conventional three electrode 500 ml cylindrical Pyrex glass cell. The cell consists of a graphite counter electrode and a silver/silver chloride, 3M KCl, reference electrode and the working electrode in different corrosive electrolytes. Working electrodes were prepared by attaching an insulated copper wire to one face of the sample using an aluminum conducting tape cold mounted in resin. Working electrodes had compositions as shown in Table 3.2. The experimental set-up is shown in Figure 3.2. Corrosion behaviour of the samples was investigated in 1 M sulphuric acid, sodium chloride and synthetic mine water solutions. Synthetic mine water solution was prepared as Human and Exner (1996) have done to represent the most aggressive mine water in gold mining industries of South Africa (Machio, 2005). The concentrations are displayed in Table 2.2, the solution had a pH of 6 (Human and Exner, 1996). Electrochemical measurements were carried out at room temperature (25 ± 1°C) with an Autolab potentiostat (PGSTAT20 computer controlled) using the General Purpose, Electrochemical Software (GPES) version $4.9._{007}$. Electrochemical measurements were conducted using open circuit potential (OCP)

measurements, potentiodynamic polarizations, and chronoamperometric determinations.

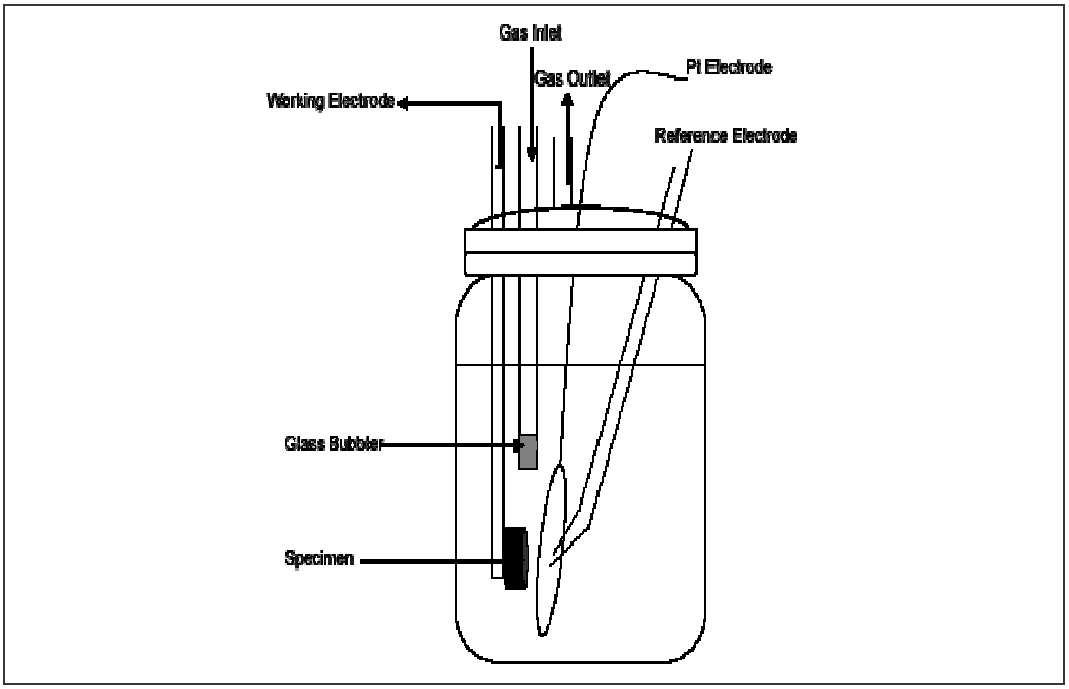



**Figure 3.2: The electrochemical measurements experimental set-up.**

**Table 3.2**: The chemical composition of synthetic mine water (Human and Exner, 1996)

| Salt | Concentration (mg/l) |
|---|---|
| $Na_2SO_4$ | 1237 |
| $MgSO_4$ | 199 |
| $CaCl_2$ | 1038 |
| NaCl | 1380 |

### *3.9.1.1 Open Circuit Potential (OCP) measurements*

The cell was left for a suitable time (about 2hours) to stabilize the OCP after the immersion of the samples in the electrolytes, before potentiodynamic polarization measurements were done.

### *3.9.1.2 Potentiodynamic polarization measurements*

Polarization curves were obtained at varying applied voltages and at constant scan rate of 2mV/s from −250 to 1200mV. The General Purpose, Electrochemical Software

(GPES) determined the corrosion potential ($E_{corr}$), corrosion current ($I_{corr}$) and corrosion current density ($i_{corr}$) from the polarization experiments, and calculated the corrosion rates. After each polarization scan, the electrolytes were replaced and the samples were polished and rinsed in water to remove the products that might form on the surface which could affect measurements.

#### *3.9.1.3 Chronoamperometry technique*

Chronoamperometry was used to investigate diffusion limitations in the pseudo-passive region of cemented carbides with ruthenium additions. Three potentials for chronoamperometry were obtained from the pseudo-passive range and the active range.

## 3.10 Surface analysis after electrochemical tests

The samples were stored in a vacuum desiccator after the corrosion tests, before performing an elemental analysis through energy dispersive X-ray spectroscopy (EDX) on the scanning electron microscope and thereafter, performing an X-ray diffraction (XRD) analysis. The degree of corrosion of a particular phase in the composite was examined. SEM/EDX analyses results were obtained for corroded regions and were used with results obtained from the polished surface to compare. X-ray diffraction (XRD) analyses were performed on the corroded surfaces to obtain diffractions patterns for comparisons with patterns obtained before corrosion. Raman spectroscopy was used to analyze sample surfaces after corrosion to determine any formation of oxide films or other corrosion products.

# *CHAPTER 4*

## 4.0 RESULTS AND DISCUSSIONS

This chapter consists of three sections: the characterisation of the materials in the as-received state, the electrochemical measurements and characterisation of the corrosion products.

### 4.1 Characterisation of the materials

The characterisation of the materials in the as-received state is presented in this section.

#### *4.1.1 Optical microscope*

The microstructures of the WC-Co-Ru alloys in the as-received condition are shown in Figure 4.1.1. The lighter regions in the micrographs correspond to the tungsten carbide while the darker regions correspond to the cobalt binder phase. The micrographs are observed to have pores that are illustrated by the arrows and are visible in most of the alloys. Shing (2000) reported that the most common causes of porosity are insufficient comminution, insufficient mixing and entrapped gases and impurities during sintering.

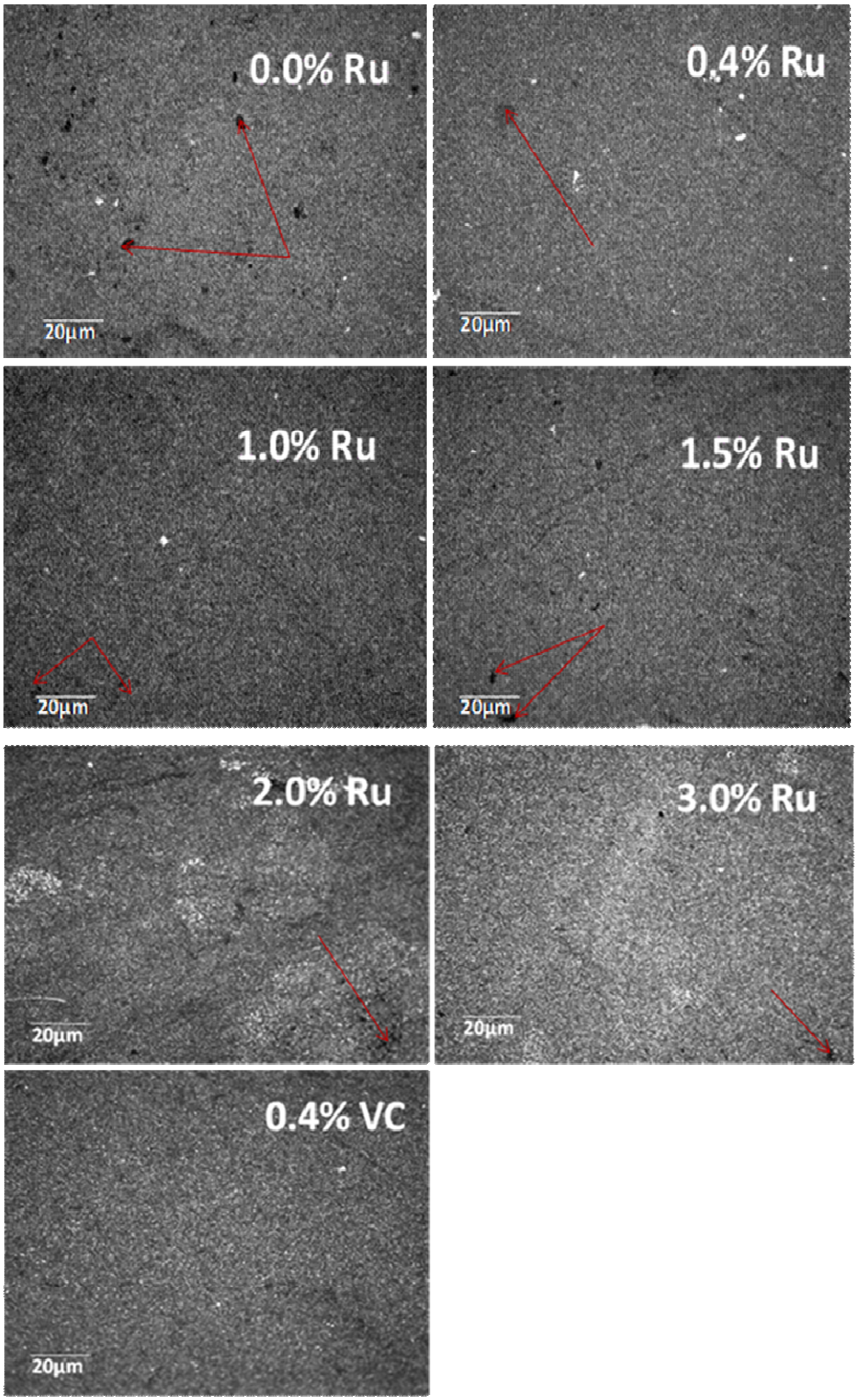



**Figure 4.1.1: Optical micrographs of the cemented carbide alloys samples in the as-received samples with arrows indicating the pores.**

### *4.1.2 Scanning electron microscope*

Analyses of the surfaces and semi-quantitative elemental compositions of the samples before corrosion occurred were obtained by using SEM/EDX and are given in the micrographs 4.1.2 - 4.1.7.

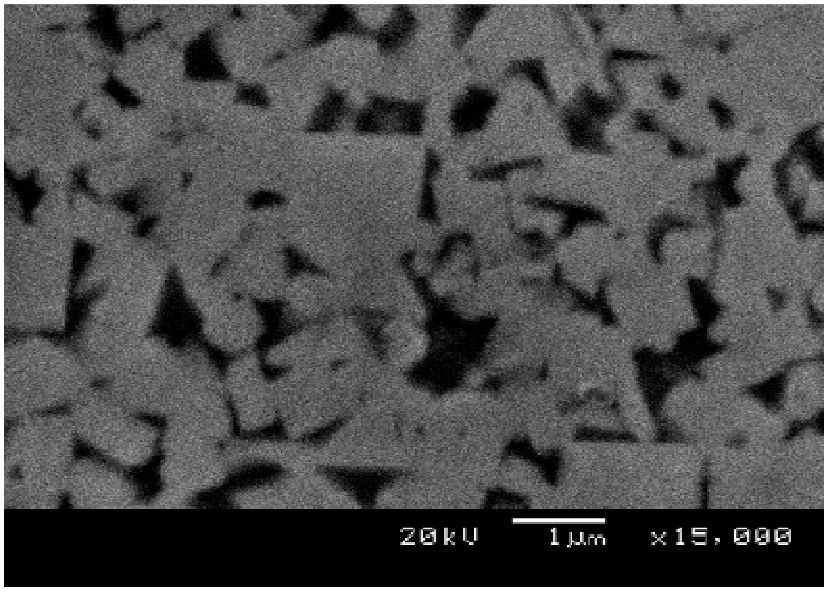



**Figure 4.1.2: SEM micrograph of WC-10%Co alloy**

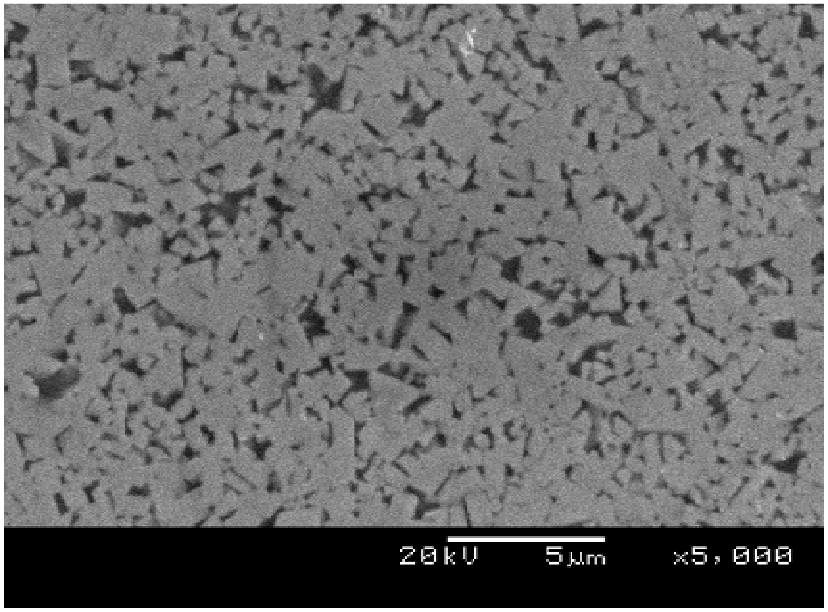



**Figure 4.1.3: SEM micrograph of WC-10%Co-0.4% Ru alloy**

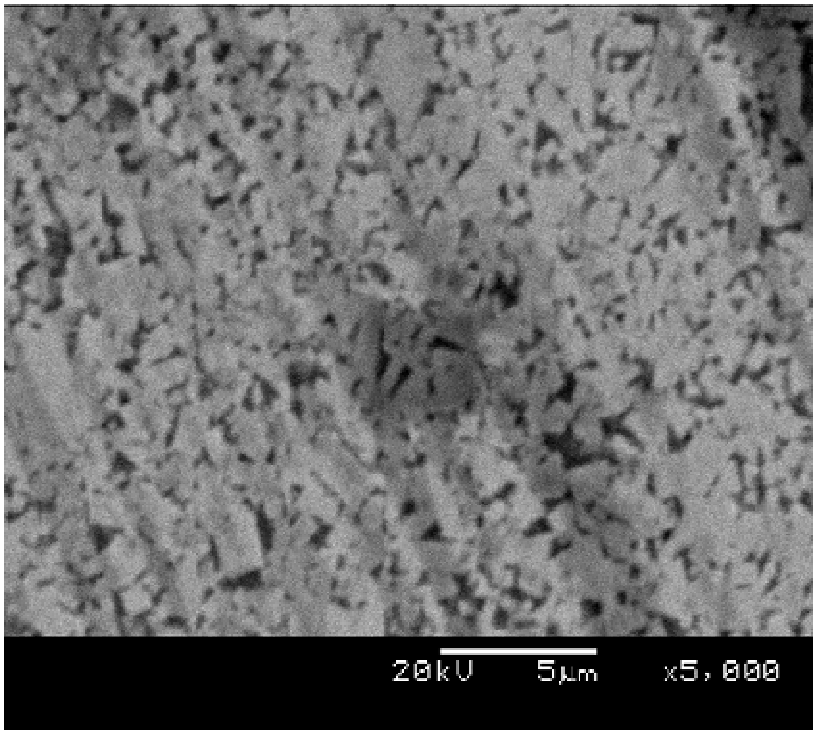



**Figure 4.1.4: SEM micrograph of WC-10%Co-1.0% Ru alloy**

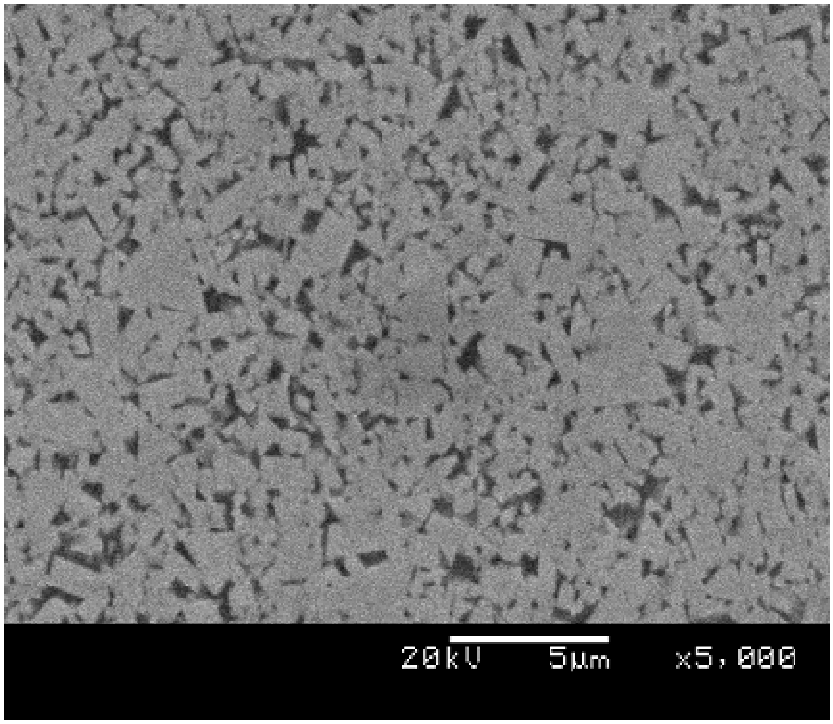



**Figure 4.1.5: SEM micrograph of WC-10%Co-1.5% Ru alloy**

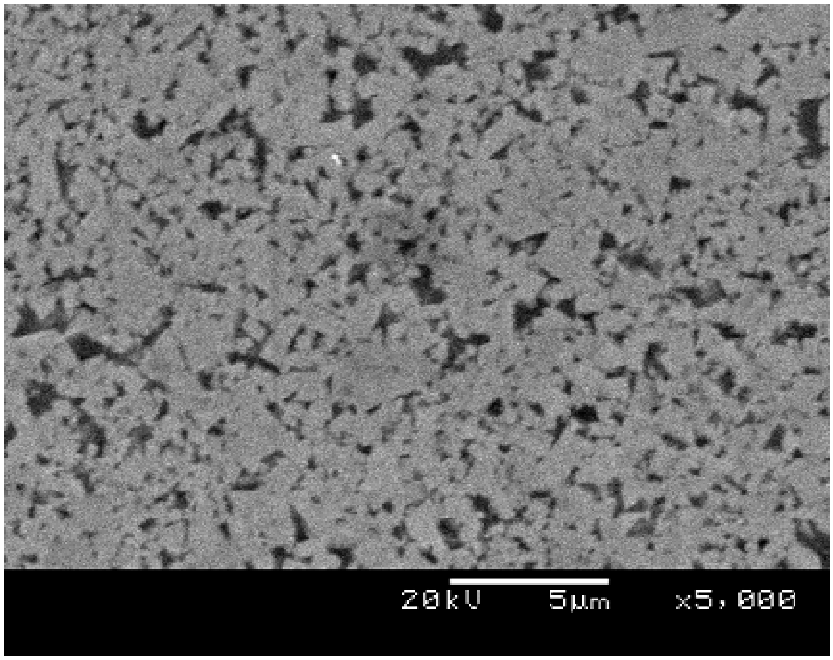



**Figure 4.1.6: SEM micrograph of WC-10%Co-2.0% Ru alloy**

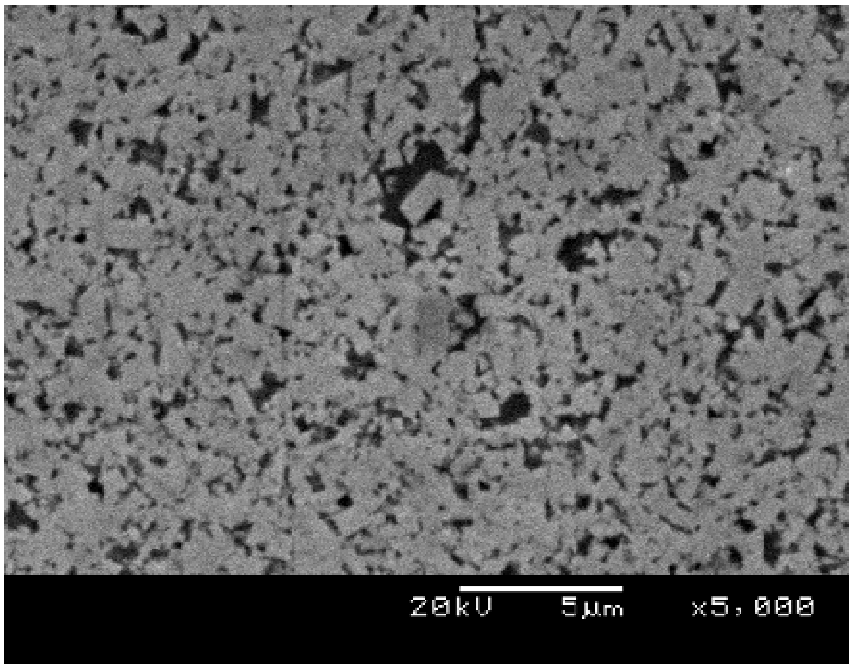
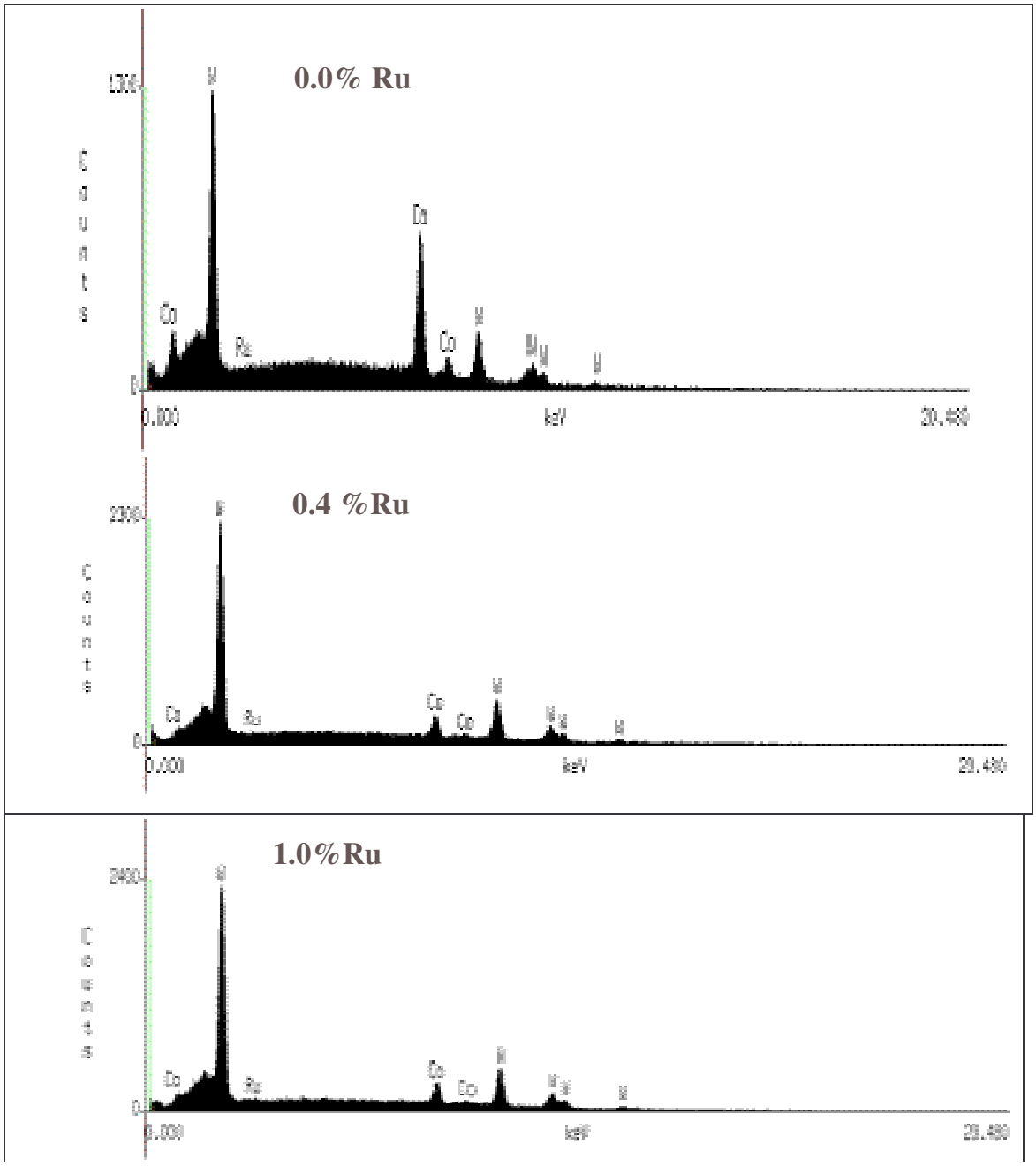



**Figure 4.1.7: SEM micrograph of WC-10%Co-3.0% Ru alloy**

Scanning electron micrographs illustrating the microstructures of the polished surface of the materials (WC-Co-Ru) in the as-received condition are shown in Figures 4.1.2 to 4.1.7. The lighter phase corresponds to tungsten carbide grains, which can be easily

observed as they are distinctly lighter and a darker cobalt binder phase. The corresponding EDX analyses are shown in Figure 4.1.8. It was observed that W showed the highest peaks in all the spectra. No ruthenium peak was obtained in WC-10%Co alloy. These observations are in agreement with the expectation that the alloys with ruthenium will show ruthenium peaks.



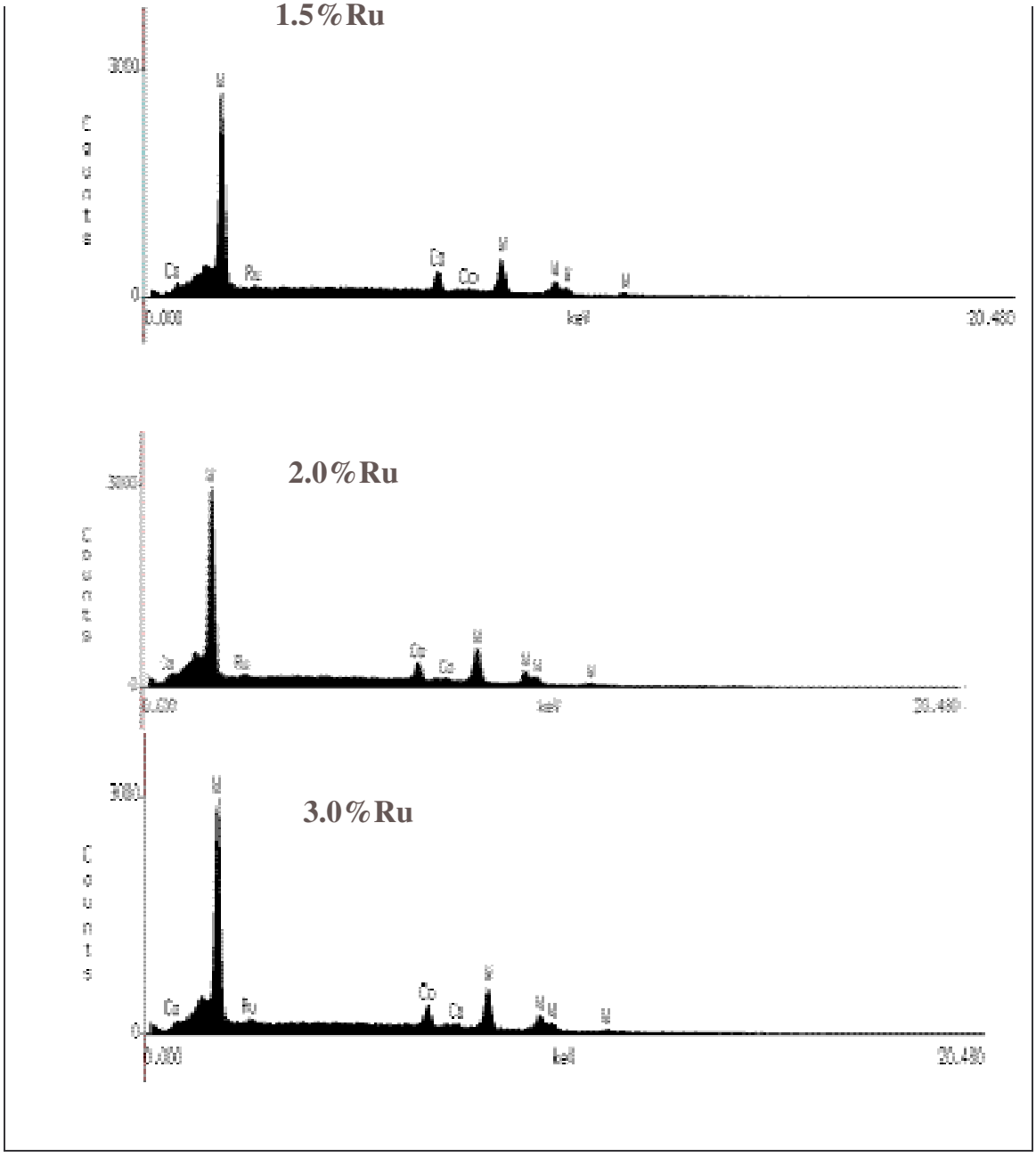



**Figure 4.1.8: EDX spectra analyses of the polished surface of the alloys used in the investigation.**

### *4.1.3 X-Ray Diffractometry (XRD)*

XRD analyses of these materials showed the presence of cobalt and WC. The ruthenium could not be detected accurately due to the detection limit of the equipment being at

least 5 wt %. For all the samples the diffraction pattern shows the cobalt peak at a 2θ value near 43º. The results are shown in Figures 4.1.9 to 4.1.14.

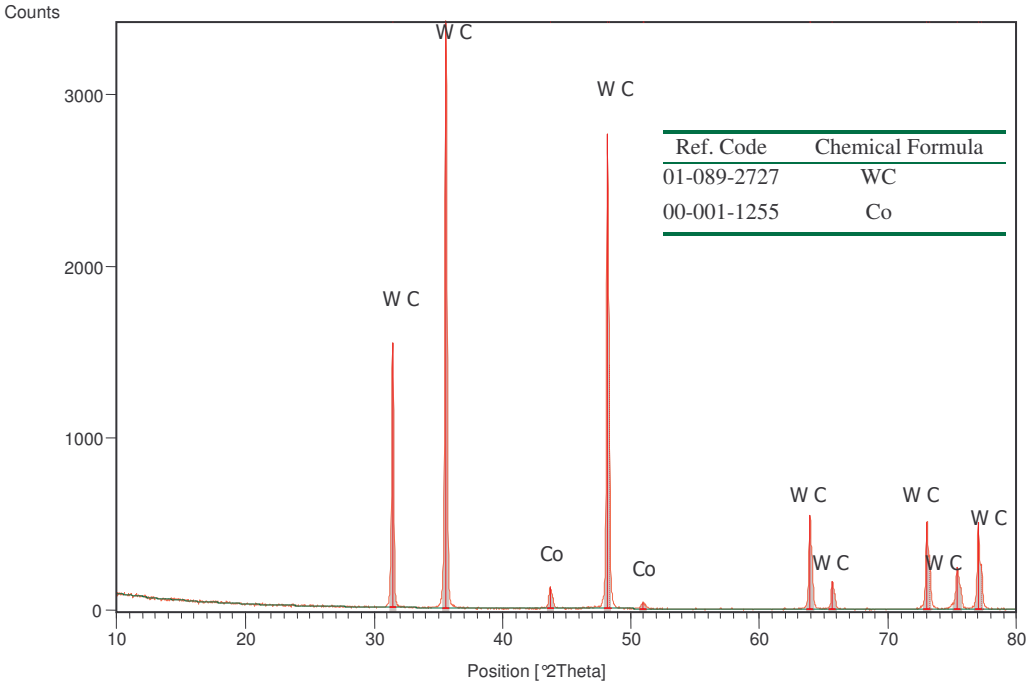



**Figure 4.1.9: XRD patterns for WC-10%Co alloy**

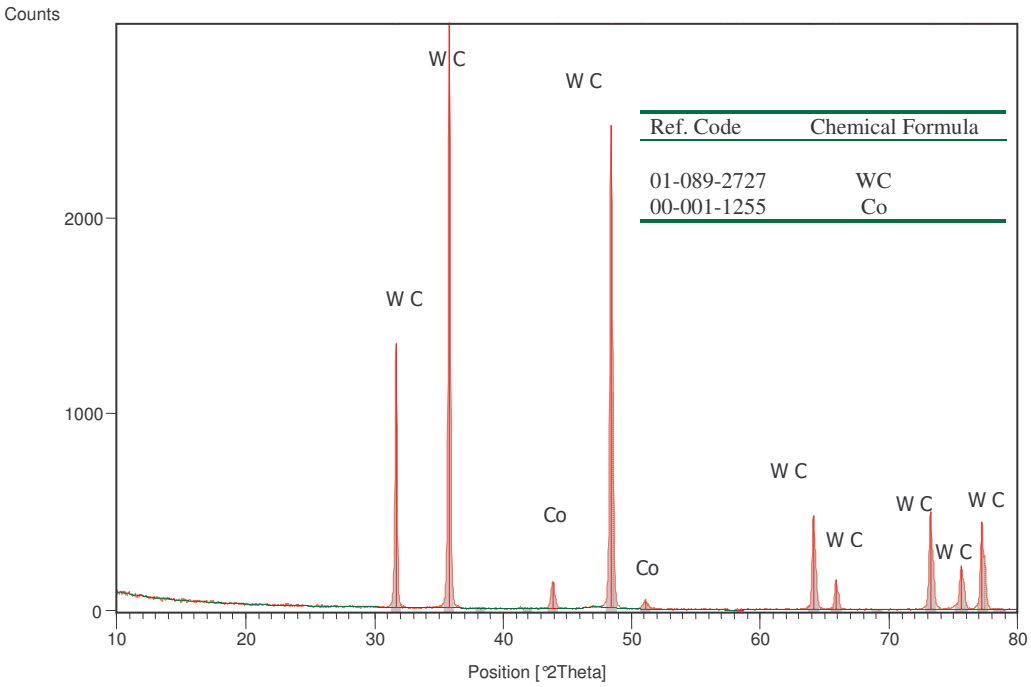



**Figure 4.1.8: XRD patterns for WC-10%Co-0.4%Ru alloy**

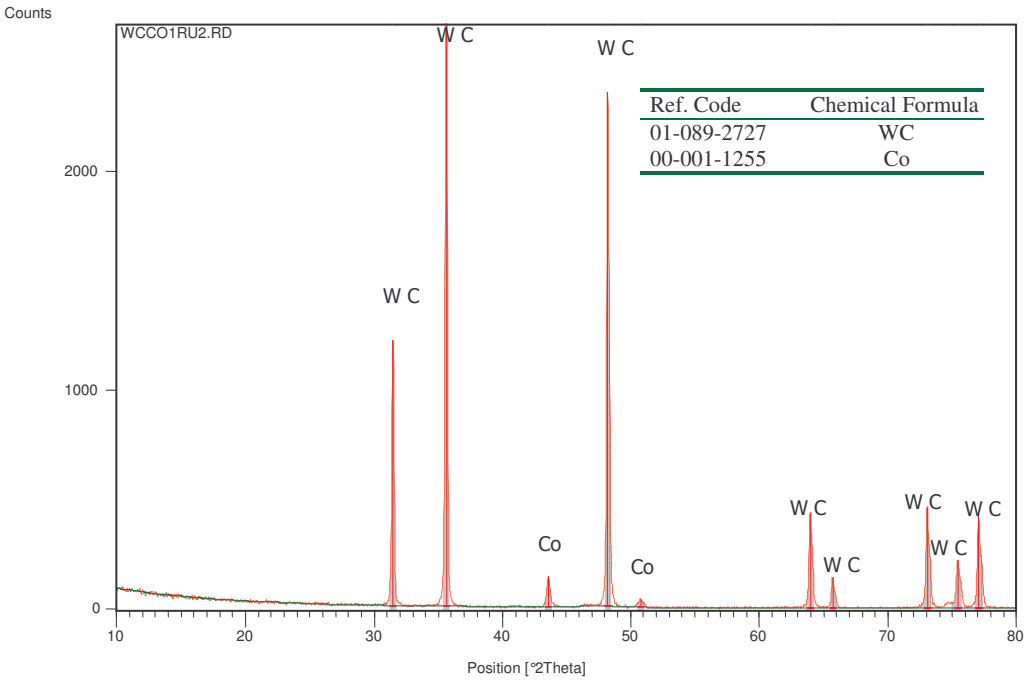



**Figure 4.1.9: XRD patterns for WC-10%Co-1.0%Ru alloy**

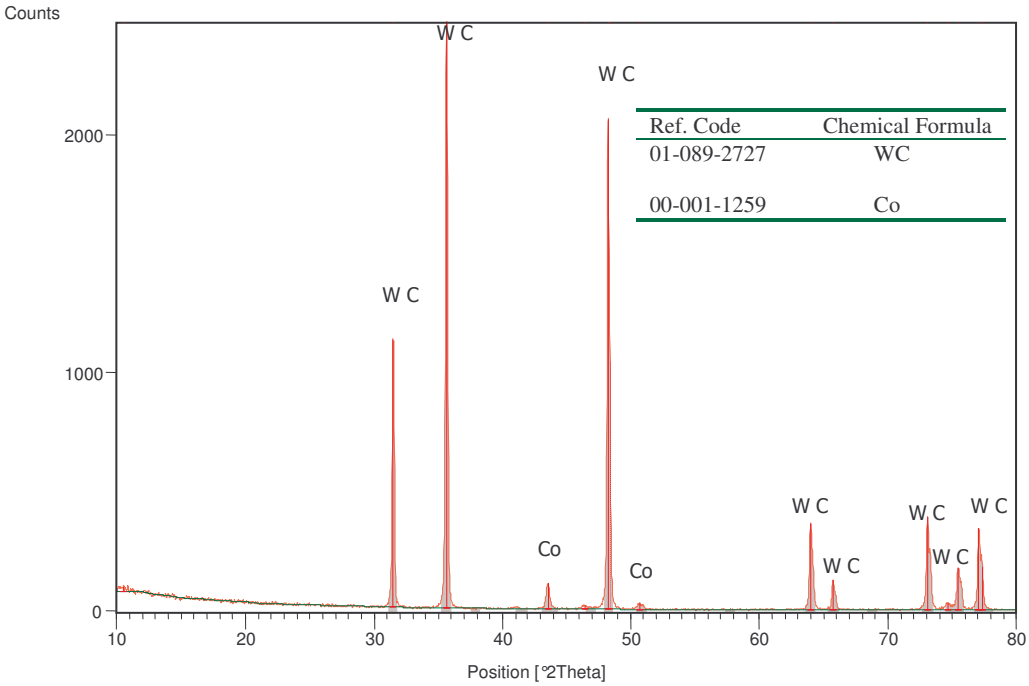



**Figure 4.1.10: XRD patterns for WC-10%Co-1.5%Ru alloy**

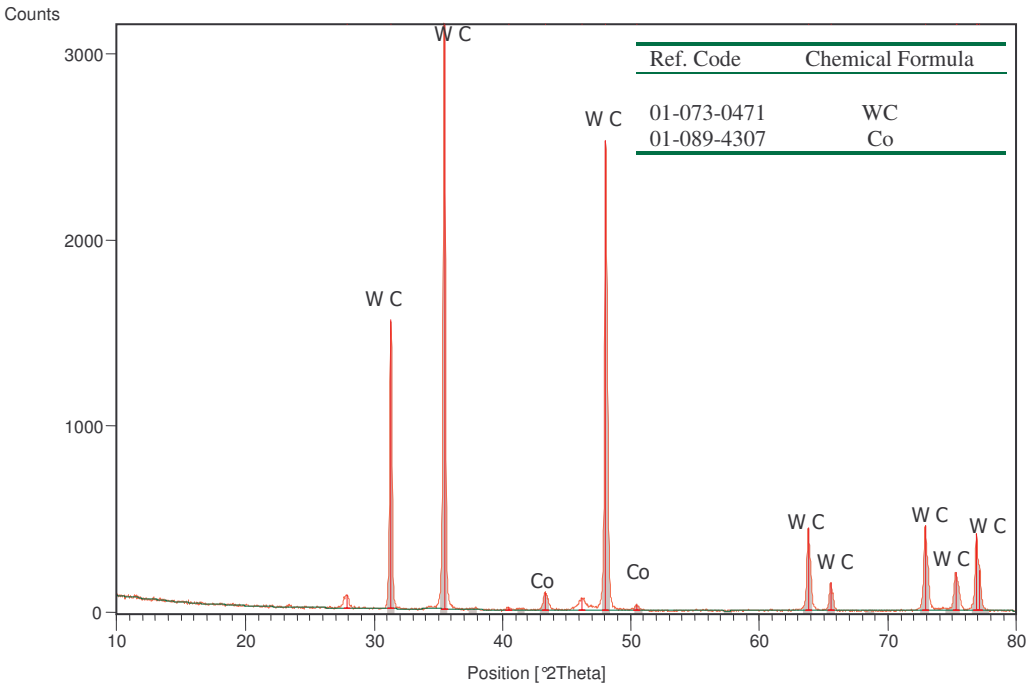



**Figure 4.1.11: XRD patterns for WC-10%Co-2.0%Ru alloy**

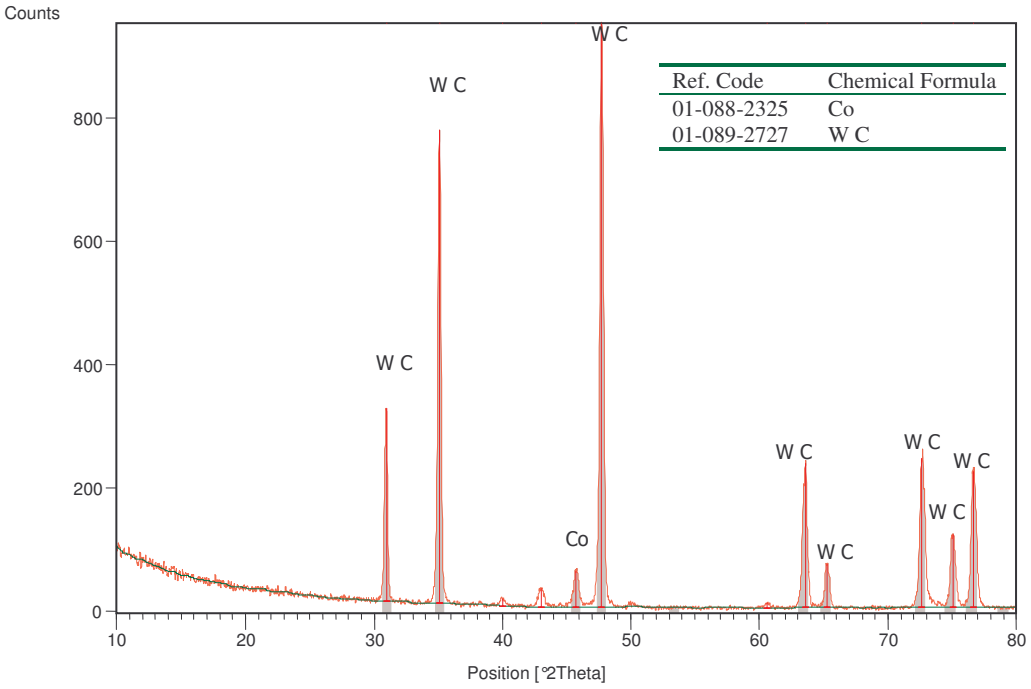



**Figure 4.1.12: XRD patterns for WC-10%Co-3.0%Ru alloy**

### *4.1.4 Raman spectroscopy*

Raman analysis was performed on each sample before corrosion occurred in order to identify the phases on the surface. Raman spectra of WC-Co-Ru were all presented in the same Figure 4.1.15 over a range of 100- 1500 $cm^{-1}$. All the visibly identifiable peaks are summarized in Table 4.1.1. The most prominent peak in all the cases is at 637 $cm^{-1}$ wavenumber. Most of the peaks for all the alloys are within the same range, therefore the average was calculated in order to give the typical range of wavenumbers for the alloys. Since the tungsten carbide was present in the highest concentration, it is assumed that these peaks detected represent tungsten carbide. Yang *et al.* (2008) also reported that the crystalline WC dominates the sample's structure and content of the alloys. These authors (Yang *et al.,* 2008) obtained prominent peaks at 685- 692 $cm^{-1}$, while a small peak was observed at 1550$cm^{-1}$.




**Figure 4.1.13: Raman spectra from the polished alloys**

**Table 4.1.1: Raman peak positions ($cm^{-1}$) of the polished sample WC-10%Co-Ru alloys**

| | | Raman peaks of polished sample | | |
|---|---|---|---|---|
| **Sample** | **Peak 1** | **Peak 2** | **Peak 3** | **Peak 4** |
| 0.0 wt% Ru | 1394 | □ | 637 | 248 |
| 0.4 wt% Ru | □ | □ | 642 | 264 |
| 1.0 wt% Ru | □ | 943 | 620 | 247 |
| 1.5 wt% Ru | 1300 | □ | 636 | □ |
| 2.0 wt% Ru | 1294 | □ | 637 | 245 |
| 3.0 wt% Ru | 1250 | □ | 651 | 254 |
| **Average** | **1310±84** | **943** | **637±14** | **257±7** |

## 4.2 Corrosion tests (Electrochemical tests)

The electrochemical tests results are presented in this section. This section includes the electrochemical behavior of WC-Co-Ru in 1M sulphuric acid, 1M sodium chloride and synthetic mine water solutions.

### 4.2.1 Sulphuric acid (1M $H_2SO_4$) electrolyte

#### *4.2.1.1 Open Circuit Potential (OCP)*

The variations in the open circuit potential ($E_{oc}$) values of the samples measured for two hours are shown in Figure 4.2.1. It was observed that the OCP values of the samples increased with increasing amount of ruthenium. This indicates that ruthenium should have a strong influence on decreasing the dissolution rate of the samples. For the alloys containing 2.0 wt% Ru and 3.0 wt% Ru, the potentials stabilized at the most noble values, i.e. at -0.075 and -0.13 V, respectively. The $E_{oc}$ of alloys containing 1.5 wt % Ru is unstable, as evidenced by the random fluctuations in their curves.

With increasing amount of ruthenium, the open-circuit potentials shifted to more noble

values with time. This positive shift of potentials could be due to the spontaneous formation of a passive film that might decrease the dissolution of the samples as the ruthenium content was increased.

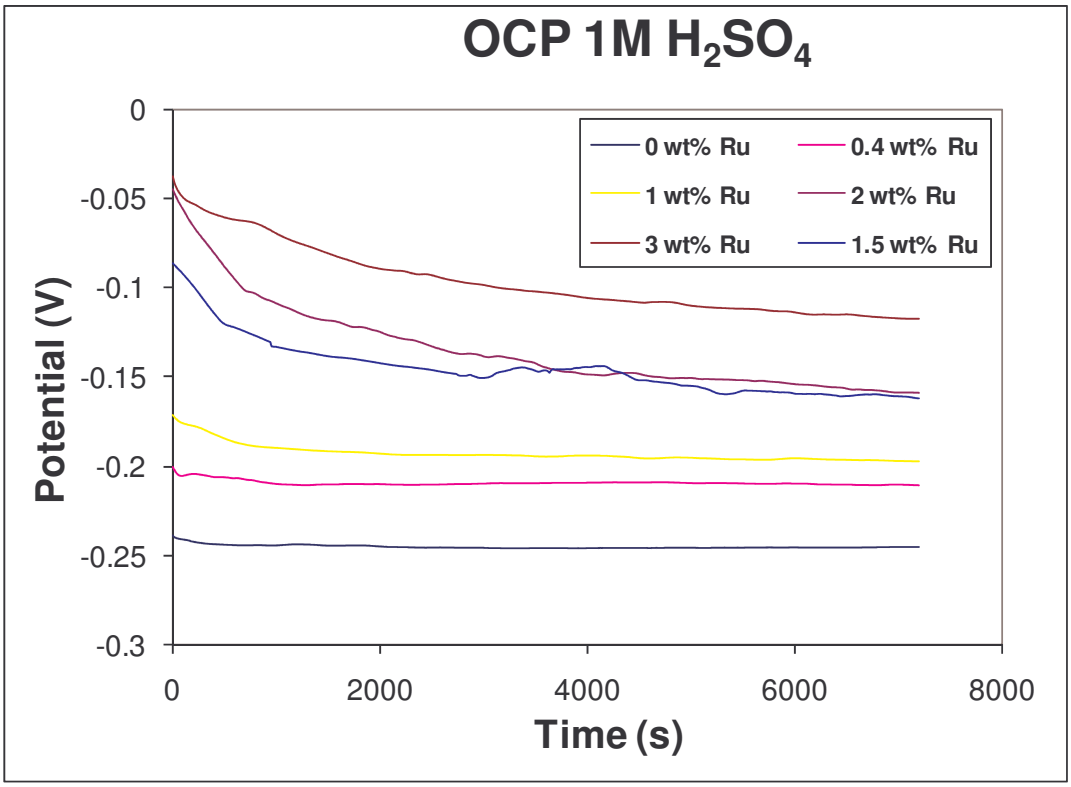



**Figure 4.2.1: Open Circuit Potential results of the samples exposure to 1M $H_2SO_4$**

### *4.2.1.2 Potentiodynamic responses*

All of the polarization curves in 1M sulphuric acid showed a typical profile representing active-passive transition behaviour to a passive state. As the ruthenium content increased, the corrosion resistance of the WC-Co alloys is increased proportionally, due to that Ru is part of the binder phase and the therefore directly influences the corrosion.

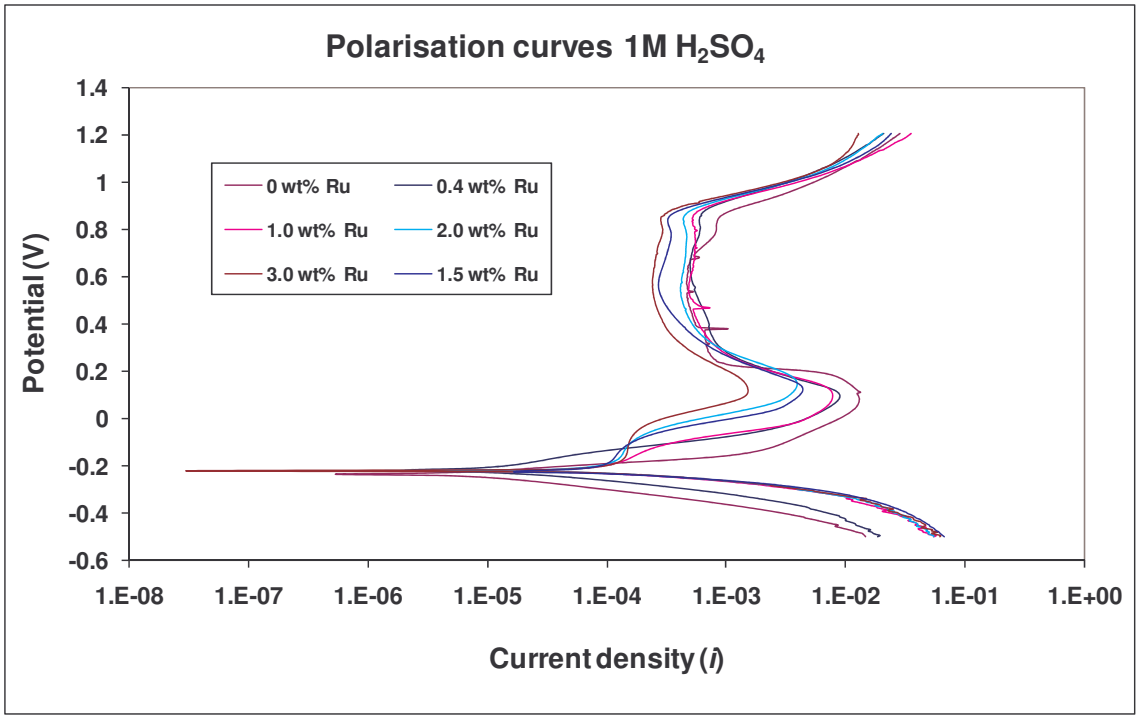



**Figure 4.2.2: Comparative behaviour of WC-Co in 1 M $H_2SO_4$ with increasing additions of Ru.**

Table 4.2.1 illustrates that the values of the corrosion potential ($E_{corr}$) had a very slight shift to more noble values, where the $E_{corr}$ value shifted to a more negative value. The critical current density ($i_{crit}$) decreases by an order of magnitude from 12.90 A/m$^2$ to 1.42 A/m$^2$ as the concentration of ruthenium is increased. This decrease in $i_{crit}$ with an increasing ruthenium content was also observed by Potgieter (1993) in work on duplex stainless steel containing increasing amount of ruthenium that were exposed to sulphuric acid solution.

**Table 4.2.1: Electrochemical parameters for the samples in 1M sulphuric acid**

| Sample | Ecorr (V) | Icorr (A) $\times 10^{-6}$ | $i_{crit}$ (A/m$^2$) $\times 10^{-3}$ | $i_{pass}$(A/m$^2$) $\times 10^{-4}$ | $b_a$ (V/Dec) | $b_c$ (V/Dec) | Corrosion rate (mm/yr) $\times 10^{-2}$ |
|---|---|---|---|---|---|---|---|
| **0.0 wt %Ru** | -0.235 | 7.09 | 12.90 | 14.30 | 0.042 | 0.055 | 14.60 |
| **0.4 wt %Ru** | -0.220 | 4.99 | 9.20 | 19.30 | 0.015 | 0.057 | 10.24 |
| **1.0 wt %Ru** | -0.230 | 5.38 | 7.45 | 19.40 | 0.018 | 0.058 | 7.35 |
| **1.5 wt %Ru** | -0.226 | 10.78 | 3.99 | 9.04 | 0.014 | 0.022 | 7.54 |
| **2.0 wt %Ru** | -0.223 | 1.19 | 3.77 | 8.66 | 0.017 | 0.010 | 2.40 |
| **3.0 wt %Ru** | -0.222 | 1.09 | 1.42 | 4.34 | 0.040 | 0.010 | 2.24 |

Similarly, the passive current density decreases by an order of magnitude for alloys containing ruthenium contents of 1.5 to 3.0 weight %. The corrosion rate of the alloys in sulphuric acid slightly decreased as the ruthenium content increased as shown in figure 4.2.3. Alloys containing 1.0 wt% and 1.5 wt% Ru showed almost similar corrosion rate. The values of $E_{corr,}$ $i_{crit}$ and corrosion rate indicate that the WC-10%Co alloy had the lowest corrosion resistance of all the materials exposed to sulphuric acid.

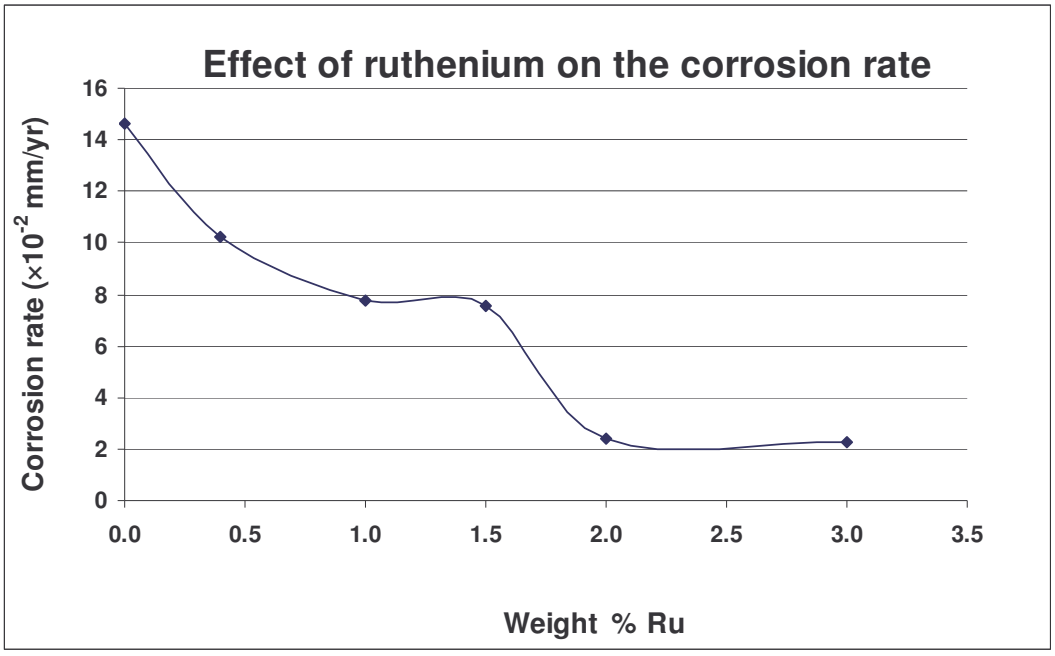



**Figure 4.2.3: The effect of ruthenium additions on corrosion rate of the alloys in 1M $H_2SO_4$**

Moreover, the data of Table 4.2.1 show that the addition of ruthenium changes both anodic and cathodic Tafel constants. The values of $ß_c$ generally decreased upon the addition of ruthenium whereas the $ß_a$ values showed no general trend. Wolff *et al.* (1998) reported that the lowering of the cathodic Tafel slopes by ruthenium is due to improved hydrogen-evolution efficiency, resulting in a decrease of the hydrogen overpotential. Therefore, these variations in anodic and cathodic Tafel constants observed illustrate that the additions of ruthenium in sulphuric acid solution influence both anodic and cathodic sites at the surface of the WC-Co-Ru, and more specifically the cathodic sites.

### *4.2.1.3 Chronoamperometry measurements*

Chronoamperometric behaviour of the samples is shown in Figure 4.2.4. In all samples, the polarization currents decreased with the increasing exposure time and increasing ruthenium content. This implies that dissolution of the samples decreases with time and this is probably due to spontaneous passivation. It was also observed that polarization currents were noticeably higher as the content of ruthenium was increased at the same applied potential of 0.6V.

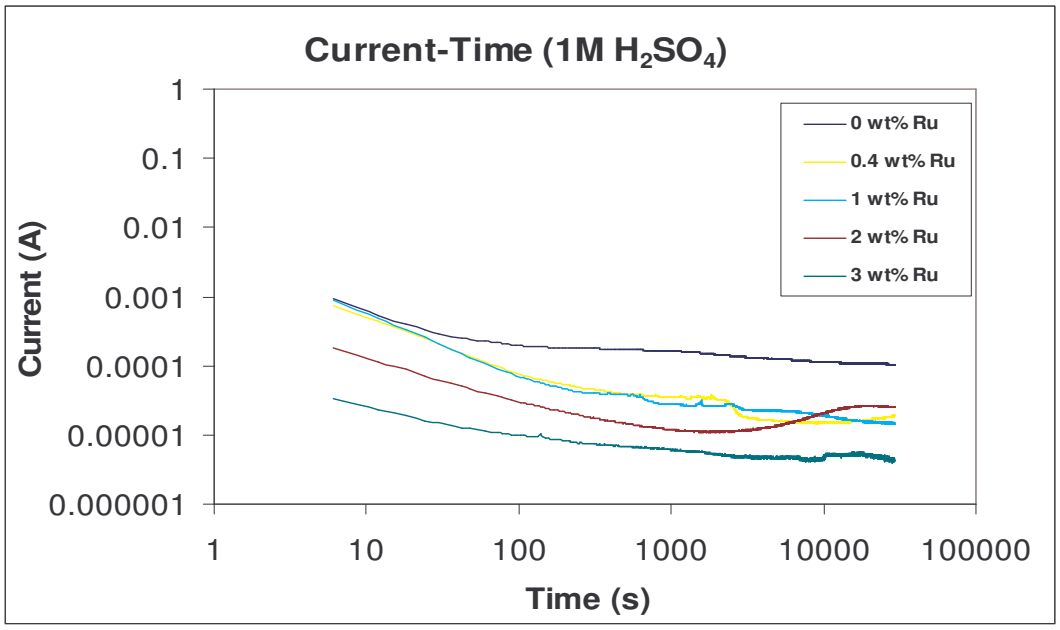



**Figure 4.2.4: Current-Time results of the samples exposure to 1M $H_2SO_4$ at 0.6V**

The passivity range observed for each alloy changed with different amounts of ruthenium content, as shown in Figure 4.2.5. The passivity range increases as the ruthenium content is increased. The oxide films formed on the surface are stable up to 5000s after which there seem to be a breakdown of the film, with increased dissolution of the metal oxide on the surface.

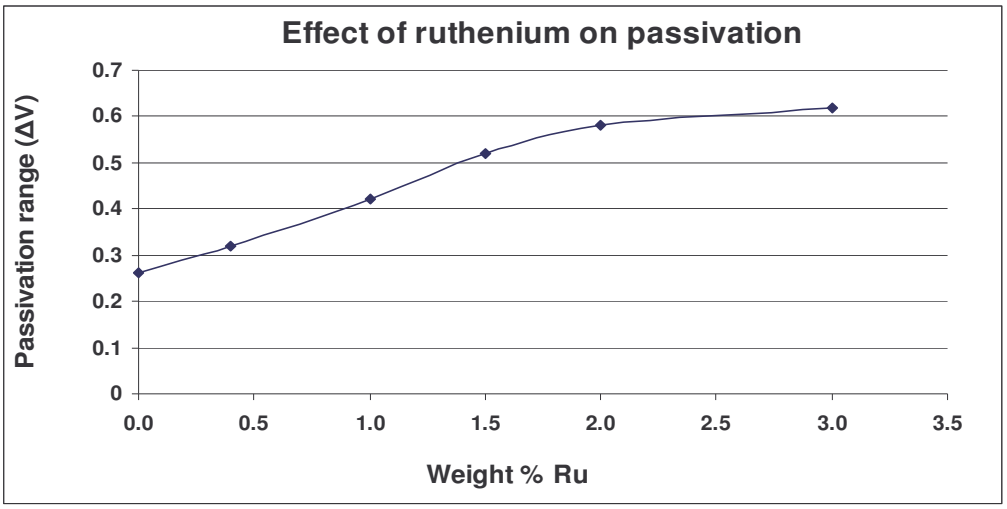



**Figure 4.2.5: The effect of ruthenium addition on passivation range of the alloys 1M $H_2SO_4$**

A general observation on the addition of the ruthenium revealed that increasing the amount of ruthenium increased the corrosion resistance of the WC-Co alloys in 1M sulphuric acid. Figure 4.2.2 and table 4.2.1 both illustrated that the highest content of ruthenium (3 wt %) gives the best optimization in resisting corrosion in WC-Co when the various materials are exposed in 1M $H_2SO_4$ acid solutions. In addition, the time for the open-circuit corrosion potential to stabilize is increased as ruthenium content of the alloys increases. The polarization curves in 1M sulphuric acid showed a typical profile representing active-passive behaviour to a passive region. This is in contrast to work reported by others. Human and Exner (1996), Human and Exner (1997) and Human *et al.,* (1998) observed that in, the polarization curves of WC-Co alloys did not undergo any active–passive transition but exhibited direct pseudo-passivation 1N sulphuric acid. Similarly, for in stainless steels containing ruthenium, Olubambi *et al.* (2008) reported that alloy containing 0.2% ruthenium did not display active–passive transition in 1M sulphuric acid, but passivated spontaneously.

### 4.2.2 Sodium chloride (1M NaCl) electrolyte

#### *4.2.2.1 Open Circuit Potential (OCP)*

The variations in the open circuit potentials ($E_{oc}$) values of the samples (measured for two hours) in 1M sodium chloride are shown in Figure 4.2.6. It was observed that the OCP values of the samples were unstable particularly alloy containing 0 wt% and 2.0 wt% Ru and showed random fluctuations in their curves. The alloy containing 3.0 wt% Ru content had the highest (more noble) starting potential compared to the other alloys containing lower ruthenium contents. However, as the time progressed, the potential dropped and this alloy stabilized at a lower potential compared to alloys containing 1.5 wt% Ru and 2.0 wt% Ru. The alloy containing 1.5 wt% Ru started at a potential of -0.14V and after 1370s it stabilized at a potential of -0.15V. As for the alloy containing 2.0 wt% Ru, it started at a lower potential of -0.21V and exhibited lot of instability (fluctuations), before it stabilized at a slightly more noble potential value of -0.15V after 6000s.

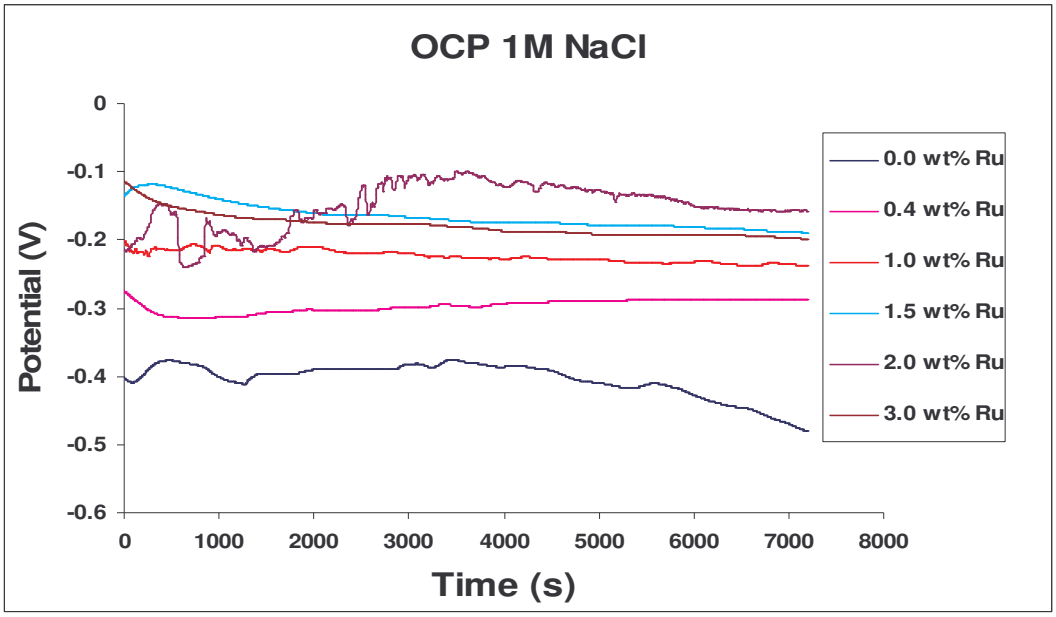



**Figure 4.2.6: Open Circuit Potential versus time for the samples exposed to 1M NaCl**

### *4.2.2.2 Potentiodynamic polarization measurements*

Figure 4.2.7 represents the electrochemical curves for the WC-Co-Ru alloys in a neutral environment of 1M sodium chloride, while Table 4.2.2 gives a summary of the electrochemical parameters of the WC-Co-Ru alloys exposed in this medium. Using WC-10%Co as the reference alloy; one notices that the corrosion potential shifted slightly towards more noble values upon the additions of ruthenium. It was observed that the corrosion potential ($E_{corr}$) of the 2.0 wt% Ru alloy reached in the most noble value when compared to the other alloys. Generally the corrosion current density decreased as the ruthenium content of the various alloys increased. The alloy with 2.0 wt% Ru showed the lowest critical and passive current density ($i_{crit}$ and $i_{pass}$) of $0.31\times10^{-3}$ A/cm$^2$ and $1.43\times10^{-4}$ A/cm$^2$ , respectively, when compared with the reference alloy.

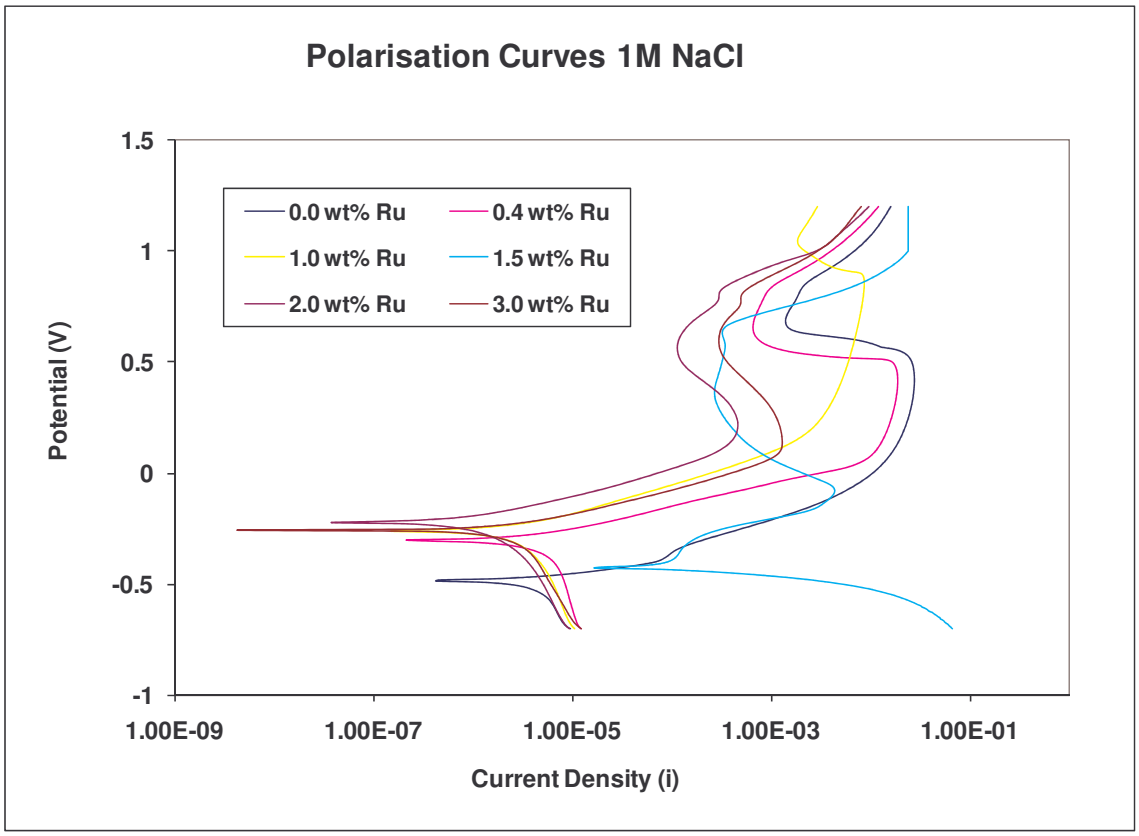



**Figure 4.2.7: Comparative behaviour of WC-Co with increasing additions of Ru in 1M NaCl**

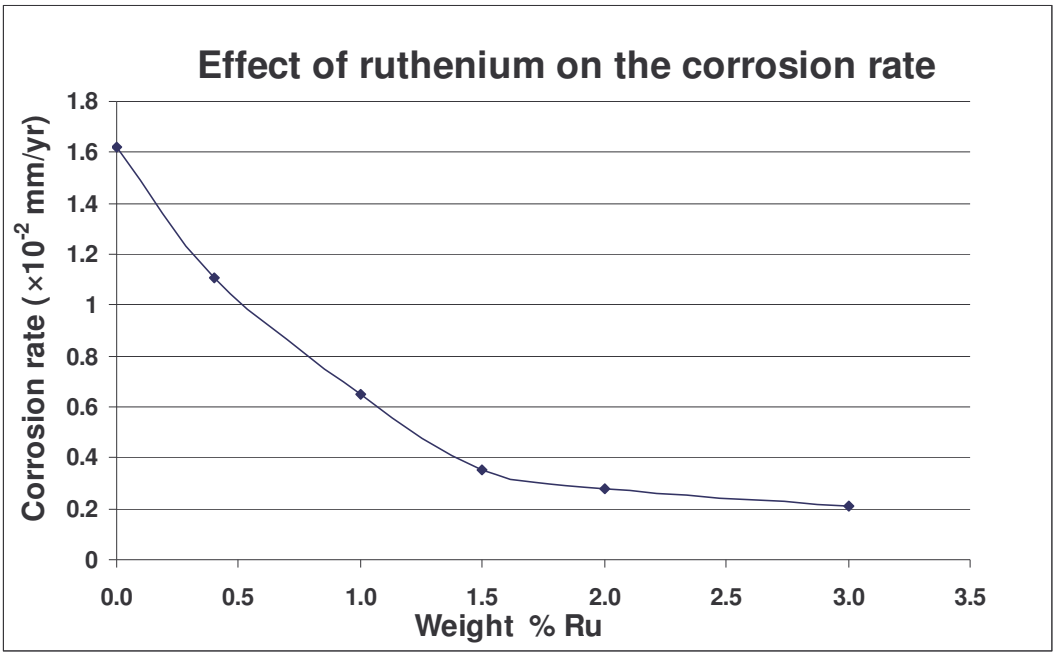



**Figure 4.2.8: The effect of ruthenium additions on corrosion rate of the various WC-Co alloys in 1M NaCl**

The anodic Tafel constant (ßa) values showed no general trend, while the cathodic Tafel constant (ßc) values decreased slightly with an increasing concentration of ruthenium. Lastly it can be observed that there is a noticeable change in corrosion rates with the addition of ruthenium. As the ruthenium content increases, the corrosion rate decreased, as is graphically illustrated in figure 4.2.8. This means that ruthenium with the highest content (3.0 wt %) has a lowest corrosion rate compared to the other alloys. One again observes a rather small difference from 2.0% Ru to 3.0% Ru, suggesting that 2.0% Ru is the optimum addition (cost wise) for improved corrosion resistance.

**Table 4.2.2: Electrochemical parameters for the samples in 1M sulphuric acid**

| Sample wt % Ru | Ecorr (V) | Icorr (A) $\times 10^{-6}$ | $i_{crit}$ ($A/m^2$) $\times 10^{-3}$ | $i_{pass}$($A/m^2$) $\times 10^{-4}$ | $b_a$ (V/Dec) | $b_c$ (V/Dec) | Corrosion rate (mm/yr) $\times 10^{-2}$ |
|---|---|---|---|---|---|---|---|
| **0.0** | -0.483 | 0.90 | 7.89 | 513 | 0.016 | 0.039 | 1.62 |
| **0.4** | -0.301 | 0.62 | 3.56 | 76.3 | 0.038 | 0.028 | 1.11 |
| **1.0** | -0.258 | 0.36 | 1.43 | 35.1 | 0.039 | 0.029 | 0.65 |
| **1.5** | -0.400 | 19.00 | 3.41 | 3.79 | 0.078 | 0.029 | 0.35 |
| **2.0** | -0.220 | 0.16 | 0.31 | 1.43 | 0.051 | 0.021 | 0.28 |
| **3.0** | -0.275 | 0.11 | 0.999 | 3.36 | 0.027 | 0.022 | 0.21 |

### *4.2.2.1 Chronoamperometry measurements*

The chronoamperometric behaviour of the samples in 1M NaCl is displayed by the curves in Figure 4.2.9. All the alloys had almost the same polarization current except for the reference alloy which showed a higher polarization current when compared to the ruthenium containing alloys. It was also observed that the alloy containing 1.5 wt% Ru has lowest polarization current at the applied potential of 0.6V.

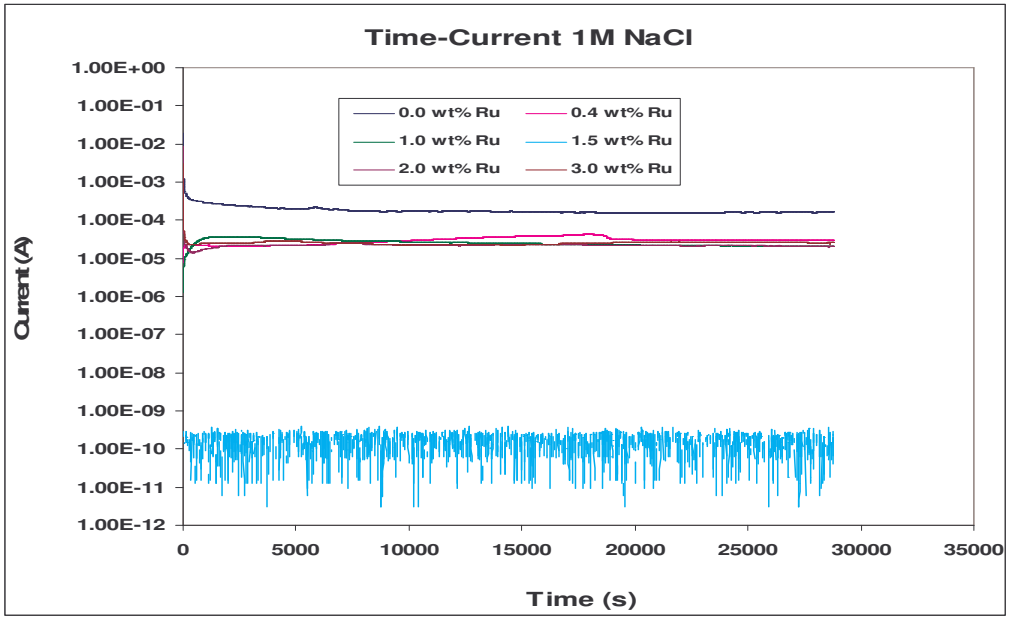



**Figure 4.2.9: Current- Time response of the samples exposure to 1M NaCl at 0.6V**

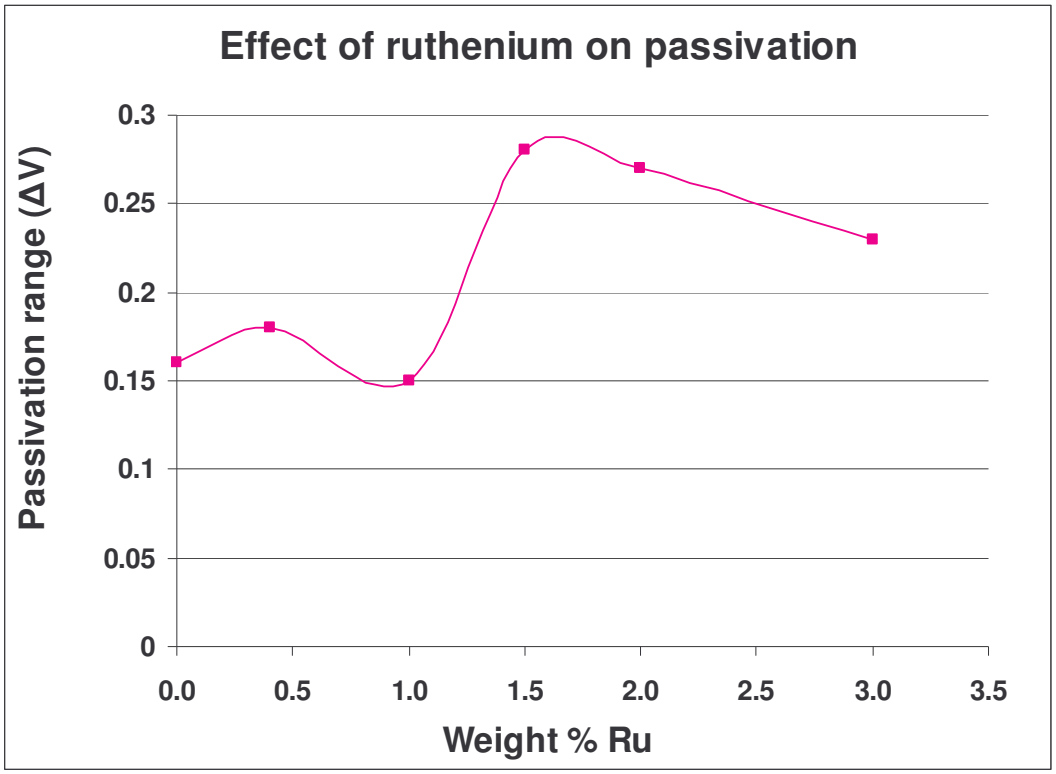



**Figure 4.2.10: The effect of ruthenium on passivation on the WC-Co in 1M NaCl**

Measurements done on the alloys in 1M sodium chloride revealed that the increasing amount of ruthenium increased the corrosion resistance of the WC-Co alloys. It was observed that alloy containing 2.0 wt% Ru showed the best corrosion resistance. This is illustrated by the highest reduction of the values of the critical current density $i_{corr}$ and the passive current density $i_{pass}$ as compared to the other alloys with ruthenium additions. Nevertheless, the alloy with the highest content of ruthenium (3.0 wt% Ru) had the lowest corrosion rate. The product film formed on the surface is stable with no indication of breakdown of the film for the investigated period of 8 hours.

The passivity range that was observed for each of the alloys changed with different amounts of ruthenium contents is shown in figure 4.2.10. It was observed that the alloys containing 1.5 wt% Ru, 2.0 wt% Ru and 3.0 wt% Ru have the largest passivation range, but that it became smaller for smaller additions than 1.5 wt% Ru. On the other hand, the reference alloy (0 wt% Ru), 0.4 wt% Ru and 1.0 wt% Ru alloy have shown a wide active–passive transition range. The passive film formed showed some stability as indicated in figure 4.2.9.

### 4.3.2 Synthetic mine water electrolyte

The variation of the OCPs of the WC-Co-Ru alloys for a periods of two hours after exposure to synthetic mine water, is shown in figure 4.2.11. The reference alloy containing 0 wt% Ru revealed the lowest OCP values when compared to the other alloys. It was observed that as the amount of ruthenium increased, the potential values slightly increased. However, there was a drastic increase in potential values of the alloy containing 3 wt% Ru, and it stabilized at a positive potential of 0.03V. The potential values at 7200s illustrate that the alloys with increasing amounts of the ruthenium are more noble than the one without ruthenium. This should therefore mean that the passive film was more stable for the alloy containing 3 wt% Ru.

***Open Circuit Potential (OCP)***

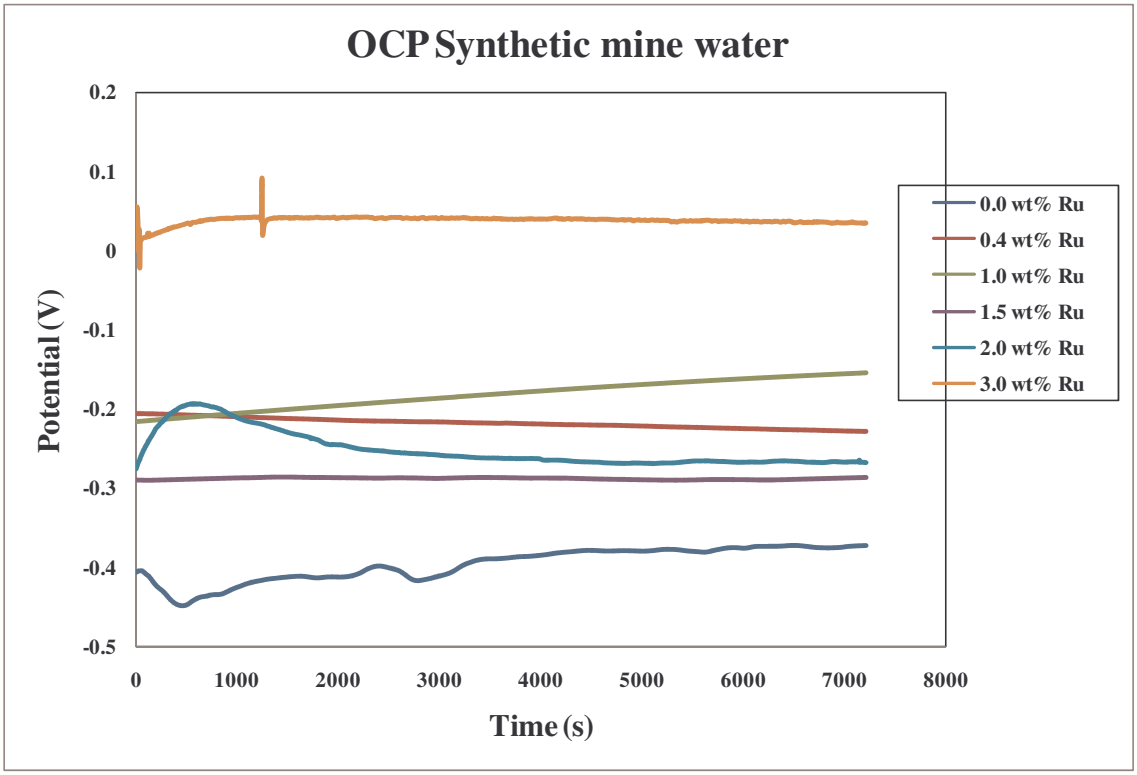



**Figure 4.2.11: Open Circuit Potential results of the WC-Co-Ru samples exposed to synthetic mine water**

#### *4.3.2.2 Potentiodynamic polarization measurements*

Figure 4.2.12 shows the polarization curves obtained in synthetic mine water solution. All the alloys containing ruthenium in turn revealed better corrosion resistance. It was also observed that the alloy containing 1.5 wt% Ru showed a lower corrosion resistance compared to alloys containing 0.4 wt% Ru and 1.0 wt% Ru. However, the alloys with 2 wt% and 3 wt% Ru had a better corrosion resistance than all the other alloys.

The results for the corrosion potentials, corrosion current, corrosion current densities, and the corrosion rates that were derived from the electrochemical tests for the samples in the synthetic mine water solution are summarized in Table 4.2.3. It was observed that the corrosion potential generally increased as the amount of ruthenium increased. It was also noted that the corrosion current density and critical current density decreased with increasing ruthenium contents in the synthetic mine water solution. The corrosion rate of the alloys as the function of their Ru content is presented in Figure 4.2.13. The corrosion rate was observed to slightly decrease with increasing ruthenium content. The alloys with 1.5%wt Ru performed out of sequence and contrary to expectations. The reasons for these are not quite clear and will require further investigation. The alloys containing 2 wt% and 3.0 wt% Ru showed a drastic decrease in corrosion current density and corrosion rate. The corrosion rate and the corrosion current density for the alloy containing 2.0 wt% Ru were reduced by three to four orders of magnitude, while for alloy containing 3.0 wt% Ru both the corrosion rate and the corrosion current density were several orders of magnitude lower (six orders of magnitude).

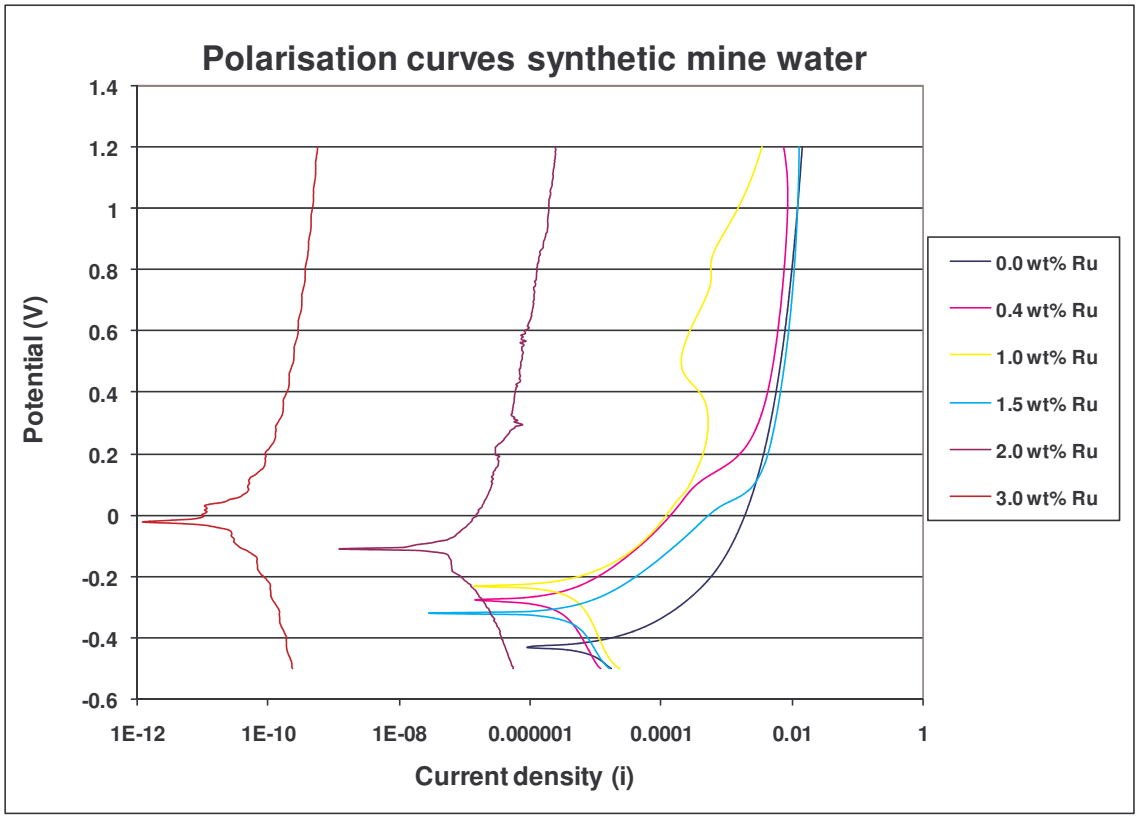



**Figure 4.2.12: Comparative potentiodynamic behaviour of WC-Co in synthetic mine water with increasing additions of Ru**

**Table 4.2.3: Electrochemical parameters for the samples in synthetic mine water**

| Sample (wt %Ru) | Ecorr (V) | Icorr (A) $\times 10^{-6}$ | $b_a$ (V/Dec) | $b_c$ (V/Dec) | Corrosion rate (mm/yr) $\times 10^{-2}$ |
|---|---|---|---|---|---|
| **0.0** | -0.429 | 4.33 | 0.037 | 0.075 | 7.79 |
| **0.4** | -0.277 | 1.04 | 0.116 | 0.058 | 1.97 |
| **1.0** | -0.230 | 0.79 | 0.027 | 0.034 | 1.42 |
| **1.5** | -0.319 | 0.90 | 0.014 | 0.026 | 1.62 |
| **2.0** | -0.135 | $5.58\times10^{-4}$ | 0.080 | 0.020 | $1.00\times10^{-3}$ |
| **3.0** | -0.020 | $2.23\times10^{-6}$ | 0.040 | 0.018 | $4.04\times10^{-6}$ |

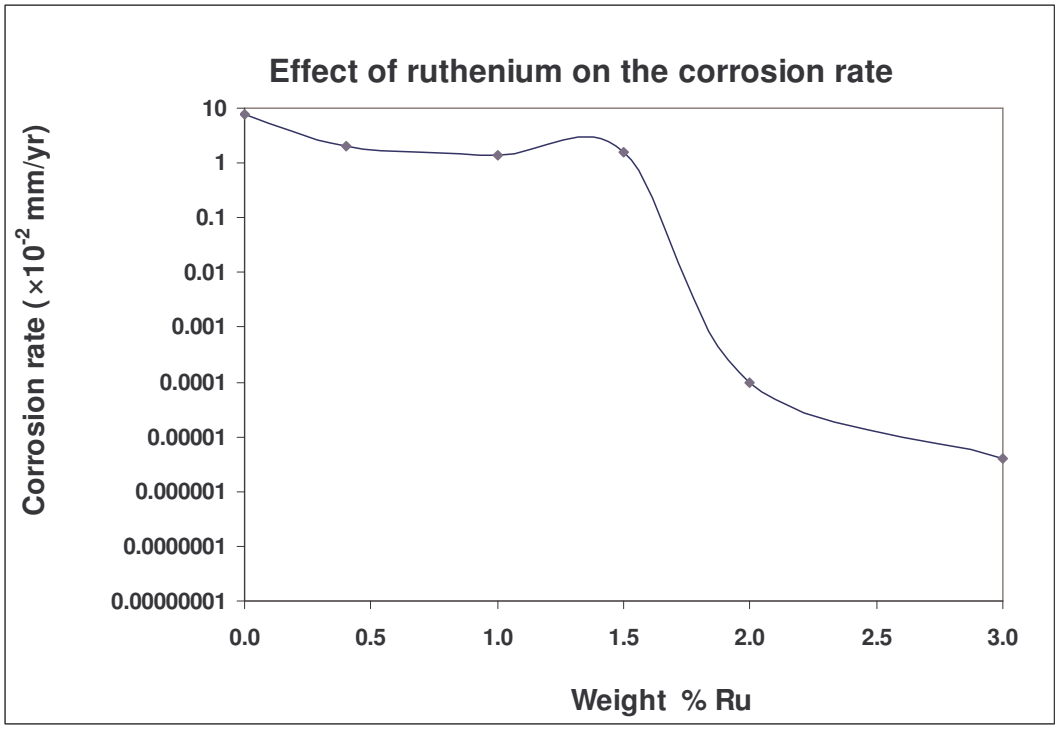



**Figure 4.2.13: The effect of ruthenium additions on corrosion rate of the alloys in synthetic mine water**

*Chronoamperometry measurements*

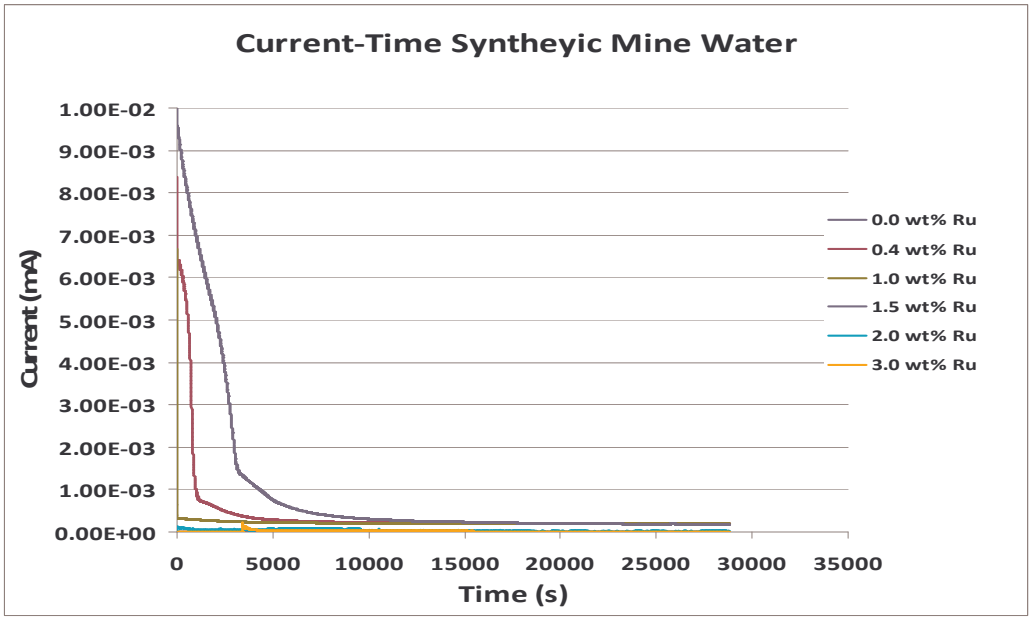



**Figure 4.2.14: Current -Time results of the samples exposure to synthetic mine water at 0.6V**

*4.3.3.3 Chronoamperometric responses*

The chronoamperometric behaviour of the WC-Co-Ru alloys in synthetic mine water solution shown in Figure 4.2.14 revealed that the current decreased as the ruthenium addition increased. The alloys all exhibited similar behaviour, except for alloys containing 0 wt%, 0.4 wt% and 1.0 wt% Ru which showed a steady decrease in current as the time progressed up till the 7000$^{th}$ second, after which it started to stabilize. This confirmed the passivation of the alloys in synthetic mine water solution observed in polarization curves. The passive films formed on the surface seem to be very stable, and there was no indication of the film breakdown occurring.

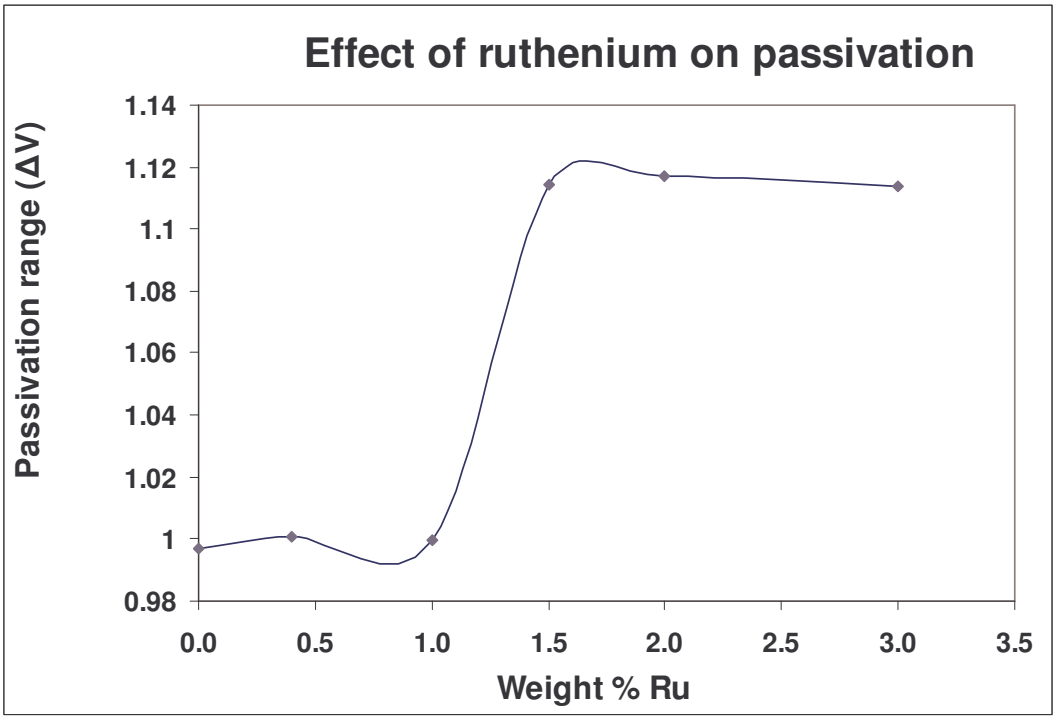



**Figure 4.2.15: The effect of ruthenium on passivation on the WC-Co in synthetic mine water**

The alloy containing 3.0wt% Ru showed better corrosion resistance in synthetic mine water than the rest. It was noted from Figure 4.2.11 that as the amount of ruthenium increased the open circuit potential values ($E_{oc}$) shifted to more noble values. The increase in open circuit potential observed could result from the formation of passive films on the surfaces of the alloys. According to Olubambi *et al.* (2008), the increase in

the potentials could signify a growth of the passivating film on the surfaces of the electrode. The passivity range of the alloys was observed in Figure 4.2.15 to be almost similar (within the same range) for all the alloys, except for the alloy containing 1.0 wt% Ru which showed uncharacteristic behaviour, as was previously alluded to.

The polarization curves in figure 4.2.12 displayed similar trends for all the alloys, without any noticeable active-passive transition. This in agreement with the observations made by Human and Exner (1997) and Machio (2005) previously. Figure 4.2.14 revealed that the film that formed on the surface did not undergo any breakdown after exposure to synthetic mine water for 8 hours. The alloy containing 0 wt% Ru showed the least corrosion resistance while the alloy containing 3.0 wt% Ru displayed the best resistance to corrosion.

## 4.3 Surface analysis after electrochemical tests

The degree of corrosion of a particular phase in the composite was examined in these sections using different techniques.

### 4.3.1 Sulphuric acid environment

#### *4.3.1.1 Scanning electron microscope*

Scanning electron micrographs of the WC-Co-Ru alloys after corrosive attack in sulphuric acid and their corresponding EDX analyses are shown in Figures 4.3.1 to 4.3.6. It is observed that area 1 showed peaks of sulphur and oxygen. These results revealed that the values of sulphur and oxygen range from 2.1% to 11.20 % and 4.76% to 13.82% respectively. This illustrates that area 1 for all the alloys represents the corrosion product formed on the surface. The corrosion product covers the entire surface but after exposure to the corrosive (wet) environment of sulphuric acid it dries up and cracks. In addition it was observed that in area 2 the amounts of oxygen and sulphur decreased dramatically showing values less than 4.00% in both cases and their peaks were no longer prominent. However the tungsten content was observed to be very

high while the cobalt content has decreased to the lowest value of 0.21%. Therefore it can be deduced that for all the alloys area 2 is the surface of the alloys.

As it was noted that the cobalt content was reduced while the tungsten content slightly increased. Srivastava *et al.* (2006) stated that this is a characteristic of selective dissolution of the binder phase. These results showed that the cobalt binder has been corroded away while the tungsten carbide is not corroded. This is in agreement with previously reported studies on the corrosion behaviour of cemented carbides (Human and Exner, 1997; Sutthiruangwong and Mori, 2003; Pugsley and Sockel, 2004; Srivastava *et al.*, 2006). Pugsley and Sockel (2004) that corrosive attack of the materials in the sulphuric acid environment proceeded through selective dissolution of the metallic binder phase leaving the hard phase skeleton of WC. SEM micrographs lead to the conclusion that the Co binder phase selectively dissolves leaving behind the WC grains. Binder dissolution may thus be represented by equation:

$$Co \rightarrow Co^{2+} + 2e^{-}$$

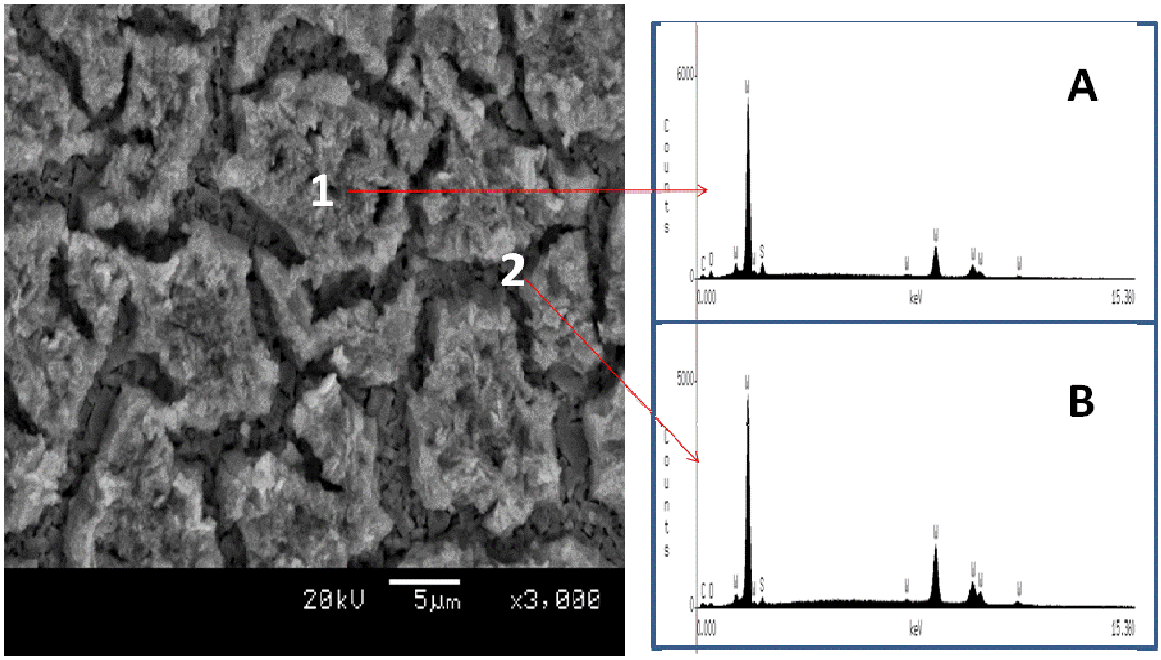



**Figure 4.3.14: SEM micrograph of the WC-10%Co alloy after exposure to 1M $H_2SO_4$ solution with corresponding EDX spectra analyses of (A) area 1 and (B) area 2.**

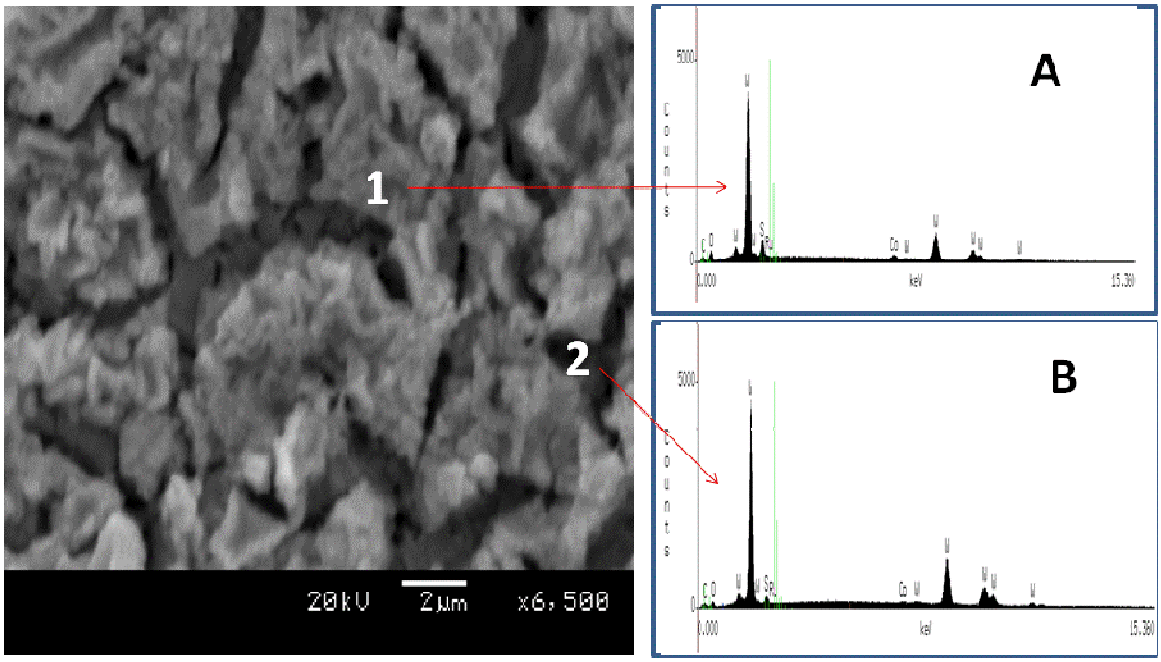



**Figure 4.3.2: SEM micrograph of the 0.4 wt% Ru containing alloy after exposure to 1M $H_2SO_4$ solution with corresponding EDX spectra analyses of (A) area 1 and (B) area 2.**

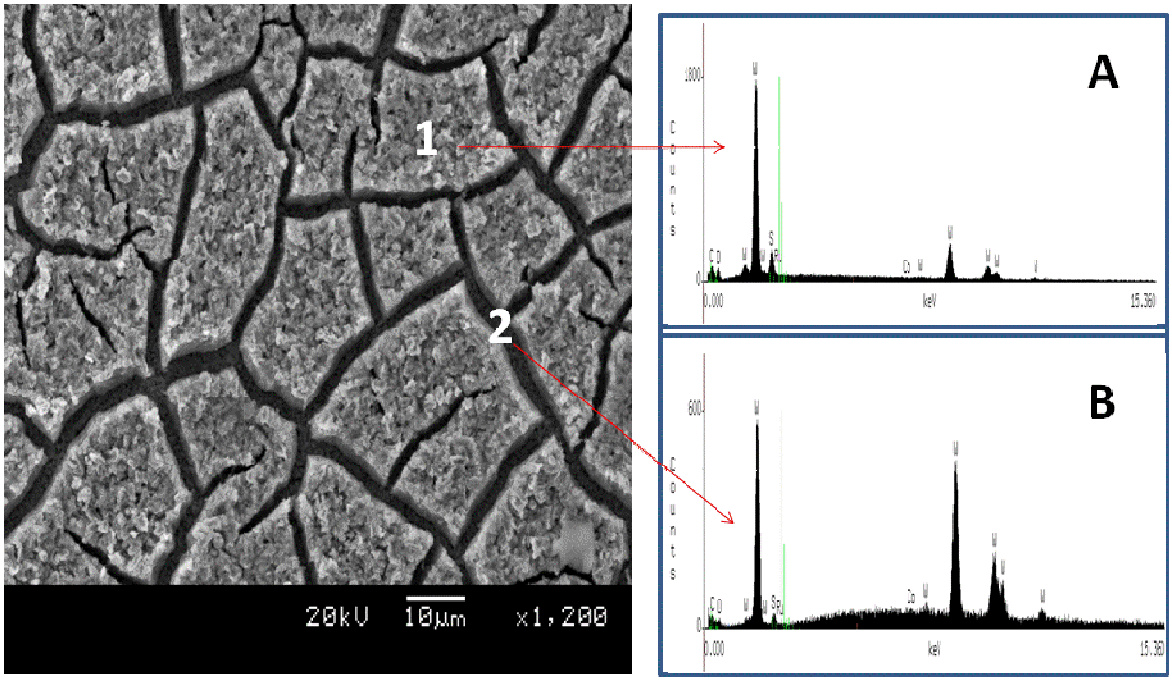



**Figure 4.3.3: SEM micrograph of the 1.0 wt% Ru containing alloy after exposure to 1M $H_2SO_4$ solution with corresponding EDX spectra analyses of (A) area 1 and (B) area 2.**

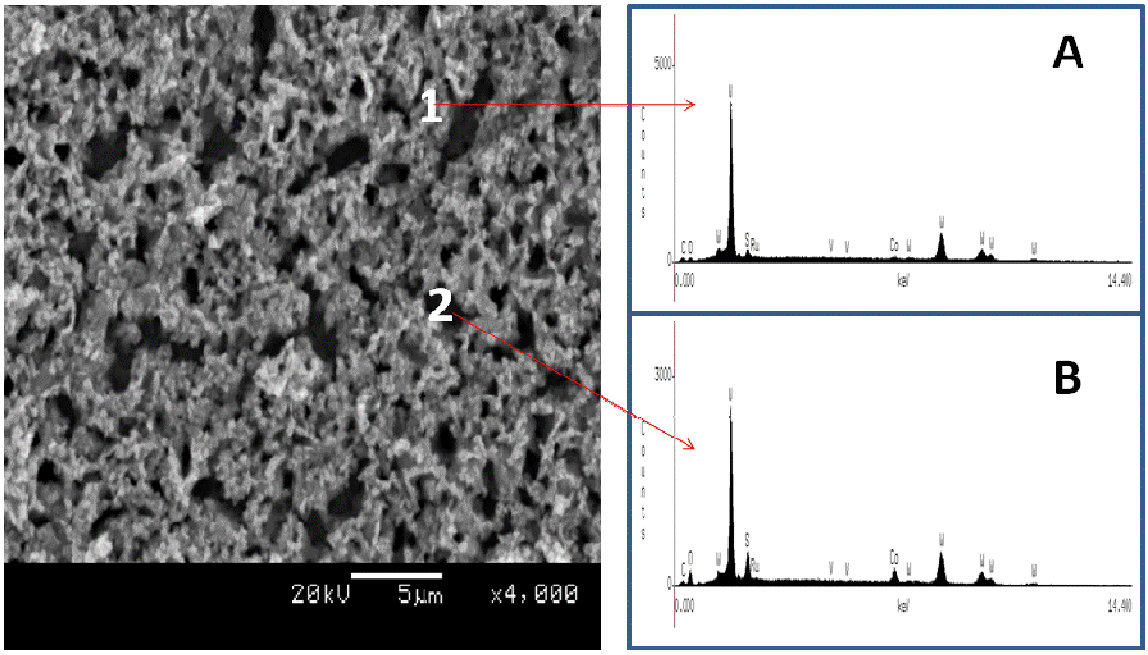



**Figure 4.3.4: SEM micrograph of the 1.5 wt% Ru containing alloy after exposure to 1M $H_2SO_4$ solution with corresponding EDX spectra analyses of (A) area 1 and (B) area 2.**

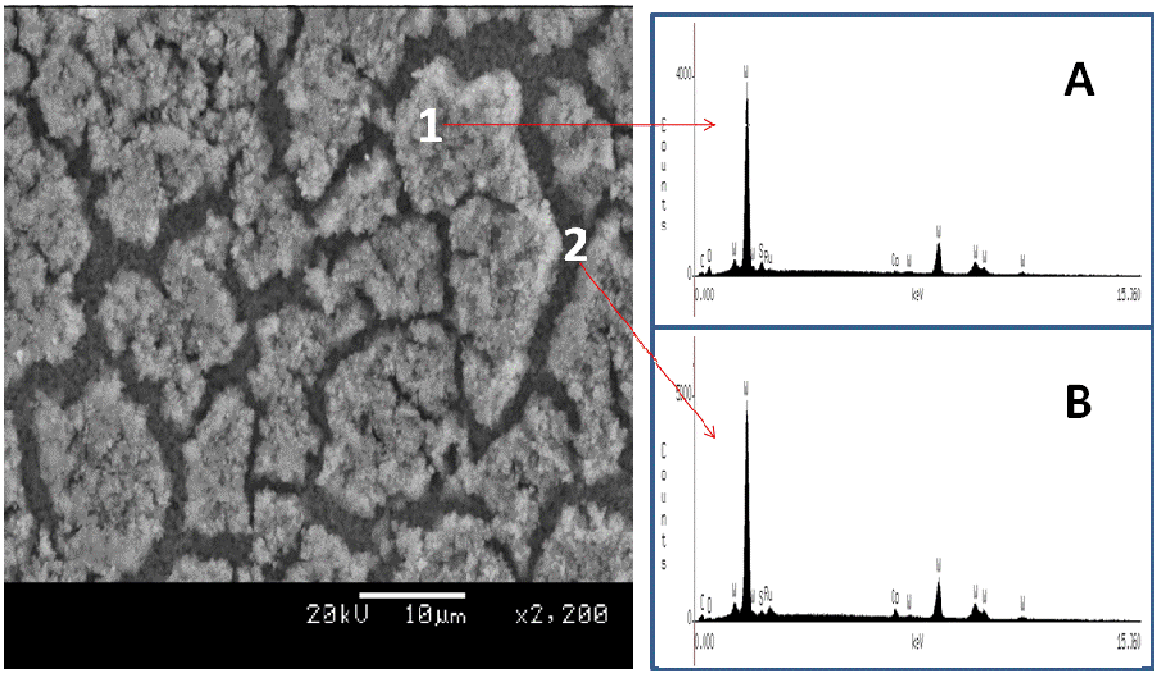



**Figure 4.3.5: SEM micrograph of the 2.0 wt% Ru containing alloy after exposure to 1M $H_2SO_4$ solution with corresponding EDX spectra analyses of (A) area 1 and (B) area 2.**

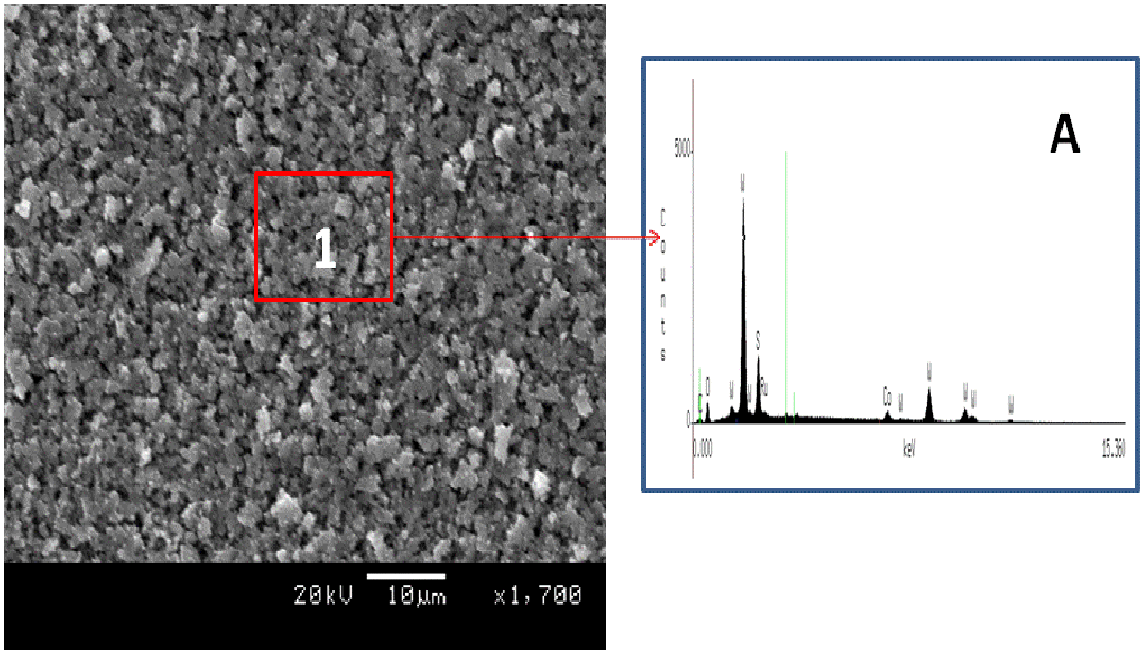



**Figure 4.3.6: SEM micrograph of the 3.0 wt% Ru containing alloy after exposure to 1M $H_2SO_4$ solution with corresponding EDX spectra analyses of (A) area 1.**

### *4.3.1.2 X-Ray diffractometry (XRD)*

XRD analyses of the samples after exposure to the 1M $H_2SO_4$ corrosive environment are presented in Figures 4.3.7 to 4.3.12. These figures are used for comparison with the diffraction spectra from the same samples before corrosion. Figures 4.3.7, 4.3.8, 4.3.9, 4.3.10, 4.3.11 and 4.3.12 showed that tungsten oxide has formed on the surface. All the above mentioned figures, except Figure 4.3.11, indicated a $WO_3$ peak around 25º. In Figures 4.3.9 and 4.3.11, it was observed that the $WO_3$ peak has shifted to 44 º and 48º respectively.

Figures 4.3.7, 4.3.8 and 4.3.11, indicate that cobalt sulphate ($CoSO_4$) has formed. This cobalt sulphate was observed to have a peak at about 16º, but in Figure 4.3.11 the cobalt sulphate peak shifted to 25º. The alloy containing 3.0 wt% Ru also formed cobalt oxide on the surface during corrosion process, and it was observed to have weak diffraction peak at around 43º. No detectable cobalt sulphate or oxide was found on alloys containing 1.0 wt% Ru and 1.5 wt% Ru. The ruthenium and vanadium carbide could not

be detected due to the detection limit of the equipment being about 5 wt %. The cobalt oxide and sulphates detected by the XRD spectra correlates well with the sulphur and oxygen species detected by EDX on the sample surfaces examined with the SEM.

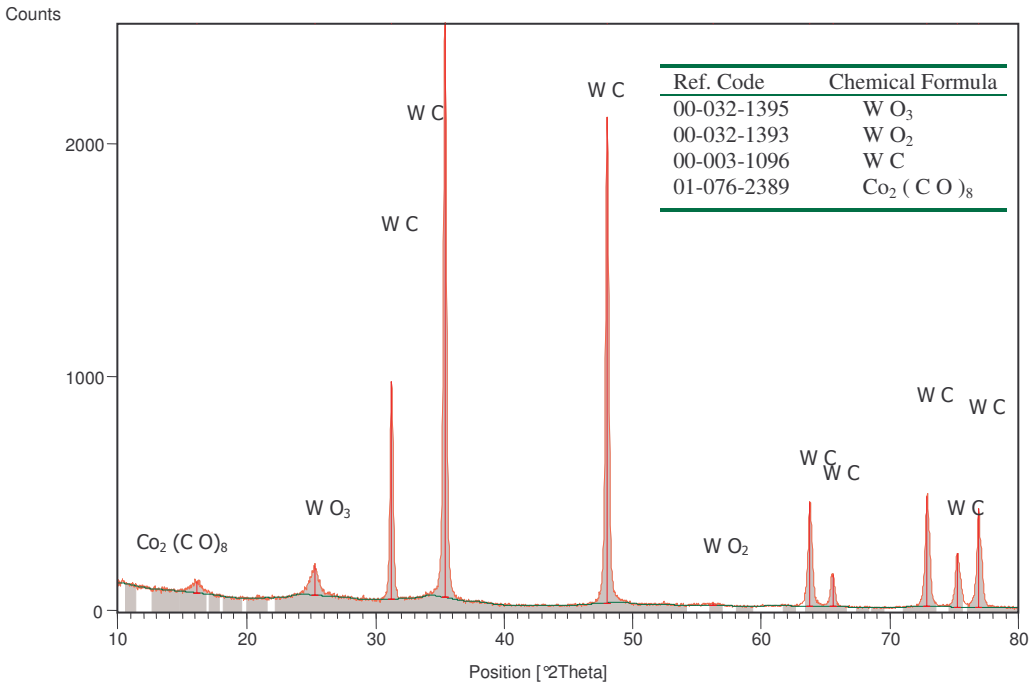



**Figure 4.3.7: XRD patterns for alloy containing 0 wt% Ru after exposure to 1M $H_2SO_4$**

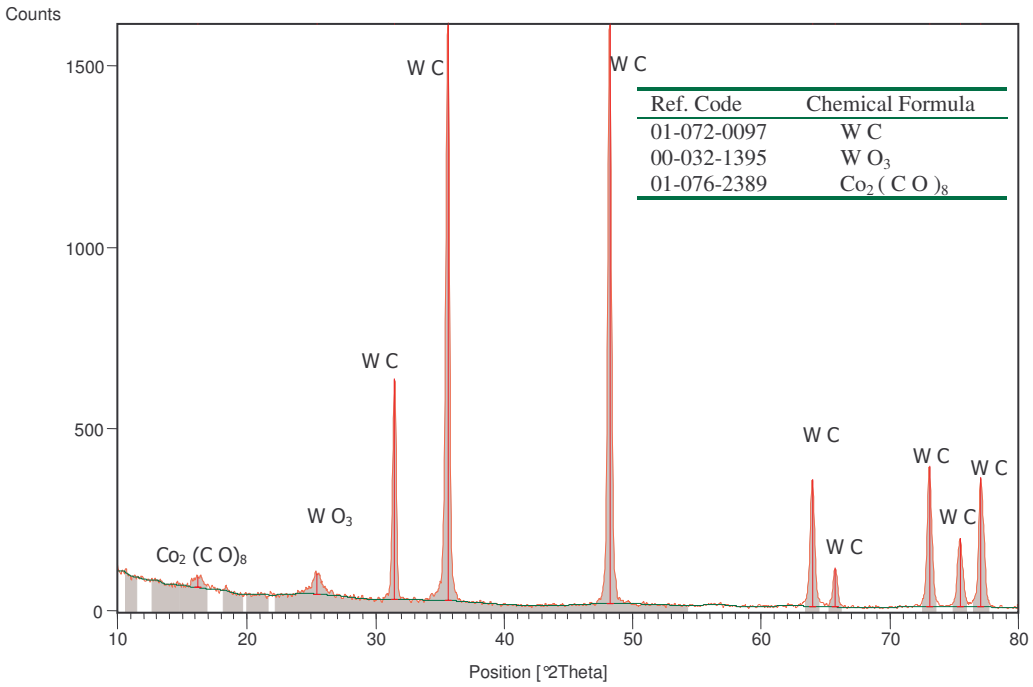



**Figure 4.3.8: XRD patterns for alloy containing 0.4 wt% Ru after exposure to 1M $H_2SO_4$**

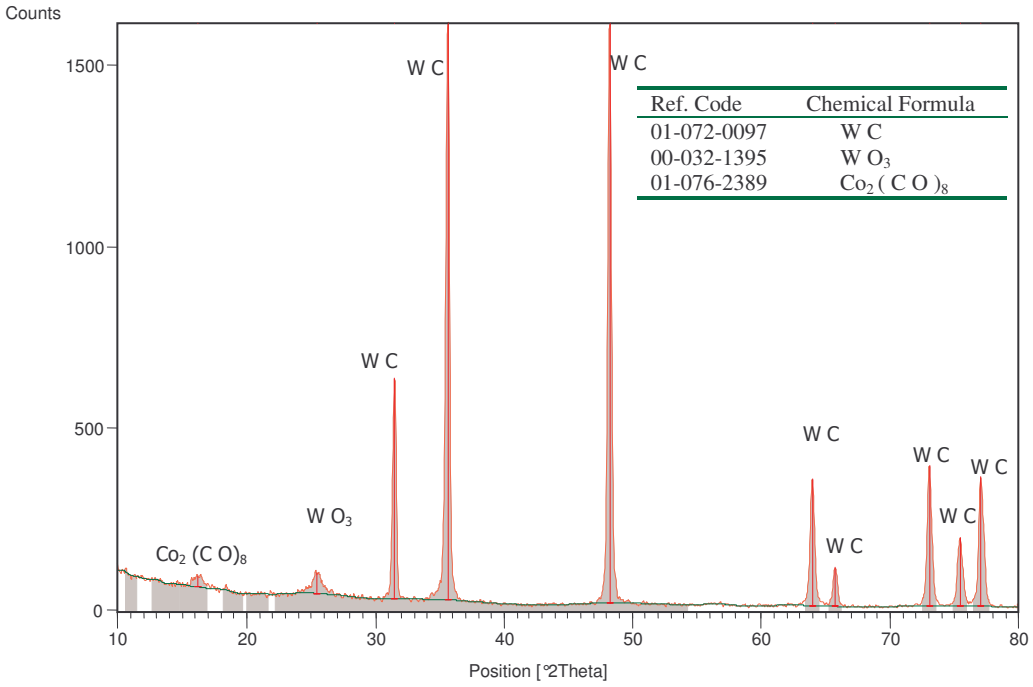



**Figure 4.3.9: XRD patterns for alloy containing 1.0 wt% Ru after exposure to 1M $H_2SO_4$**

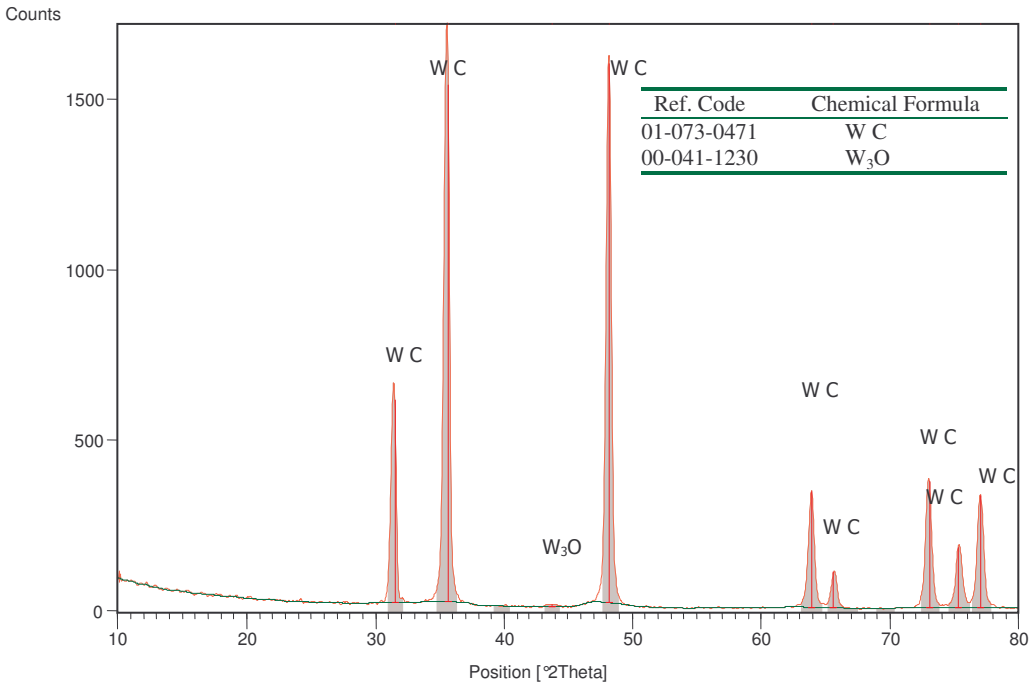



**Figure 4.3.10: XRD patterns for alloy containing 1.5 wt% Ru after exposure to 1M $H_2SO_4$**

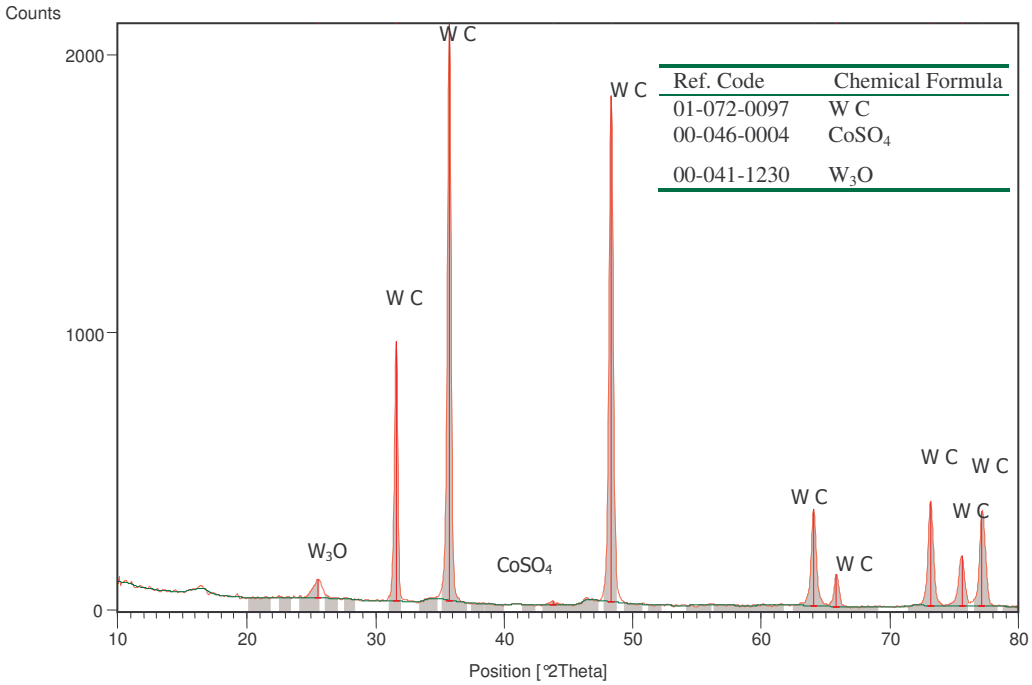



**Figure 4.3.11: XRD patterns for alloy containing 2.0 wt% Ru after exposure to 1M $H_2SO_4$**

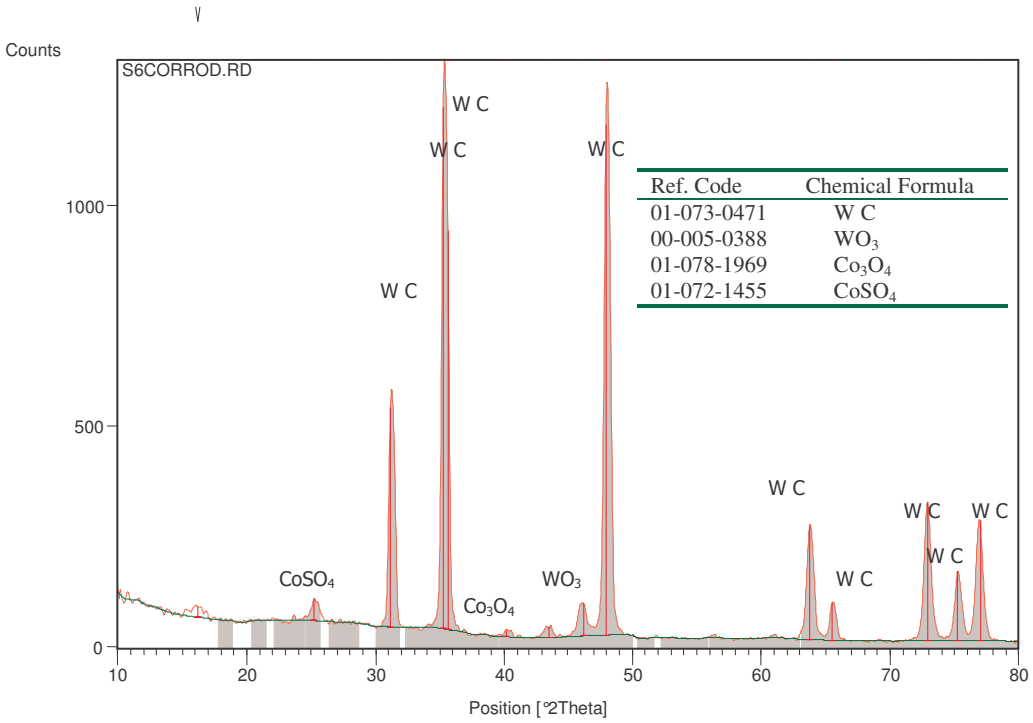



**Figure 4.3.12: XRD patterns for alloy containing 3.0 wt% Ru after exposure to 1M $H_2SO_4$**

### *4.3.1.3 Raman analysis*

Raman analyses were performed on surfaces of the corroded alloys to confirm compounds formed on the surface. Raman spectra of WC-Co-Ru after exposure to 1M sulphuric acid are all presented in the same Figure 4.3.13 over a range of 100- 1500 $cm^{-1}$. All visible peaks are summarized in Table 4.3.1.

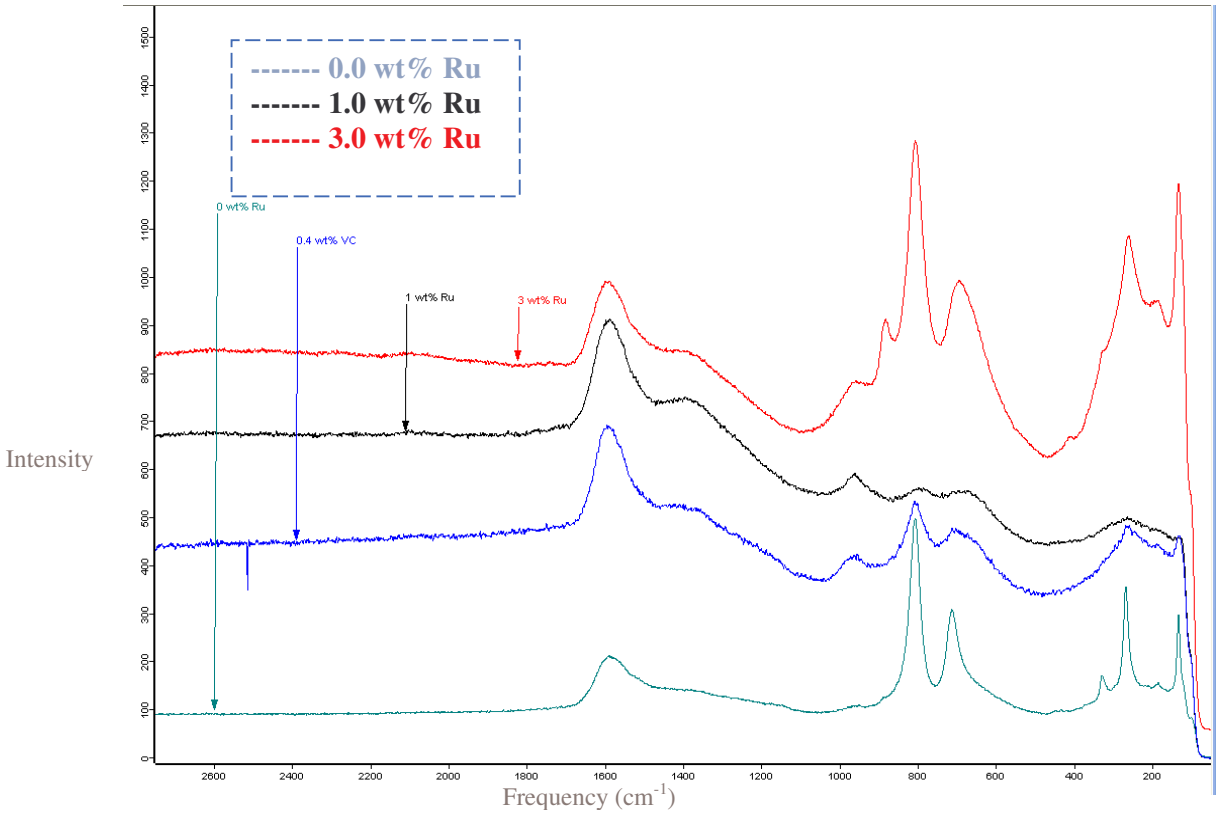



**Figure 4.3.13: Raman spectra of the WC-Co-Ru after exposure to 1M sulphuric acid**

**Table 4.3.1: Peak positions ($cm^{-1}$) found on the surface of WC-Co-Ru alloys after exposure in 1M sulphuric acid solution**

| | **Raman peaks of samples after exposure to sulphuric acid** | | | | | | |
|---|---|---|---|---|---|---|---|
| **Sample** | **Peak 1** | **Peak 2** | **Peak 3** | **Peak 4** | **Peak 5** | **Peak 6** | **Peak 7** |
| 0.0 wt% Ru | 1588 | | 808 | 715 | 327 | 267 | 125 |
| 1.0 wt% Ru | 1583 | 956 | 792 | | | 265 | |
| 3.0 wt% Ru | 1590 | 884 | 803 | 689 | | 255 | 130 |
| **Overall** | **1589±7** | **933±26** | **802±10** | **701±14** | **327** | **262±7** | **128±3** |
| | | | | | | | |
| **Arai *et al*. (1990).** | | | **808** | **719** | | **300** | **150** |
| **Shiyanovskaya *et al.* (1995)** | | **955** | **755** | **670** | **416** | | |

The peaks of the investigated alloys have the average values of 1589 $cm^{-1}$, 933 $cm^{-1}$,

802 $cm^{-1}$, 701 $cm^{-1}$, 327 $cm^{-1}$, 262 $cm^{-1}$and 128 $cm^{-1}$. Some of the peaks were in the same range with the ones obtained by Aria *et al.* (1990); Shiyanovskaya *et al.* (1995) illustrated in the table 4.3.2. Aria *et al.* (1990) reported that the peak around 800 $cm^{-1}$ is usually attributed to W-O stretching modes, while the peaks around 300 $cm^{-1}$ and 150 $cm^{-1}$ are attributable to W-O deformation and O-O deformation modes, respectively. It was suggested that the analysis detected $WO_3$ while Shiyanovskaya *et al.* (1995) detected $WO_3.1/3(H_2O)$.

It was observed that the cobalt is depleted after exposure of the corrosive environment of sulphuric acid, (Figures 4.3.1 to 4.3.7, compared with Figures 4.1.2 to 4.1.8). The chemical composition determined by EDX indicated the presence of oxides and sulphates, which is in agreement with the XRD analyses. EDX analysis showed that after exposure to sulphuric acid corrosion, the element that showed the highest amount was the tungsten, followed by the oxygen, which indicate a tungsten oxide layer has formed on the surface. These EDX results are confirmed by the XRD and Raman analyses which showed that $WO_3$ and $WO_3.H_2O$ formed on the surface, as shown by the peaks obtained. In addition some of the cobalt has been oxidised by oxygen to form cobalt oxides in the form of CoO and $Co_3O_4$. A sulphate layer also formed on the surface, as illustrated by the XRD analysis and was identified as $CoSO_4$.

### 4.3.2 Sodium chloride environment

#### 4.3.2.1 *Scanning electron microscope*

Scanning electron micrographs of the WC-Co-Ru alloys after corrosive attack of sodium chloride and their corresponding EDX analyses are shown in Figures 4.3.14 to 4.3.19. It was observed that there are some chloride compounds on the surface, which covered some parts of the samples' surfaces in this solution.

*0 wt% Ru*

Area 1 is the light phase that has formed on the surface. This phase show prominent peaks of chlorine and sodium with less prominent tungsten and cobalt peaks. Therefore area 1 represents corrosion product. On the other hand Area 2 shows values of chlorine and sodium which are much lower and their peaks are no longer as prominent as in area

1. However the weight percentage of cobalt has slightly increased which could imply that some of the tungsten has dissolved in the 1M sodium chloride solution.

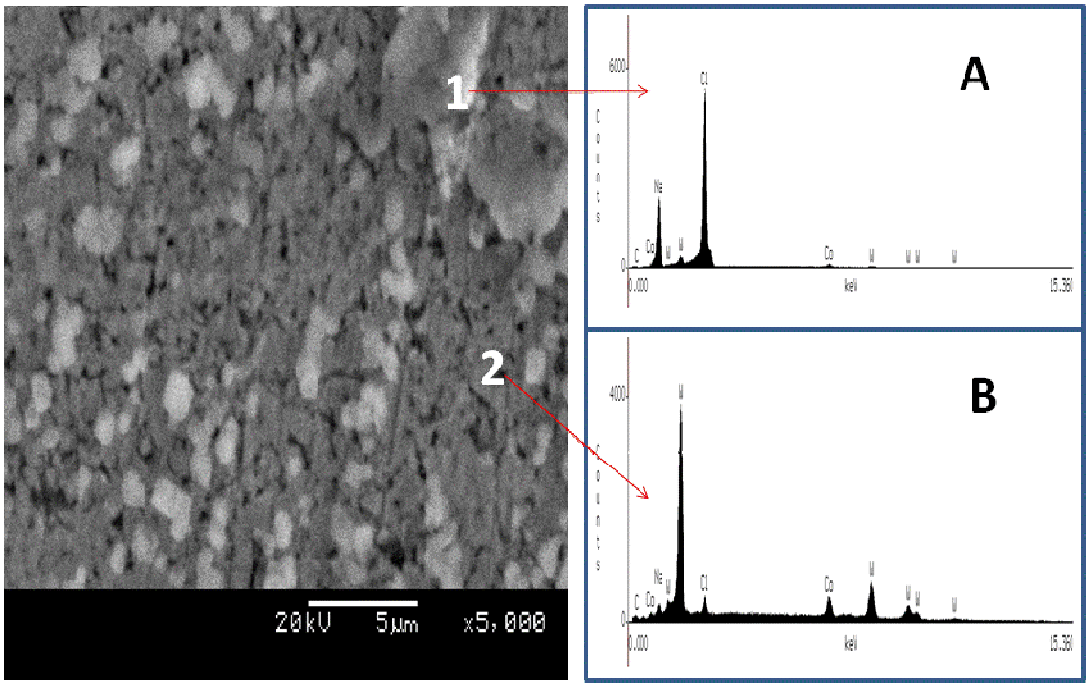



**Figure 4.3.14: SEM micrograph of the 0.0 wt% Ru containing alloy after exposure to 1M NaCl solution with corresponding EDX spectra analyses of (A) area 1 and (B) area 2.**

*0.4 wt% Ru*

A micrograph of 0.4 wt% Ru shows two distinct regions, namely firstly region A which has high amounts of chlorine and sodium, and therefore it contains corrosion product. This region is represented by Area 1. The second region in Area 2 had a high tungsten level, while the cobalt, chlorine and sodium concentrations were low.

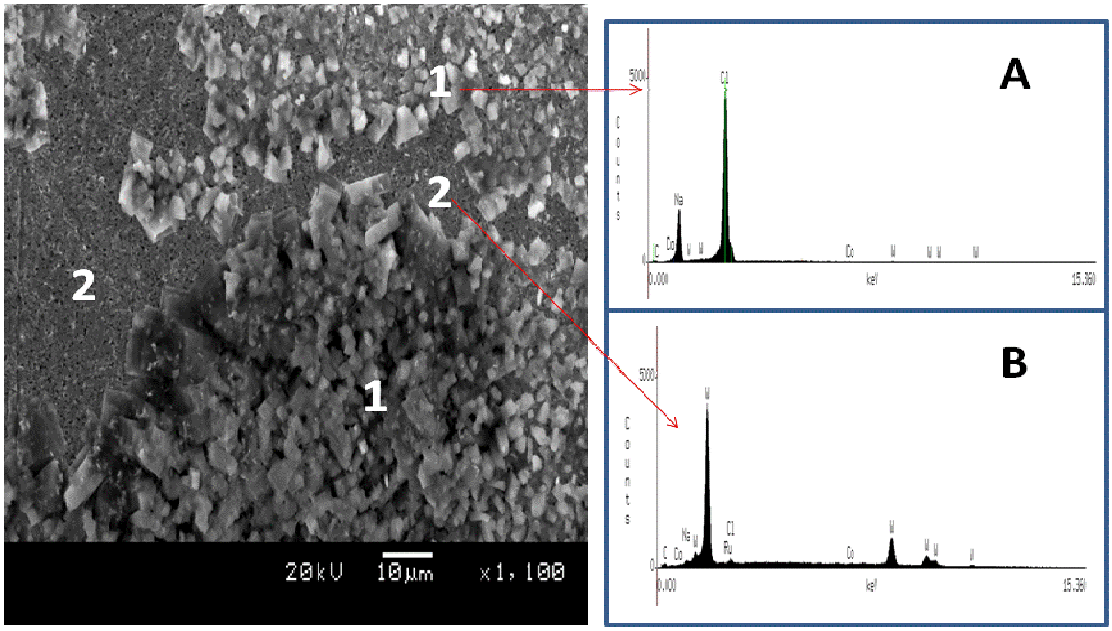



**Figure 4.3.15: SEM micrograph of the 0.4 wt% Ru containing alloy after exposure to 1M NaCl solution with corresponding EDX spectra analyses of (A) area 1 and (B) area 2.**

*1.0 wt% Ru*

It is observed that the peaks of the chlorine and sodium are very weak while the tungsten peak is prominent. There is not much of the corrosion product on the surface of this alloy.

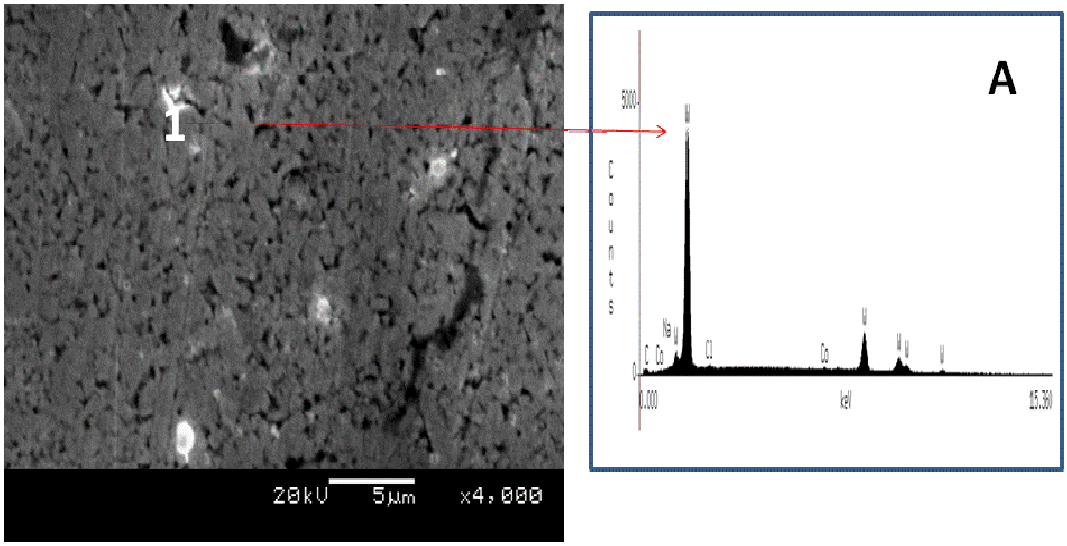



**Figure 4.3.16: SEM micrograph of the 1.0 wt% Ru containing alloy after exposure to 1M NaCl solution with corresponding EDX spectra analyses of (A) area 1 and (B) area 2.**

*1.5 wt% Ru*

This alloy exhibited a very similar behaviour to the alloy containing 0.4 wt% Ru. Two distinct regions are visible: Area 1 represents the corrosion product and Area 2 represents the surface of the alloy with small amounts of chlorine and sodium.

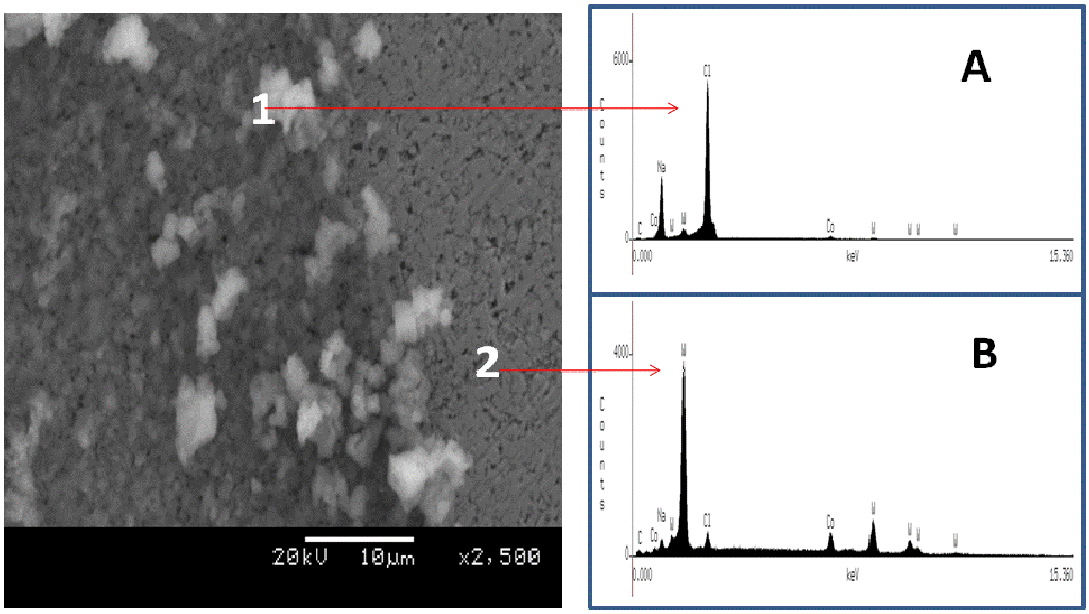



**Figure 4.3.17: SEM micrograph of the 1.5 wt% Ru containing alloy after exposure to 1M NaCl solution with corresponding EDX spectra analyses of (A) area 1 and (B) area 2.**

*2.0 wt% Ru*

This alloy displayed three different regions on its surface. Area 1 is probably the corrosion product, due to high amounts of chlorine and sodium as compared to tungsten and cobalt detected. Area 2 might be the surface of the alloy, and had low amounts of chlorine and sodium and a high amount of tungsten. Finally, Area 3, might also be corrosion product and it is quite porous, showing prominent peaks of tungsten and chlorine.

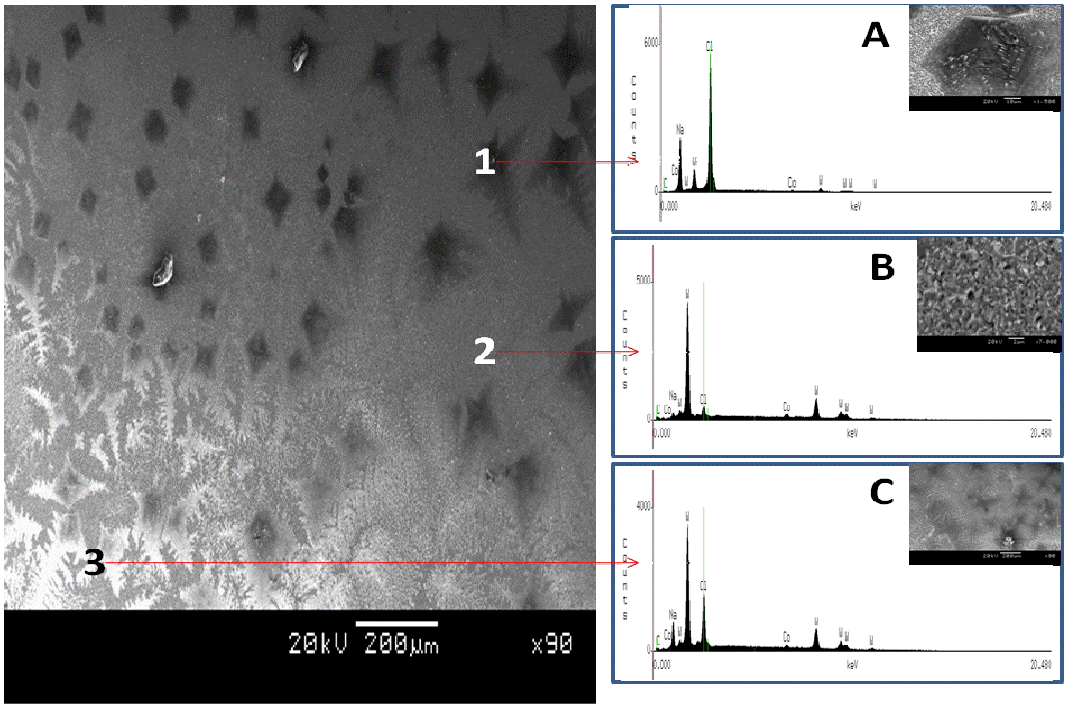



**Figure 4.3.18: SEM micrograph of the 2.0 wt% Ru containing alloy after exposure to 1M NaCl solution with corresponding EDX spectra analyses of (A) area 1 and (B) area 2.**

*3.0 wt% Ru*

This alloy exhibited a very similar behaviour to the alloy containing 2.0 wt% Ru. Again three regions could be distinguished on the surface: Area 1 represents the surface of the alloy, Area 2 represents the porous corrosion product and Area 3 also represents corrosion product.

In summary, in all the alloys there were at least two distinct areas visible on the

corroded surfaces, i.e. the corrosion product and the area of the surface with only small amounts of sodium and chlorine. In most cases the surface of the alloy was observed to have a slightly reduced amount of tungsten. This could mean that tungsten carbide actually dissolves in 1M NaCl. These observations are in agreement with a previously reported study that stated that Co actively dissolves in acidic and in neutral solutions, while it shows passivation behaviour at alkaline pH, while WC, in contrast, shows active dissolution in neutral and alkaline solutions (Hochstrasser-Kurz *et al.,* 2007).

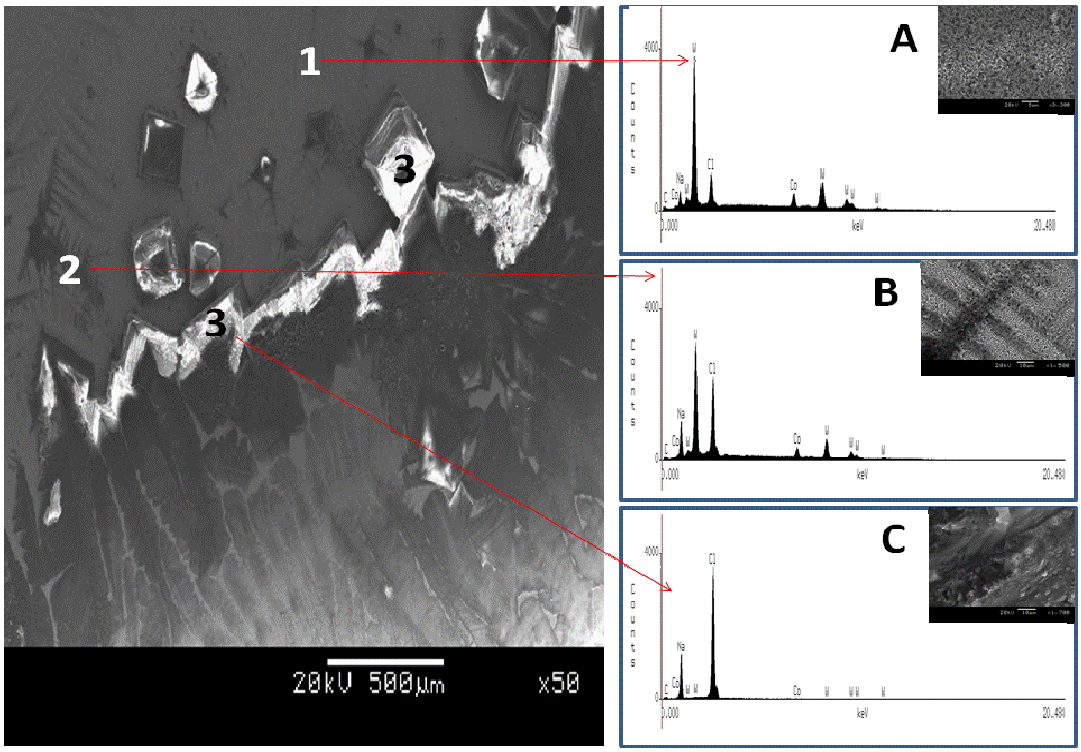



**Figure 4.3.19: SEM micrograph of the 3.0 wt% Ru containing alloy after exposure to 1M NaCl solution with corresponding EDX spectra analyses of (A) area 1 and (B) area 2.**

### *4.3.2.2 X-Ray diffractometry (XRD)*

XRD analyses of the samples after the exposure to the 1M NaCl corrosive environment are presented in Figures 4.3.20 to 4.3.25. These figures are used for comparison with the diffraction spectra from the same samples before corrosion. All the figures illustrate that after the exposure of the alloys to 1M NaCl solution there are still peaks of cobalt binder

around 44$^{o}$ peak. These cobalt peaks have very low intensities as compared to the tungsten carbide. This could still confirm the results obtained from section 4.3.2.1 (i.e. the SEM and EDX results after exposure to 1M sodium chloride) that the tungsten carbide shows dissolution in 1M sodium chloride whereas not much cobalt dissolved in the same solution. These observations are in agreement with a previous study on corrosion behaviour of WC-Co based hardmetal in neutral chloride and acid sulphate media (Bozzini *et al.,* 2003).

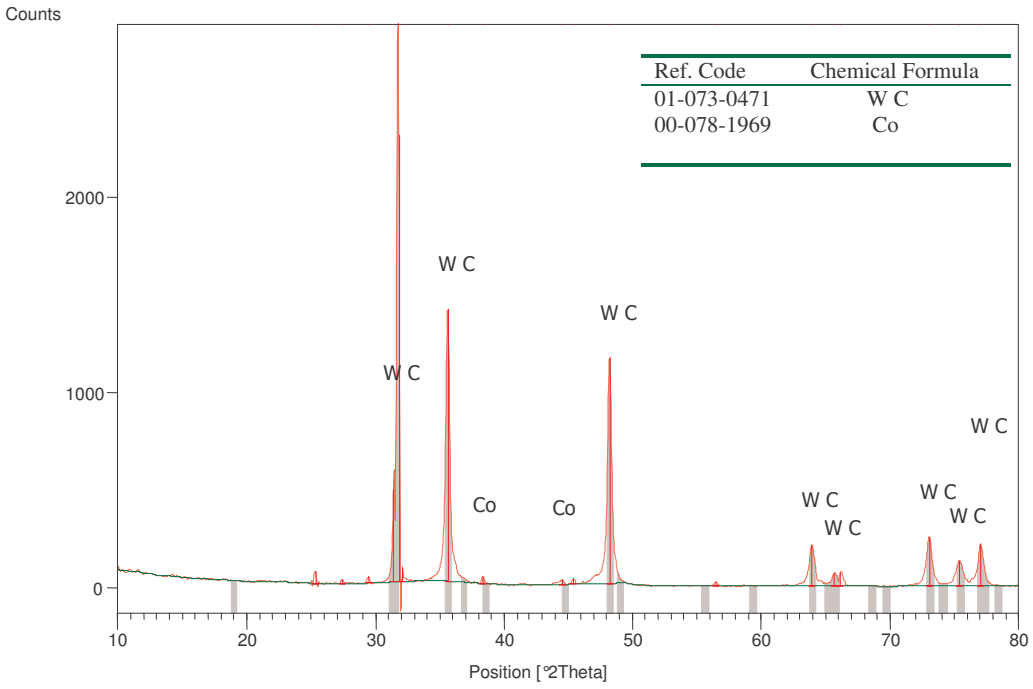



**Figure 4.3.20: XRD patterns for 0.0 wt% Ru after exposure to 1M NaCl**

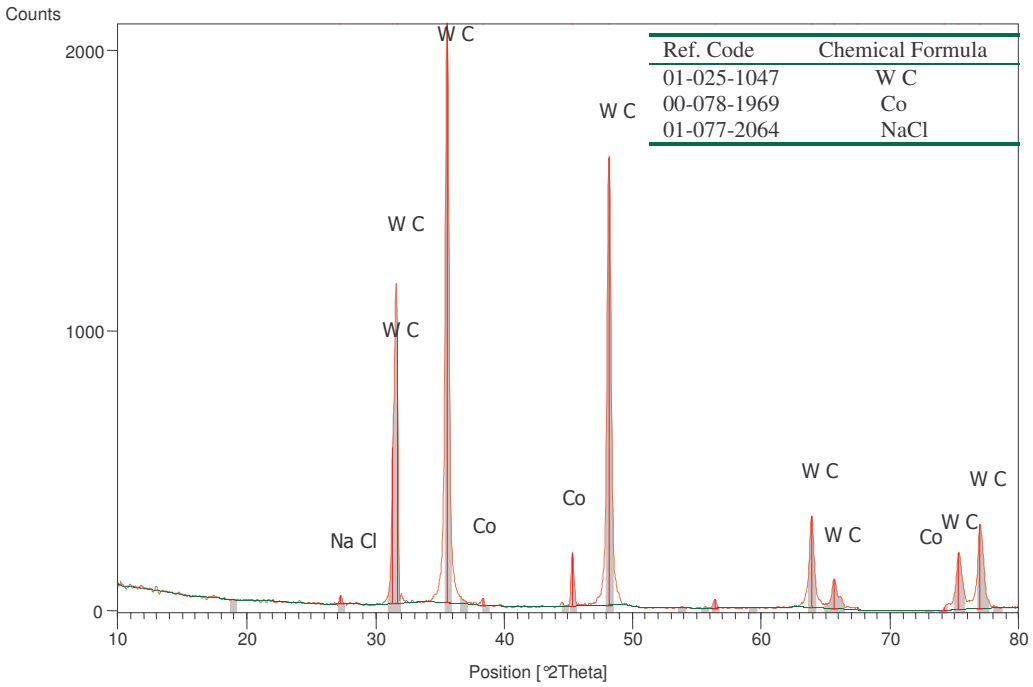



**Figure 4.3.21: XRD patterns for 0.4 wt% Ru after exposure to 1M NaCl**

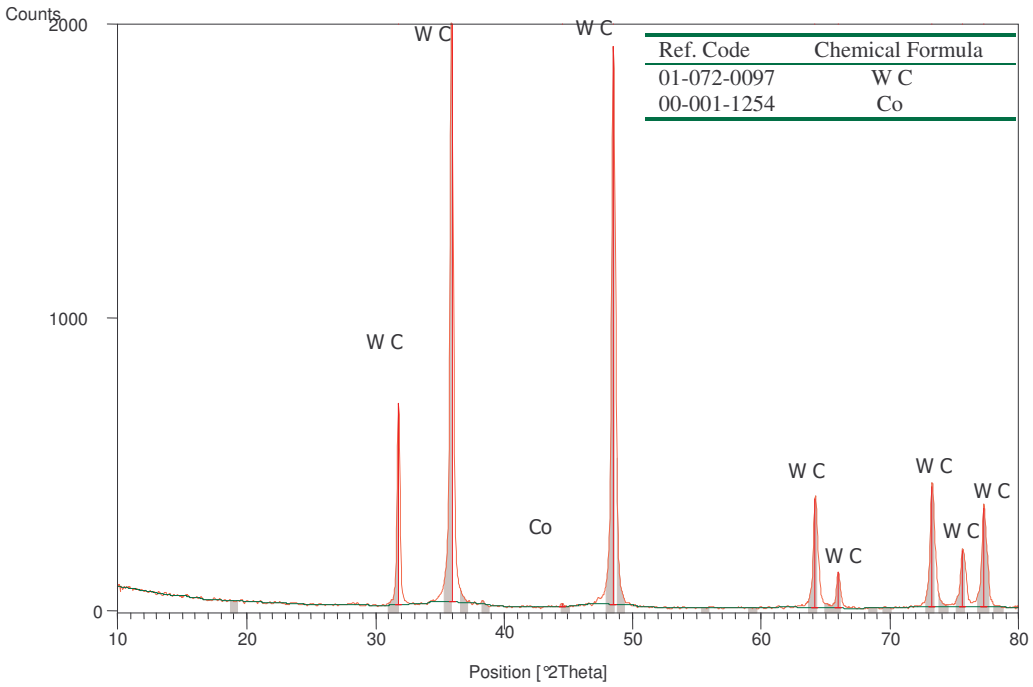



**Figure 4.3.22: XRD patterns for 1.0 wt% Ru after exposure to 1M NaCl**

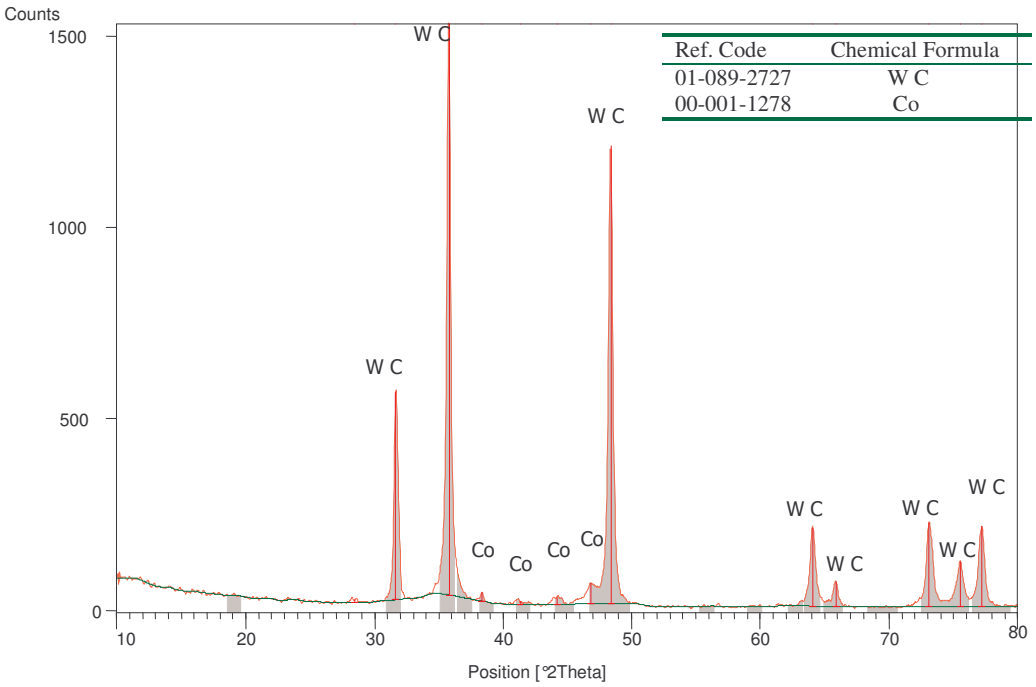



**Figure 4.3.23: XRD patterns for 1.5 wt% Ru after exposure to 1M NaCl**

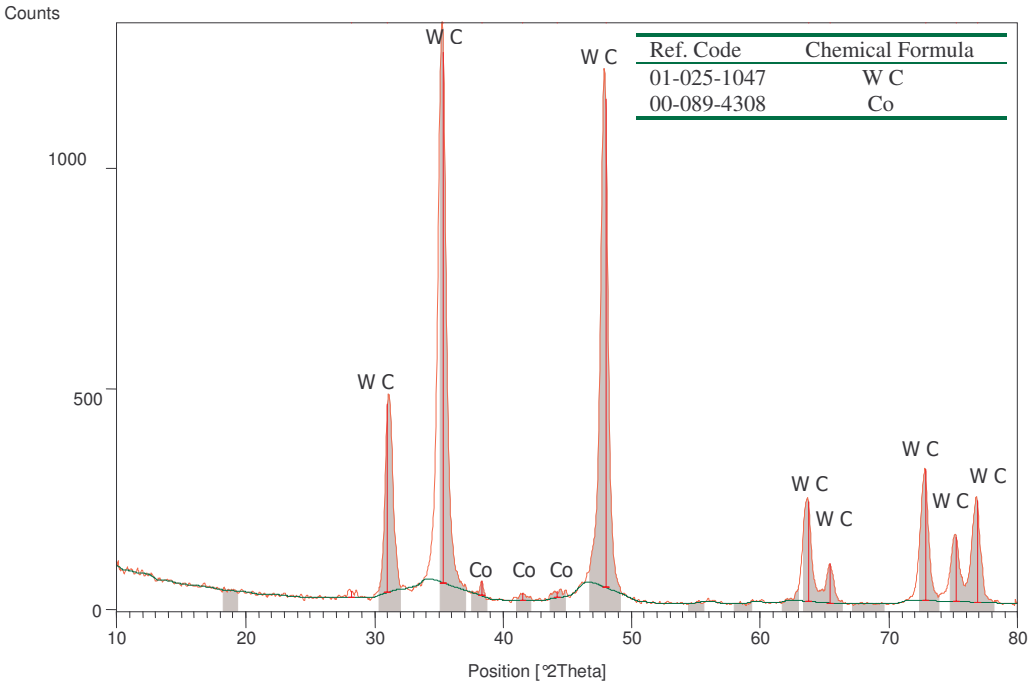



**Figure 4.3.24: XRD patterns for 2.0 wt% Ru after exposure to 1M NaCl**

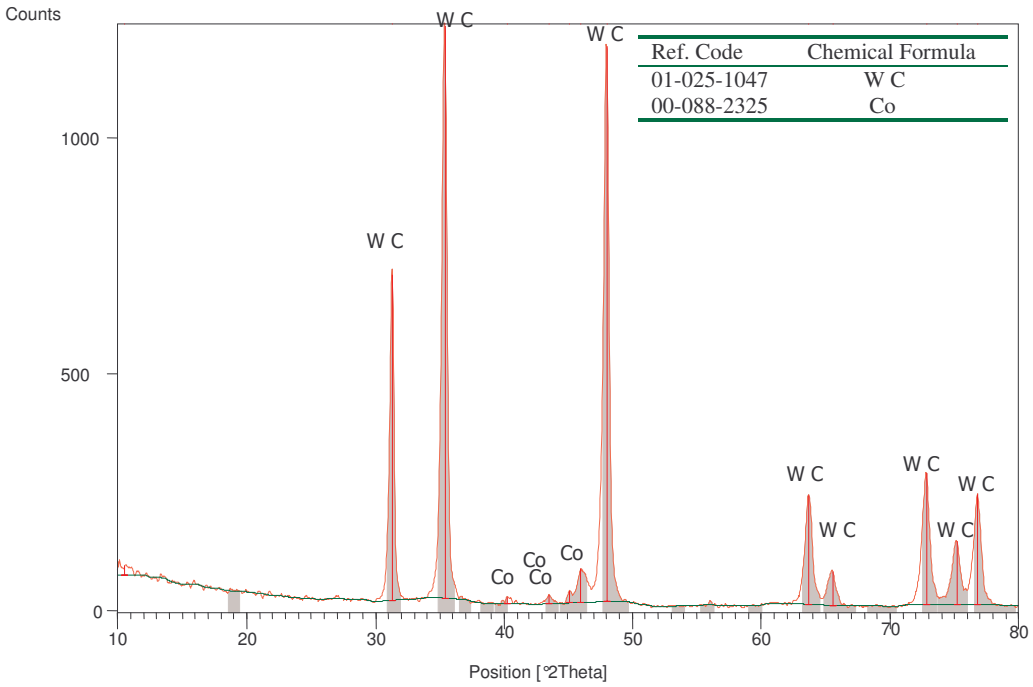



**Figure 4.3.25: XRD patterns for 3.0 wt% Ru after exposure to 1M NaCl**

### 4.3.2.3 *Raman analysis*

Raman analyses were performed on surfaces of the corroded alloys to confirm compounds formed on the surface. Raman spectra of WC-Co-Ru after exposure to 1M sodium chloride are all presented in the same Figure 4.3.26 over a range of 100- 1500 $cm^{-1}$. All the most prominent visible peaks are summarized in Table 4.3.4. Alloys containing 0.0 wt% Ru, 0.4 wt% Ru and 1.5 wt% Ru have similar peaks with the average values of 647 $cm^{-1}$, 520 $cm^{-1}$, 456 $cm^{-1}$and 223 $cm^{-1}$ .

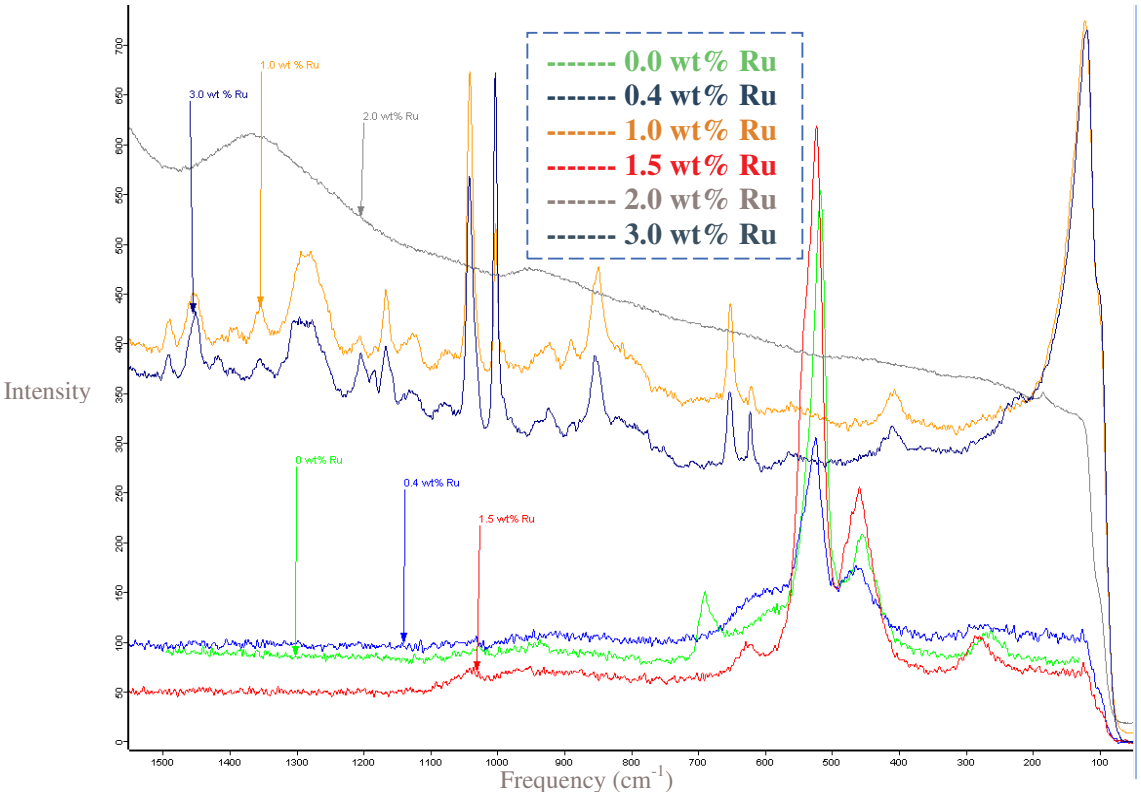



**Figure 4.3.26: Raman spectra from the alloys after exposure to 1M sodium chloride solution**

These peaks were in the same range with those reported by Gu *et al*. (2007); Jiang and Li (2007); Tripathy *et al.* (2008) presented in table 4.3.5. The peaks around 666 and 575 $cm^{-1}$ are attributed to the characteristic of the ν (Co–O) modes which confirms the formation of $Co_3O_4$ (Gu *et al*., 2007; Jiang and Li, 2007; Tripathy *et al.*, 2008). This results showed that the cobalt reacted with oxygen, this oxygen might be from air and distilled water used to make-up an electrolyte The remaining alloys in Table 4.3.4 have similar peaks with the average values of 1421 $cm^{-1}$, 1022 $cm^{-1}$, 861 $cm^{-1}$, 662 $cm^{-1}$, 406 $cm^{-1}$ and 142 $cm^{-1}$.

**Table 4.3.2: Raman peak positions ($cm^{-1}$) found on the surface of WC-Co-Ru alloys after exposure in 1M sodium chloride solution**

| | **Raman peaks of samples after exposure to sodium chloride** | | | | | | |
|---|---|---|---|---|---|---|---|
| **Sample** | **Peak 1** | **Peak 2** | **Peak 3** | **Peak 4** | **Peak 5** | **Peak 6** | **Peak 7** |
| 0.0 wt% Ru | | | 687 | | 516 | 456 | 261 |
| 0.4 wt% Ru | | | | 628 | 519 | 456 | 128 |
| 1.5 wt% Ru | | | | 627 | 525 | 456 | 281 |
| **Average** | | | **687** | **647±1** | **520±5** | **456±0** | **223±95** |
| | | | | | | | |
| **Jiang and Li, (2007)** | | | **671** | **606** | **512** | **469** | **191** |
| **Tripathy, (2008)** | | | **670** | **610** | **510** | **470** | **191** |
| **Gu *et al.*, (2007)** | | | **690** | **618** | **521** | **482** | |
| 1.0 wt% Ru | 1451 | 1041 | 845 | 663 | | 406 | 123 |
| 2.0 wt% Ru | 1362 | | 886 | | | | 184 |
| 3.0 wt% Ru | 1449 | 1002 | 853 | 661 | | 406 | 118 |
| **Average** | **1421±59** | **1022±20** | **861±25** | **662±1** | | **406±0** | **142±42** |

### 4.3.3 Synthetic Mine Water environment

#### *4.3.3.1 Scanning electron microscope*

Micrographs of the microstructures, along with the chemical composition of the various elements observed in the alloys after exposure to synthetic mine water, are given in Figures 4.3.27 - 4.3.32. The surfaces of the alloys examined after the polarization tests in the electron microscope showed that all samples experienced corrosion during the tests. It was observed that the surfaces were completely covered by the corrosion product. The EDX analysis (Figures 4.3.27 - 4.3.32) revealed that this corrosion product constitute of high amounts of oxygen, sulphur and chloride. It is apparent from these micrographs that area 1 (the lighter region) consists of more oxygen, sulphur, chloride and calcium compared to area 2 (darker phase). These results are consistent with those reported previously (Machio, 2005) which reported that EDX analysis showed the

presence of calcium and chloride in corrosion product because the electrolyte was made up of these elements in the salt form.

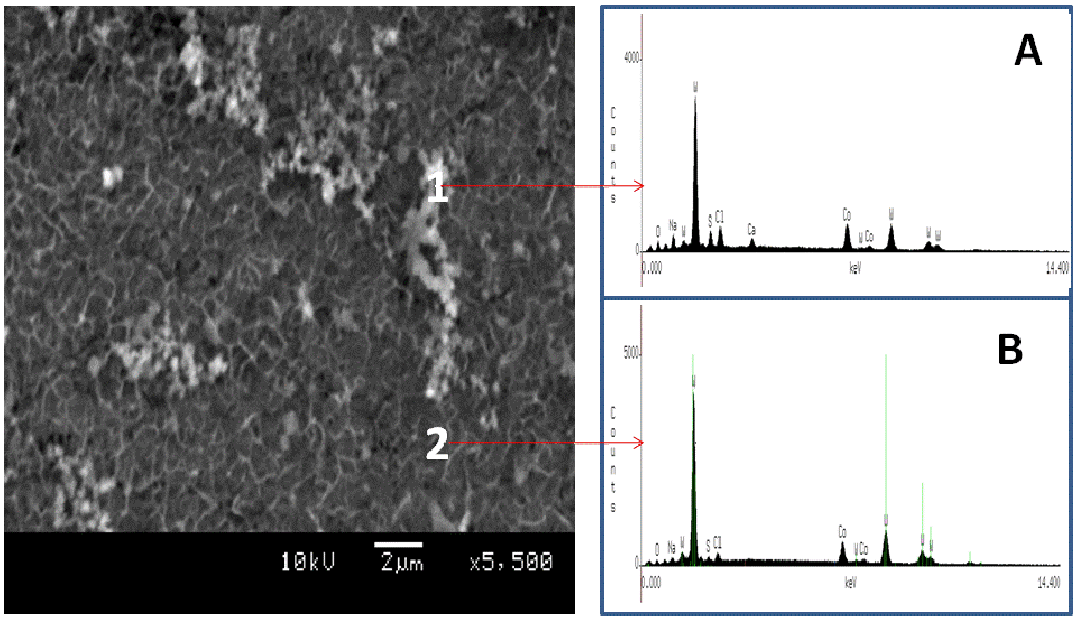



**Figure 4.3.27: SEM micrograph of the WC-10%Co alloy after exposure to synthetic mine water solution with corresponding EDX spectra analyses of (A) area 1 and (B) area 2.**

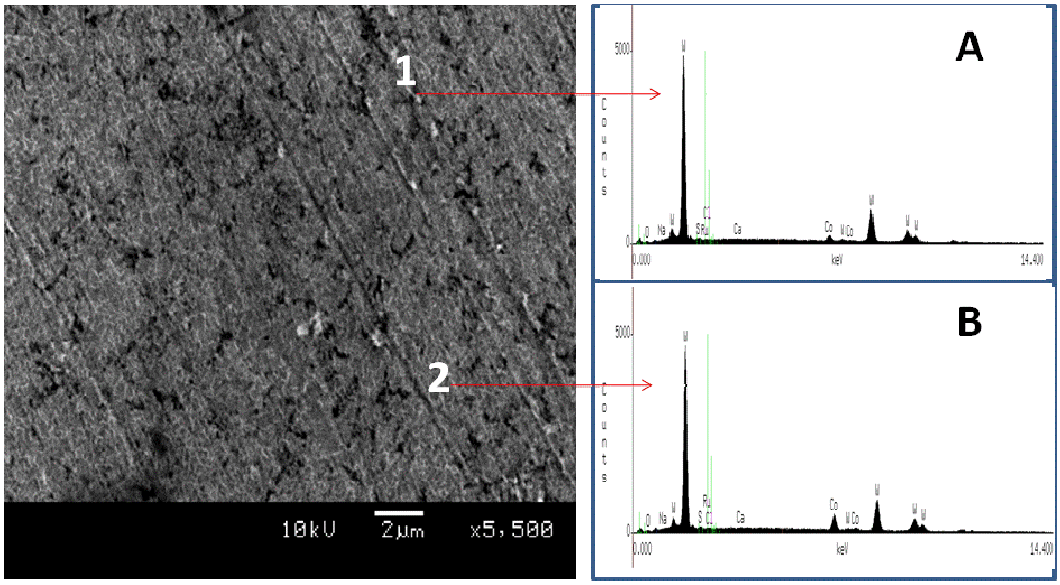



**Figure 4.3.28: SEM micrograph of the 0.4 wt% Ru containing alloy after exposure to synthetic mine water solution with corresponding EDX spectra analyses of (A) area 1 and (B) area 2.**

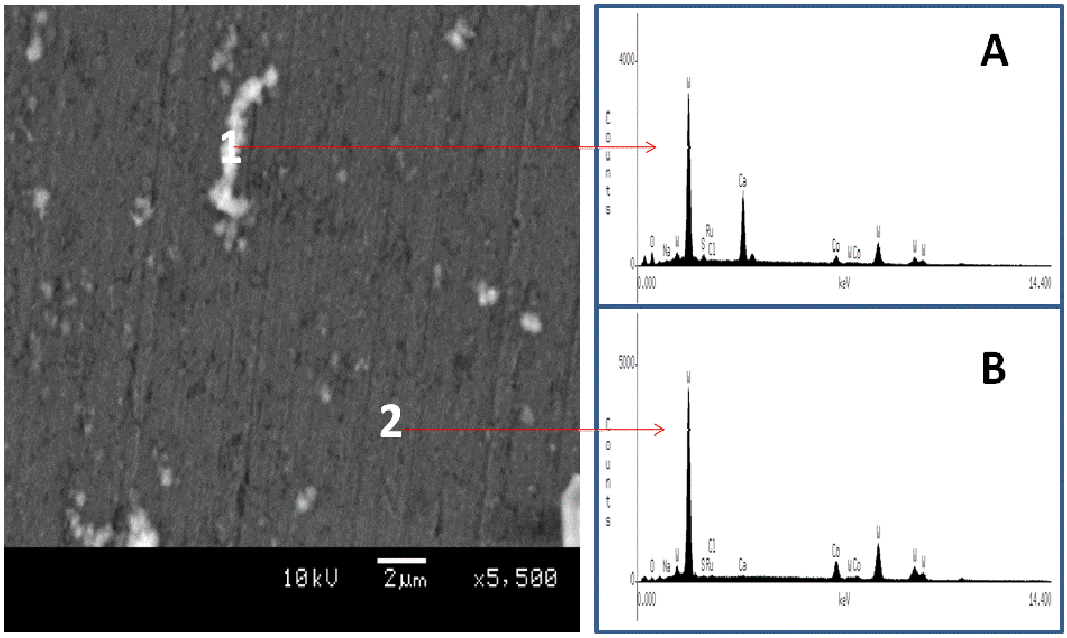



**Figure 4.3.29: SEM micrograph of the 1.0 wt% Ru containing alloy after exposure to synthetic mine water solution with corresponding EDX spectra analyses of (A) area 1 and (B) area 2.**

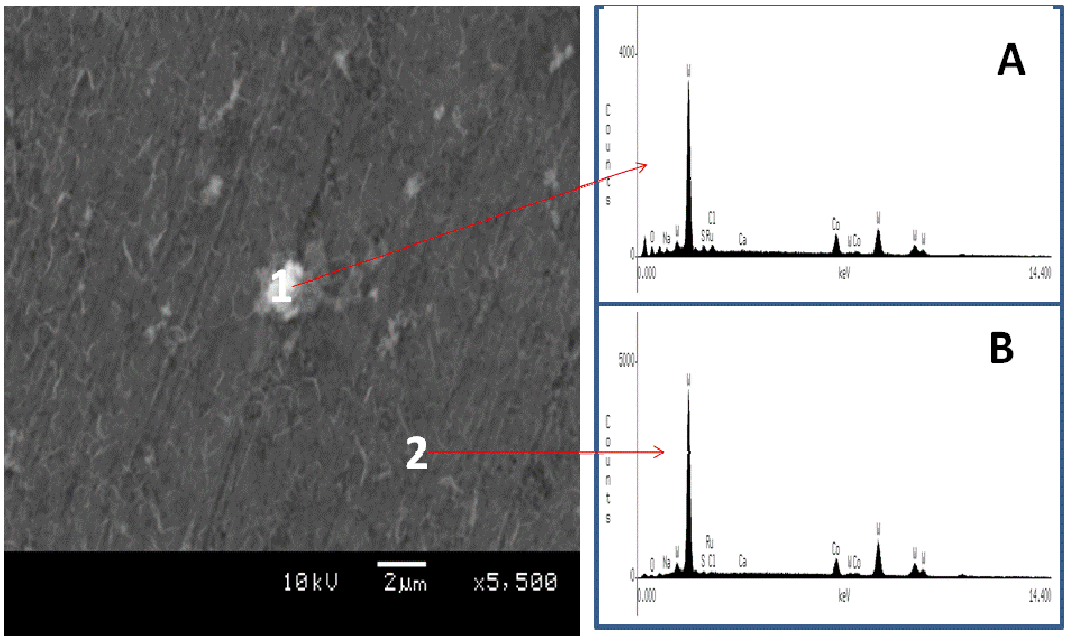



**Figure 4.3.30: SEM micrograph of the 1.5 wt% Ru containing alloy after exposure to synthetic mine water solution with corresponding EDX spectra analyses of (A) area 1 and (B) area 2.**

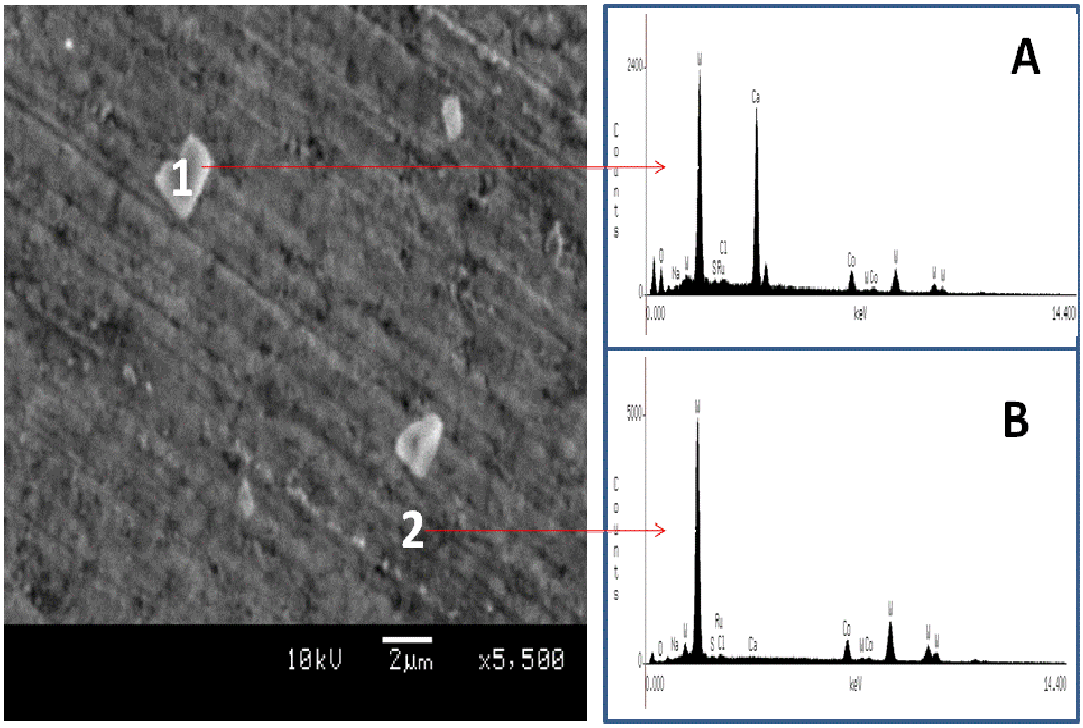



**Figure 4.3.31: SEM micrograph of the 2.0 wt% Ru containing alloy after exposure to synthetic mine water solution with corresponding EDX spectra analyses of (A) area 1 and (B) area 2.**

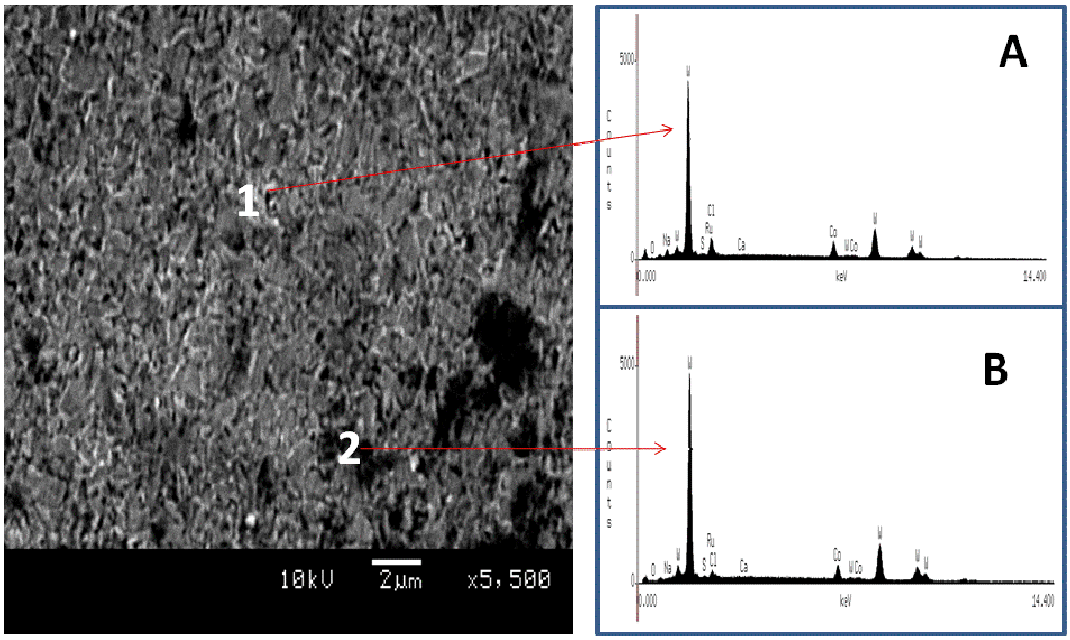



**Figure 4.3.32: SEM micrograph of the 3.0 wt% Ru containing alloy after exposure to synthetic mine water solution with corresponding EDX spectra analyses of (A) area 1 and (B) area 2.**

### *4.2.3.3 X-Ray Diffractometry (XRD)*

The XRD analyses which are presented in Figures 4.3.33- 4.3.38 show the corrosion species formed on the external surfaces of the investigated alloys. It was observed from XRD that the peaks were only for WC and Co compounds. In some of the alloys no cobalt peaks were obtained. Since WC phase was detected in all the alloys it illustrates that the cobalt might have been corroded away, thus leaving very small amounts of cobalt that could not be detected by XRD. This in agreement with the work reported by Machio (2005) that the corroded surfaces appeared to have retained the phase composition they had before corrosion. EDS analysis revealed the presence of calcium, chloride and oxygen on the surfaces of the alloys. However, the corrosion species that could have formed on the surface could not be detected by XRD equipment. This could mean that the corrosion film on the surface was very thin. The insufficient resolution of XRD as a surface analysis technique has to be bore in mind also.

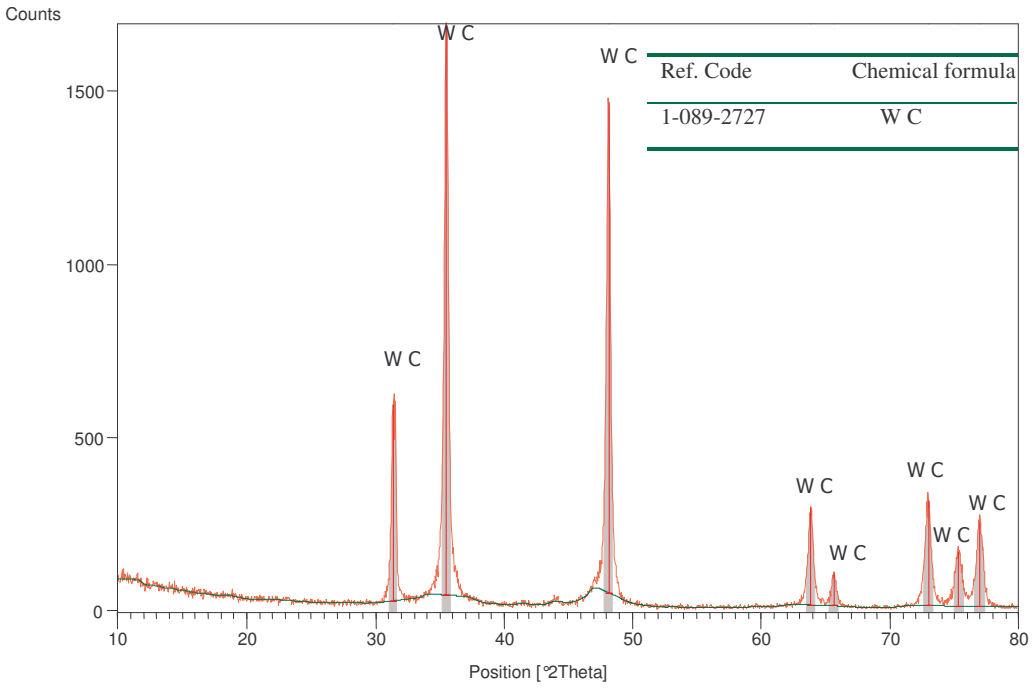



**Figure 4.3.33: XRD patterns for 0 wt% Ru after exposure to synthetic mine water**

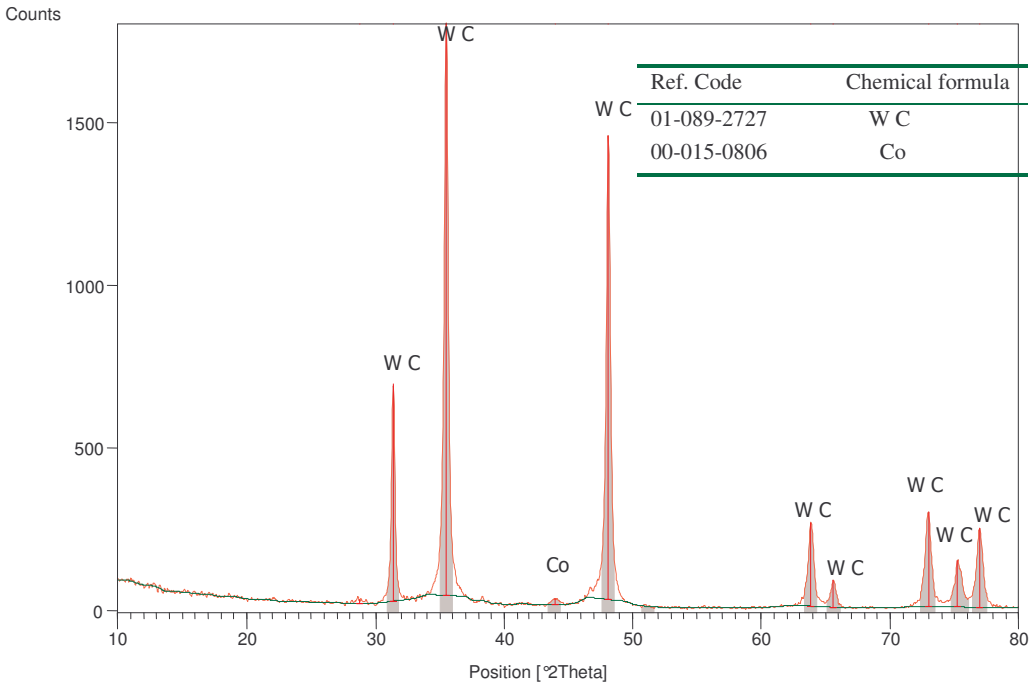



**Figure 4.3.34: XRD patterns for 0.4 wt% Ru after exposure to synthetic mine water**

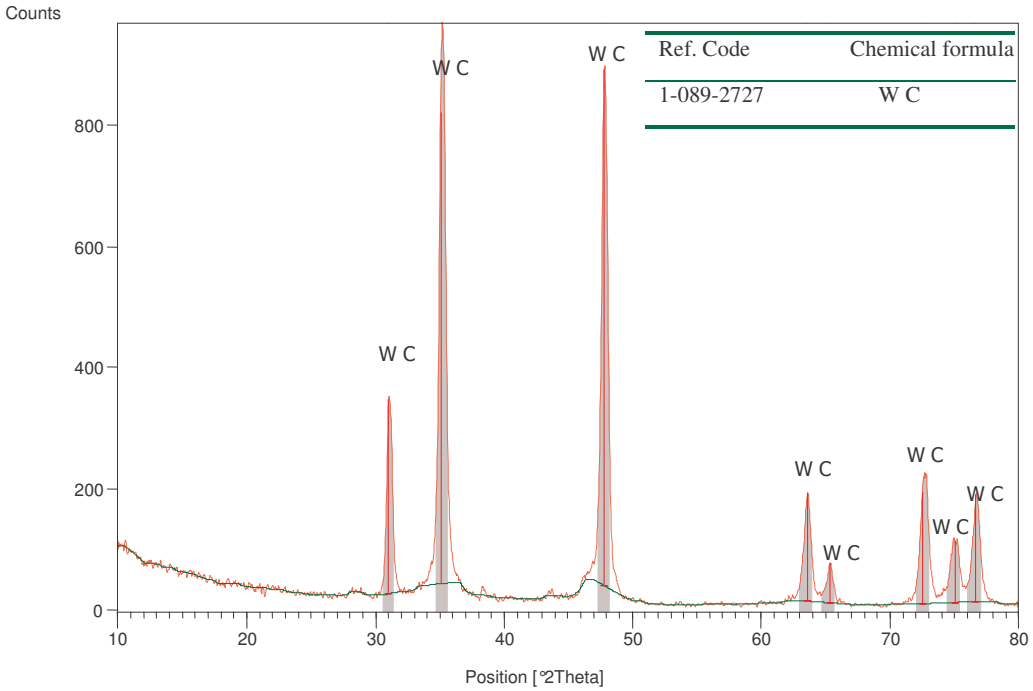



**Figure 4.3.35: XRD patterns for 1.0 wt% Ru after exposure to synthetic mine water**

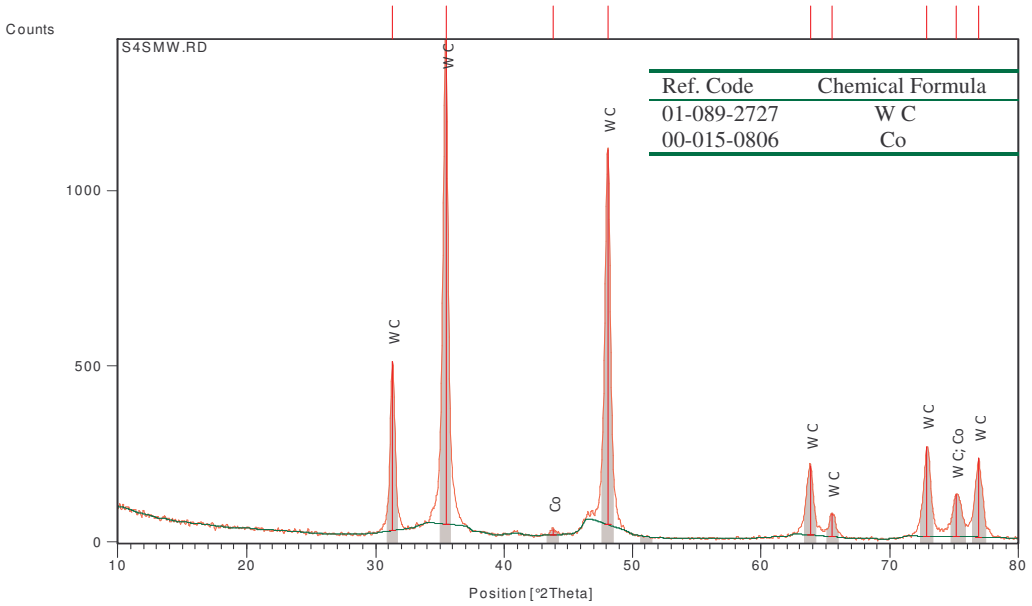



**Figure 4.3.36: XRD patterns for 1.5 wt% Ru after exposure to synthetic mine water**

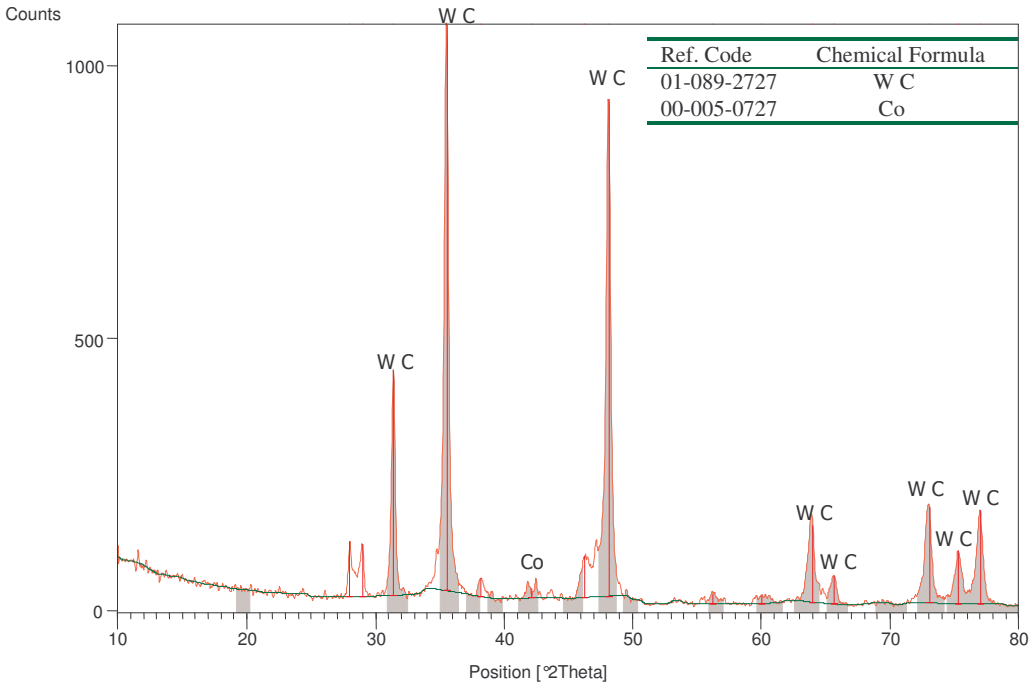



**Figure 4.3.37: XRD patterns for 2.0 wt% Ru after exposure to synthetic mine water**

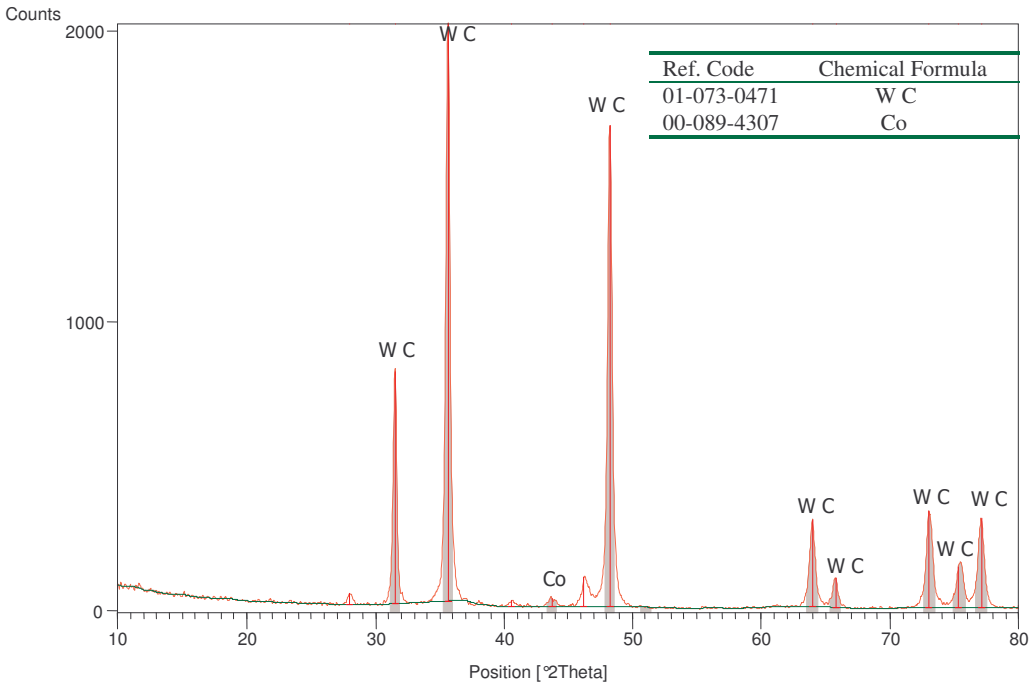



**Figure 4.3.38: XRD patterns for 3.0 wt% Ru after exposure to synthetic mine water**

### *4.2.3.4 Raman Spectrometry*

Raman spectra of the WC-Co-Ru alloys after exposure to synthetic mine water are illustrated in figure 4.3.39. Raman identifiable peaks of samples are summarised in tables for each alloy exposed to synthetic mine water. The most prominent spectrum of all the alloys is at an average of 523±13 $cm^{-1}$ and the lower peak at 152±38 $cm^{-1}$.

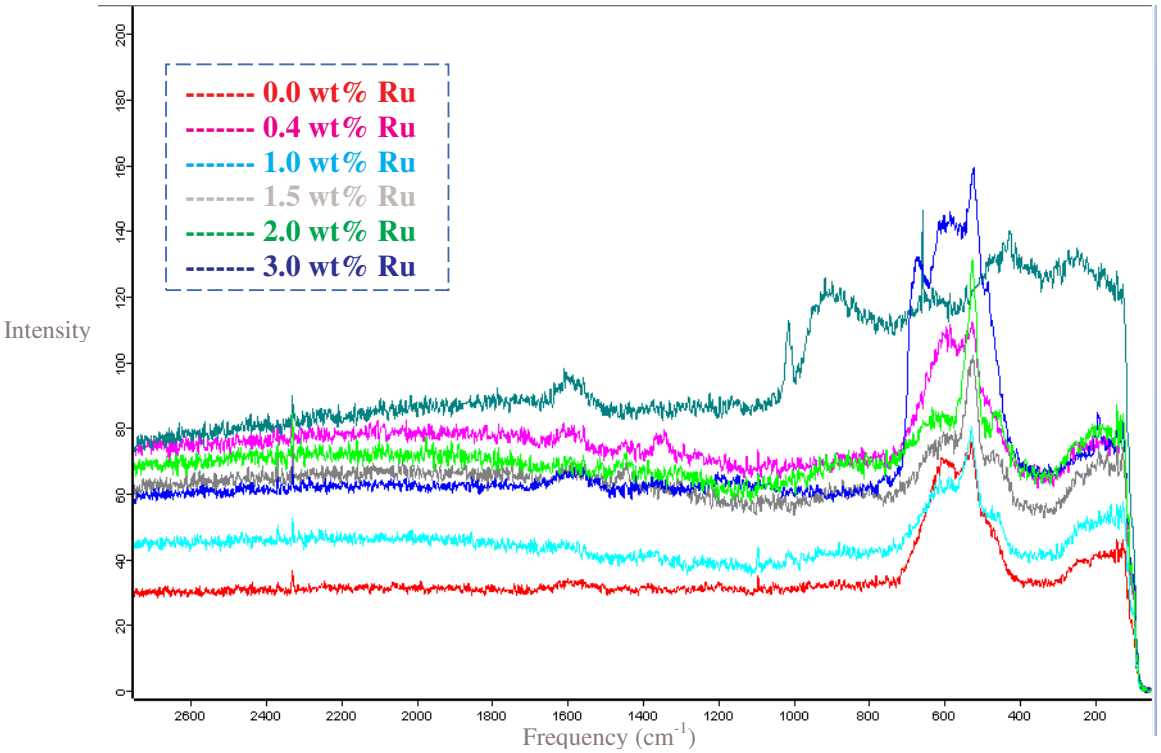



**Figure 4.3.39: Raman spectra from the alloys after exposure to synthetic mine water solution**

**Table 4.3.3: Raman peak positions ($cm^{-1}$) found on the surface of WC-Co-Ru alloys after exposure in synthetic mine water solution**

| | **Raman peaks of samples after exposure to synthetic mine water** | | | | | |
|---|---|---|---|---|---|---|
| **Sample** | **Peak 1** | **Peak 2** | **Peak 3** | **Peak 4** | **Peak 5** | **Peak 6** |
| 0.0 wt% Ru | 1582 | 1232 | □ | 598 | 527 | 128 |
| 0.4 wt% Ru | 1596 | 1337 | □ | 581 | 527 | 139 |
| 1.0 wt% Ru | 1613 | 1374 | 857 | 619 | 520 | 122 |
| 1.5 wt% Ru | 1586 | 1436 | 867 | 598 | 530 | 152 |
| 2.0 wt% Ru | 1572 | □ | □ | 656 | 510 | 186 |
| 3.0 wt% Ru | 1596 | 1014 | 898 | 625 | 525 | 144 |
| **Average** | **1588±25** | **1263±173** | **874±24** | **620±46** | **523±13** | **152±38** |

## 4.4 GENERAL DISCUSSIONS

### 4.4.1 Comparisons of the electrochemical behaviour of WC-Co with the additions of ruthenium

It was observed that in all the investigated solutions, the corrosion current density and the critical current density decreased while the corrosion potential slightly shifted to more positive values as Ru content increases. There was no general trend in the anodic Tafel constant values, while the cathodic Tafel constant values were decreased with increasing amounts of ruthenium. The electrochemical behaviour in all the investigated solutions indicated positive effects of ruthenium additions in decreasing the corrosion rate of the WC-Co cemented carbides.

According to these observations, it is apparent that the additions of ruthenium to the binder phase (cobalt) improved the corrosion resistance of the WC-Co cemented carbides in the investigated solutions. The alloy without any ruthenium showed the smallest passivation range in all the solutions when compared to the other alloys with the additions of ruthenium in the same solutions. However, in 1M sodium chloride, the alloy with no ruthenium showed a wide active–passive transition which contributes to the high corrosion rate observed when compared to the alloy containing 3.0 wt% Ru. On the other hand, no passive-to-active transition was observed in the polarization curves of the alloys in synthetic mine water solution. It was observed that an alloy containing 3.0 wt% Ru had increased corrosion resistance in synthetic mine water which was shown by its lowest corrosion rate.

### 4.4.2 Comparisons of sulphuric acid, sodium chloride and synthetic mine water

The comparative behaviour of the two alloys (0 wt% Ru and 3 wt% Ru) in 1M sodium chloride, synthetic mine water and 1M sulphuric acid solutions is shown in Figure 4.4.1. Results revealed that the alloy with 3.0 wt% Ru showed better corrosion resistance in synthetic mine water compared to 1M NaCl and 1M $H_2SO_4$. To the contrary, the alloy containing no ruthenium (reference alloy) revealed the lowest corrosion resistance in synthetic mine water compared to the other solutions. The effect of ruthenium on WC-

Co in 1M sulphuric acid is not as significant as in synthetic mine water and 1M sodium chloride solutions. The corrosion rate and the corrosion current density in 1M sodium chloride was lower than in 1M sulphuric acid solution, showing that the alloy corroded less in sodium chloride than in sulphuric acid. These observations are in agreement with the study that was reported by Tomlinson and Ayerst (1989).

These researchers reported that the corrosion rate in neutral NaCl solution was much less than that in sulphuric acid solution. It was also observed that in neutral NaCl solution the value of $i_{pass}$ was slightly increased compared that in the acid solution, but still remains of the same order of magnitude. Moreover, the alloy containing 3.0 wt% Ru corroded less in synthetic mine water than sodium chloride and sulphuric acid. This confirms the results reported by Human and Exner (1996), who reported that the critical current density is significantly reduced in synthetic mine water compared to sulphuric acid. It is interesting to observe that the alloys containing Ru corroded less in media containing aggressive $Cl^-$ ions compared to the acidic solution. Based on the observation of stainless steels containing Ru, one would expect a more dramatic effect of the Ru in decreasing the alloys corrosion rate in sulphuric acid compared to the chloride containing solution.

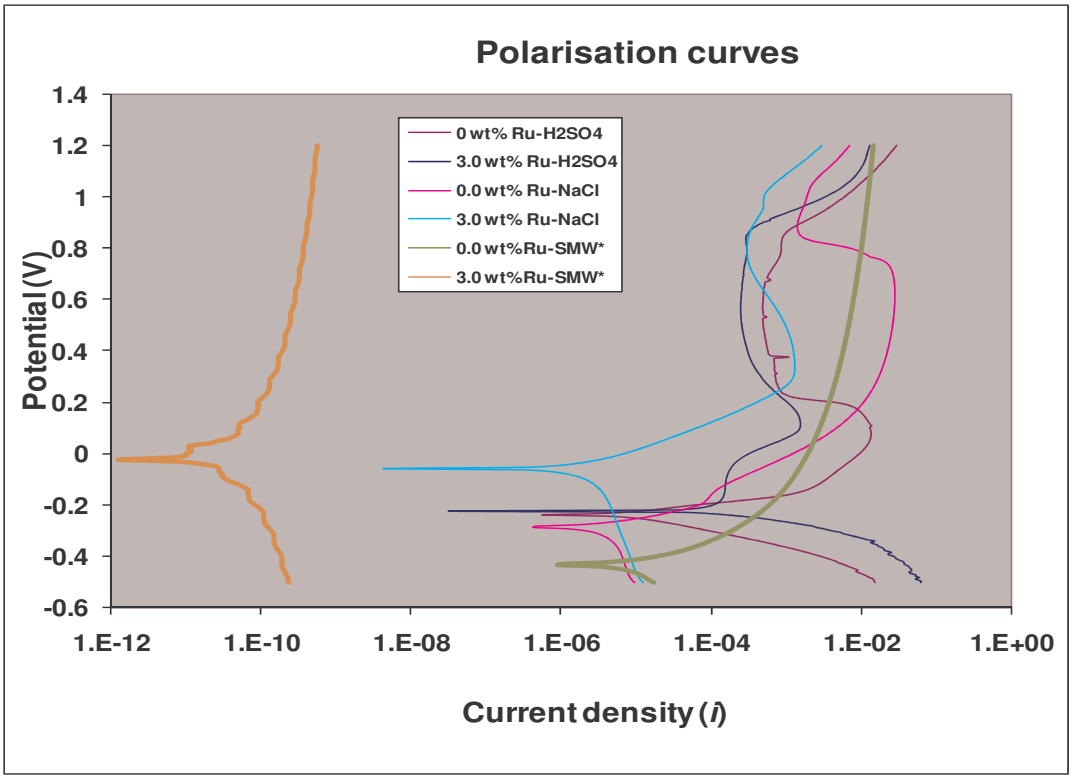



**Figure 4.4.1: Polarization curves showing the influence of ruthenium on the corrosion behaviour of the WC-Co alloys in 1M NaCl and 1M $H_2SO_4$ solutions.**

**Table 4.4.1: Electrochemical parameters for the samples in 1M sulphuric acid and 1M NaCl and SMW (synthetic mine water) solutions**

| Sample | Ecorr (V) | Icorr (A) $\times 10^{-6}$ | $i_{crit}$ ($A/m^2$) $\times 10^{-3}$ | $i_{pass}$($A/m^2$) $\times 10^{-4}$ | $b_a$ (V/Dec) | $b_c$ (V/Dec) | Corrosion rate (mm/yr) $\times 10^{-2}$ |
|---|---|---|---|---|---|---|---|
| **0%Ru- NaCl** | -0.483 | 0.90 | 7.89 | 513 | 0.016 | 0.039 | 1.62 |
| **3%Ru- NaCl** | -0.275 | 0.11 | 0.10 | 3.36 | 0.027 | 0.022 | 0.21 |
| **0%Ru-$H_2SO_4$** | -0.235 | 7.09 | 12.90 | 14.30 | 0.042 | 0.055 | 14.60 |
| **3%Ru-$H_2SO_4$** | -0.222 | 1.09 | 1.42 | 4.34 | 0.040 | 0.010 | 2.24 |
| **0%Ru-SMW** | -0.429 | 4.33 | | | 0.037 | 0.075 | 7.79 |
| **3%Ru-SMW** | -0.200 | 2.23 | | | 0.040 | 0.018 | 4.04 |

Electrochemical parameters for the samples in 1M sulphuric acid and 1M NaCl and SMW (synthetic mine water) solutions are presented in Table 4.4.1. It was observed that

the corrosion potential values ($E_{corr}$) are generally more negative in 1M NaCl than in 1M $H_2SO_4$ and synthetic mine water, whereas the corrosion current density ($i_{corr}$) was generally greater (i.e. more dissolution and corrosion) in 1M $H_2SO_4$ than in synthetic mine water and 1M NaCl. The 3.0 wt% Ru alloy showed corrosion rates that were generally an order of magnitude larger in 1M $H_2SO_4$ compared to those in NaCl. Ruthenium affects $\beta_c$ in 1M $H_2SO_4$ and synthetic mine water, but not really much in NaCl. This is in agreement with the cathodic modification mechanism. $i_{crit}$ is smaller in NaCl than $H_2SO_4$. However $i_{pass}$ is larger in NaCl than in $H_2SO_4$ for the alloy without ruthenium, and similar for the alloy containing 3% Ru.

These observations indicate that the alloys were more susceptible to corrosion in sulphuric acid than in sodium chloride and synthetic mine water solutions. In contrast, Human and Exner (1996) reported that in synthetic mine water, the corrosion potential of a WC-Co composite was markedly shifted to a more negative value, the current density increases with increasing polarisation and the pseudo-passivation is not as pronounced as in sulphuric acid. The passivity range increased with an increasing amount of ruthenium. It was also observed that the passivity range of the alloys depends on the nature of the corrosive media, and it decreases in the following order: passivity range (synthetic mine water) > passivity range (sodium chloride) > passivity range (sulphuric acid).

Recently Olubambi *et al.* (2008) reported that an increase in passivity with increasing ruthenium contents might be an indication that ruthenium increases the passivation region, possibly through the replacement and substitution of cobalt binder after its selective dissolution. It is possible that after cobalt is lost from the alloy, ruthenium could diffuse and accumulate on the defect sites within the surface of the alloys, thereby inducing passivity. Tjong *et al.* (1997) observed that the accumulation of the ruthenium atoms on the surface of the alloy could promote the efficiency for hydrogen evolution, thereby moving the corrosion potential towards the noble direction, and resulting in spontaneous passivation when the surface concentration of ruthenium reaches a critical value. This correlates well with the observed decrease in the cathodic Tafel constants with increased ruthenium content in the alloys in this investigation, as well as the shift of the open circuit corrosion potential to more noble values. Furthermore, the ruthenium adatoms on the surface of the corroded alloys are also more corrosion resistant than the

cobalt atoms, and this contributes to the increased corrosion resistance against sulphuric acid. This is corroborated by the observed decrease in $i_{crit}$ recorded during potentiodynamic scans.

### 4.4.3 The corrosion products formed on the surface

The semi-logarithmic plots of the anodic polarization curves in 1M $H_2SO_4$ and NaCl show four distinct regions. The first region is the cathodic one, where the current density gradually decreases, where the corrosion current density is derived. In the active region (second region), the current density slowly increases until the critical current density is reached, i.e. the starting of the third (active to passive transition) region. In this region the current density decreases slowly and shortly thereafter it remains constant while the potential continuously increases. This last region is termed the passive region (fourth region). This behaviour is attributed to the formation of the layers which can be observed on the surface as corrosion products. The current density was observed not to have reduced significantly. This behaviour is termed pseudo-passivity.

Other researchers also observed and reported that the WC-Co alloys undergo pseudo-passivation, not true passivation (Human and Exner, 1997; Human *et al.,* 1998; Mori *et al.,* 2001; Bozzini *et al*., 2003; Sutthiruangwong and Mori, 2003; Sutthiruangwong *et al.,* 2005). Human *et al.* (1998) defined pseudopassivity as a film that forms on Co (W, C) alloys causing the current to become relatively independent of potential but remaining very high. Human and Exner (1996) reported that pseudopassive behaviour is due to the formation of a porous corrosion layer on the surface which is supported by the WC network. Sutthiruangwong and Mori (2003) stated that the pseudopassivity of WC-Co was due to diffusion limitations of mass transport current flow which decreased and caused pseudopassive behaviour. Bozzini *et al*. (2004) agreed with Human and Exner (1996) and stated that since current densities of several tens of $mA/cm^{-2}$ are typically measured, it cannot result from diffusion or ionic mobility through a coherent film.

During anodic polarization, the formation of various oxide films can be observed on the WC–Co surface using XRD. The various oxides films that were observed were $Co_3O_4$,

CoO, $WO_3$ and $WO_3.xH_2O$ surface layers. In sulphuric acid, it was observed that the $WO_3$ film was formed. The formation of the $WO_3.xH_2O$ species might relate to the passivation of the hardmetals with formation of a continuous layer of oxides inhibiting the reaction of the binder phase (Bozzini *et al.,* 2003). Cobalt oxides were reported to continuously dissolve in acidic solution, but stabilized in neutral and alkaline solutions (Hochstrasser -Kurz *et al.,* 2007)

After corrosion in 1M sulphuric acid, XRD analysis revealed that the surfaces of the WC-Co-Ru alloys were covered with corrosion product containing tungsten oxide ($WO_3$), cobalt oxide ($Co_3O_4$) and cobalt sulphate ($CoSO_4$), while no distinctive cobalt binder peaks were identified. The passivation of the various alloys in sulphuric acid may be due to the presence of tungsten oxide ($WO_3$) that is formed on the surface during the corrosion tests (Human *et al.,* 1998). No significant information was obtained on the XRD analysis of the corroded samples in 1M sodium chloride and synthetic mine water solutions. EDS analysis however revealed that chloride products (species) were formed on the surface of the samples (but does not cover the entire alloy surface) in a 1M sodium chloride environment. Surface cracks were observed on the surfaces of the samples corroded in 1M sulphuric acid and synthetic mine water, while no cracking was observed in samples corroded in 1M sodium chloride. These observations are in agreement with the previously reported studies (Bozzini *et al.,* 2002; Pugsley and Sockel, 2004).

### 4.4.4 Effects of ruthenium on binding effects of cobalt on the WC-Co cemented carbide and hypotheses validation

#### *4.4.4.1 Hypothesis one*

The first hypothesis states that ruthenium is a nobler metal than cobalt; a tungsten carbide containing cobalt will therefore be less noble than the one with the additions of ruthenium, and thus the latter would have better corrosion resistance than the one without Ru. This is due to the partial substituting of the conventional cobalt binder with a more corrosion resistant element that reduces the current density (Human and Exner 1997). The addition of up to 3 wt% ruthenium to cobalt results in changes in the polarisation behaviour. A major influence of Ru alloying is a shifting of the corrosion

potential in a positive direction while reducing the $i_{crit}$, $i_{corr}$, $i_{pass}$ and corrosion rate, as well as changing the values of the cathodic Tafel constant. No general trend in the anodic Tafel slope changing could be seen.

Increasing ruthenium contents have been observed to play an important role in the increased corrosion resistance of the WC-Co alloys. Varga *et al.* (1997), as well as Wolff *et al.* (1998); confirmed the fact that ruthenium is a major factor in improving the corrosion resistance of the stainless steels. The improvement of corrosion resistance as ruthenium is added could be due to the cathodic modification effects of ruthenium which results in more noble corrosion potential values and a decrease in values of $ß_c$. These observations are in agreement with previous studies on the effect of ruthenium in other alloys such as chromium, titanium and stainless steels (Stern and Wissenberg, 1959; Potgieter, 1991; Potgieter, 1993; Potgieter *et al.*, 1997; Varga *et al.,* 1997; Wolff *et al.,* 1998; Van der Lingen and Sandenbergh, 2001; Olubambi *et al.,* 2008). It was observed that small ruthenium additions can significantly increase the corrosion resistance of the stainless steels, displacing their open-circuit corrosion potentials towards more positive values. In addition, reduced corrosion, critical and passive current densities in all the solutions indicate that the ruthenium content also inhibits the anodic dissolution of the alloys.

Therefore the first hypothesis correlates well with the corrosion results. As the ruthenium content is increased, so does the corrosion resistance of the WC-Co alloys.

#### *4.4.4.2 Hypothesis two*

The second hypothesis states that ruthenium has a stabilizing effect on the fcc phase of the cobalt binder, thus the improvement of corrosion resistance as ruthenium is added to WC-Co could also be due to the stabilizing effects of ruthenium on the crystal structure of cobalt binding phase. A XRD analysis obtained for the WC-Co alloys with ruthenium additions revealed that cobalt retained its fcc crystal structure after the additions of ruthenium. However for the alloy containing no ruthenium, the cobalt crystal structure is hcp as illustrated in table 4.4.2. However in this study it was observed that in all the electrolytes (i.e. 1M sulphuric acid, 1M sodium chloride and synthetic mine water) the fcc crystal structure showed improved corrosion resistance compared to the hcp crystal structure. This implied that ruthenium actually stabilizes the cobalt phase to retain the

fcc crystal structure. It could be inferred from these observations that the samples containing ruthenium (i.e. where the cobalt alloys had fcc structure) exhibited better corrosion resistance than those containing no ruthenium (i.e. those with hcp structure). Similar observations that the presence of the fcc phase displayed improved corrosion resistance compared to those cobalt phases exhibiting hcp structures have also been reported by Human *et al.* (1998) and Srivastava *et al.* (2006).

**Table 4.4.2: Effect of ruthenium in the crystallographic structure of WC-Co**

| **Samples** | **Reference code** | **Crystallographic structure** |
|---|---|---|
| 0.0 wt% Ru | 00-001-1277 | Hexagonal (HCP) |
| 0.4 wt% Ru | 00-015-0806 | Cubic (FCC) |
| 1.0 wt% Ru | 01-089-4307 | Cubic (FCC) |
| 1.5 wt% Ru | 00-001-1259 | Cubic (FCC) |
| 2.0 wt% Ru | 01-088-2325 | Cubic (FCC) |
| 3.0 wt% Ru | 01-088-2325 | Cubic (FCC) |

# *CHAPTER 5*

# 5.0 CONCLUSIONS AND RECOMMENDATIONS

## 5.1 Conclusions

### 5.1.1 Effect of ruthenium additions on WC-Co alloys

From the investigation, it was found that ruthenium additions of up to 3 wt% Ru in the WC-10%Co alloy increased the corrosion resistance of the WC-Co alloys. Corrosion rates were observed to decrease with increasing Ru content. This is attributed to the stabilization of the cobalt fcc phase due to ruthenium additions as well the increased passivation range and reduced current densities observed as the ruthenium content increased.

### 5.1.2 Corrosion behaviour of WC-Co-Ru

The alloy with 3.0 wt% Ru showed better corrosion resistance in synthetic mine water compared to 1M NaCl and 1M $H_2SO_4$. To the contrary, the alloy containing no ruthenium (reference alloy) revealed the least corrosion resistance in synthetic mine water compared to the other two solutions. Ruthenium affects $\beta_c$ in 1M $H_2SO_4$ and synthetic mine water, but not really in NaCl. It was also observed that the passivity range and corrosion resistance decreases in order of synthetic mine water> sodium chloride> sulphuric acid.

### 5.1.3 Validation of Claims

In the literature, the improvement of corrosion resistance caused by added ruthenium is due to the cathodic modification and anodic inhibition effects of ruthenium, which is observed by the reduced critical current density, more noble corrosion potential values and the decrease in values of $ß_c$. The results of this investigation confirm these previous reports.

### 5.1.4 Validation of the hypothesis

The two hypotheses were confirmed as follows:

The first hypothesis was confirmed, namely that the corrosion resistance increase as the ruthenium content is increased.

The second hypothesis was confirmed with the XRD analysis, which indicated the samples containing ruthenium (i.e. where the cobalt alloys had fcc structure) exhibited better corrosion resistance than those containing no ruthenium (i.e. those with hcp structure)

In summary, ruthenium additions of up to 3 wt% Ru of the WC-10%Co alloy increased the corrosion resistance of the WC-Co alloys.

## 5.2 Recommendations

According to the literature, large amounts of VC improve the corrosion resistance of the WC-Co alloys. It is recommended that the VC additions are compared with the effect of ruthenium additions on the corrosion behaviour of WC-Co alloys.

It is also stated that the high cobalt contents improve the corrosion resistance of the WC-Co alloys with the addition of vanadium carbide. It is recommended the cobalt contents should be increased (i.e. more than 10 wt% Co) and the corrosion behaviour of the WC-Co alloys investigated.

It is also recommended that in-situ investigations (in-situ Raman and potentiostatic characterisation) should be carried out in order to determine the corrosion mechanism to understand the precise role of ruthenium and to analyse the film to determine whether ruthenium is incorporated into the passive film or layer.

# *REFERENCES*


Almond, E. A. and Roebuck, B. (1988). Identification of Optimum Binder Phase Compositions for Improved WC Hard Metals. *Materials Science and Engineering*, A 105/106, 237-248

Arai, M., Hayashi, S. and Yamamoto, K. (1990). Raman studies of phase transitions in gas-evaporated $WO_3$ microcrystals. *Solid State Communications*, 75, 613-616

Aw, P. K., Tan, A. L. K., Tan, T.P. and Qiu, J. (2007). Corrosion resistance of tungsten carbide based cermet coatings deposited by High Velocity Oxy-Fuel spray process. *WC Thin Solid Films.* In-press

Beste, U., Hartzell, T. Engqvist, H. and Axéna, N. (2001). Surface damage on cemented carbide rock-drill buttons. *Wear*, 249, 324–329

Bonjour, C. (2004). Effects of Ruthenium Additions on the Properties and Machining Behaviour of WC-Co Hard Metals. *Powder Metallurgy Tool Material*, 529-535 *University of Applied Sciences of Western Switzerland.*

Bonjour, C. and Actis-Data, A. (2004). Effects of Ruthenium Additions on the Properties of WC-Co Ultra Micrograins. *Powder Metallurgy Tool Material*, 543-549 *University of Applied Sciences of Western Switzerland.*

Bozzini, B., De Gaudenzi, G.P., Serra, M., Fanigliulo, A. and Bogani, F. (2002). Corrosion behaviour of WC-Co based hardmetal in neutral chloride and acid sulphate media. *Materials and Corrosion*, 53, 328-334

Bozzini, B., De Gaudenzi, G.P., Fanigliulo, A. and Mele, C. (2003). Anodic behaviour of WC-Co type Hardmetal. *Materials and Corrosion*, 54, 295-303

Broccardo, S.P. (2003). An investigation into the corrosion resistance of WC-VC-Co hardmetals, *M.Sc dissertation*, University of the Witwatersrand, Johannesburg

Brookes, K.J.A. (2001). The secretive world of 1950s hard metals. *Metal Powder Report,* 56, 28

Exner, H. E. (1979) Physical and chemical nature of cemented carbides, *International Metal Reviews*, 4, 149–173

Fernandes, P.J.L., Luckyx, S.B., Human, A.M. and Robinson, F.P.A. (1992). Does the Cobalt Mean free Path Affect the Corrosion behaviour of WC-Co? *Journal of Hard Materials*, 3, 185-194

Festeau, G., Fang, D.X. and Wills, D.J. (2007). PVD coated ruthenium featured cutting tools. *US Patent*

Guilemany, J. M., Sanchiz, I., Mellor, B. G., Llorca, N. and Miguel, J. R. (1993-1994). Mechanical-Property Relationships of Co/WC and Co-Ni-Fe/WC Hard Metal Alloys. *International Journal of Refractory Metals & Hard Materials*, 12, 199-206

Heumann, Th, and Stolica, N. (1971). The electrochemical behaviour of tungsten-I. the dissolution of tungsten and tungsten oxides in buffer solutions. *Electrochimica Acta,* 16, 643 – 651

Hochstrasser-Kurz, S., Mueller, Y., Latkoczy, C., Virtanen, S. and Schmutz, P. (2007). Analytical characterization of the corrosion mechanisms of WC–Co by electrochemical methods and inductively coupled plasma mass spectroscopy. *Corrosion Science*, 49, 2002–2020

Human, A. M. and Exner, H. E. (1996). Electrochemical behaviour of tungsten-carbide hardmetals. *Materials Science and Engineering*, A209, 180-19l

Human, A. M. and Exner, H. E. (1997). The Relationship Between Electrochemical Behaviour and In-service Corrosion of WC Based Cemented Carbides. *International Journal of Refractory Metals & Hard Materials*, 15, 65-71

Human, A. M., Roebuck, B. and Exner, H. E. (1998). Electrochemical polarisation and corrosion behaviour of cobalt and (Co, W) alloys in 1N sulphuric acid. *Material Science and Engineering A*, 241, 202-210

Jia, K., Fischer, T.E. and Gallois, B. (1998). Microstructure, hardness and toughness of nanostructured and conventional WC-Co composites. *Nanostructured Materials,* 10, 875-891

Jiang, J. and Li, L. (2007). Synthesis of sphere-like $Co_3O_4$ nanocrystals via a simple polyol route. *Materials Letters*, 61, 4894–4896

Kny, E., Bader, T. Hohenrainer, Ch.and Schmid, L. (1986). Corrosion and highly wear resistant hard metals. *Werkstoffe und Korrosion.* 37, 230

Krakhmalev, P.V., Sukumaran, J. and Gåård, A. (2007a). Effect of microstructure on edge wear mechanisms in WC–Co. *International Journal of Refractory Metals & Hard Materials*, 25,171–178

Krakhmalev, P.V., Adeva Rodil, T. and Bergstrom J. ((2007b). Influence of microstructure on the abrasive edge wear of WC–Co hardmetals. *Wear*, 263, 240–245

Llopis, J., Tordesillas, I. M. and Alfayatb, J. M. (1966). Anodic Corrosion of

Ruthenium In Hydrochloric Acid Solution. *Electromichica Acta*, 11, 623- 632

Lisovsky, A. F., Tkachenko, N. V. and Kebko, V. (1991). Structure of a Binding Cemented Carbides Phase in Re-Alloyed WC-Co. *International Journal of Refractory Metals & Hard Materials*, 10, 33-36

Machio, C.N. (2005). Preparation, characterization and testing of WC-VC-Co HP/HVOF thermal spray coatings. *Ph.D thesis*, University of the Witwatersrand, Johannesburg

Milman, Y.N., Luyckx, S., Northrop, I.T., (1999). Influence of hardness, grain size and cobalt content on the behaviour of WC-Co alloys. *International Journal of Refractory Metals & Hard Materials*, 17, 39-44

Mori, G., Zitter, H., Lackner, A. and Schretter, M. (2001). Influencing the corrosion resistance of cemented carbides by addition of $Cr_2C_3$, TiC and TaC. *15th International Plansee Seminar Editions (HM 29)*, 222-236

Myburg, G., Varga, K., Barnard, W.O., Baradlai, P., Tomcs´anyi, L., Potgieter, J.H., Louw, C.W. and van Staden, M.J. (1998). Surface composition of Ru containing duplex stainless steel after passivation in non-oxidizing media. *Applied Surface Science*, 136, 29–35

Nascimentoa, M. L., Muellera, W.D., Carvalhoa, A. C. and Tomas, H. (2007). Electrochemical characterization of cobalt-based alloys using the mini-cell system. *Dental Materials*, 23, 369–373

Ogundipe, A., Greenberg, B., Braida, W., Christodoulatos, C. and Dermatas, D. (2006). Morphological characterisation and spectroscopic studies of the corrosion behaviour of tungsten heavy alloys. *Corrosion Science*, 48, 3281-3297

Olubambi, P.A. (2008). Influence of microwave pretreatment on the bioleaching behaviour of low-grade complex sulphide ores. *Hydrometallurgy*

Olubambi, P. A., Potgieter, J. H. and Cornish, L. (2008). Corrosion behaviour of superferritic stainless steels cathodically modified with minor additions of ruthenium in sulphuric and hydrochloric acids. *Materials & Design*, In Press

Penrice, T. W. (1997). Some Characteristics of the Binder Phase in Cemented Carbides. *International Journal of Refractory Metals & Hard Materials*, 15, 113-121

Polini, R., Delogu, M. and Marcheselli, G. (2006). Adherent diamond coatings on cemented tungsten carbide substrates with new Fe/Ni/Co binder phase. *Thin Solid Films*, 494, 133-140

Potgieter, J. H. (1991). Alloys cathodically modified with noble metals. *Journal of*

*Applied Electrochemistry*, 21, 471 – 482

Potgieter, J. H. (1993). Effects of minor ruthenium additions on the corrosion behaviour of duplex stainless steel in sulphuric acid. *South African Journal of Chemistry*, 46, 58 – 64

Potgieter, J.H., Skinner, W. and Heyns, A.M. (1990). Cathodic modification as a means of improving the corrosion resistance of alloys. *Journal of Applied Electrochemistry*, 20, 711 – 715

Potgieter, J.H., Skinner, W. and Heyns, A.M. (1993). The nature of the passive film on cathodically modified stainless steels. *Journal of Applied Electrochemistry*, 23, 11 - 18

Potgieter, J. H., Barnard, W. O., Myburg G., Varga, K., Baraglai, P. and Tomcsanyi, L. (1996). Corrosion behaviour of duplex stainless steels containing minor ruthenium additions in reducing acid media. *Journal of Applied Electrochemistry*, 26, 1103-1110

Pugsley, V.A. and Sockel, H. G. (2004). Corrosion fatigue of cemented carbide cutting tool materials. *Materials Science and Engineering*, A366, 87–95

Ringas, C., Robinson, F.P.A., Luyckx, S.B. and Sellschop, J.P.F. (1990) Corrosion behaviour of ion implanted WC-Co and WC-Ni alloys in acid and chloride containing media. *Surface Engineering*, 6, 194 -198

Schnyder, B., Stössel-Sittig, C., Kötz, R., Hochstrasser-Kurz, S., Virtanen, S., Jaeggi, C., Eichenberger, N. and Siegenthaler, H. (2004). Investigation of the electrochemical behaviour of WC–Co hardmetal with electrochemical and surface analytical methods. *Surface Science*, 566-568, 1240-1245

Scholl, H., Hofman, B. and Rauscher, A. (1992). Anodic polarization of cemented carbides of the type [(WC, M); M = Fe, Ni or Co] in sulphuric acid solution. *Electrochimica Acta*, 37, 447-452

Sebeya, T.T. (2005). An investigation into the cause of the difference in the corrosion behaviour of WC- Co and WC-VC-Co hardmetals, *MSc dissertation*, University of the Witwatersrand, Johannesburg

Shing, T.L. (2000). An investigation on the effect of Ruthenium Additions on Properties of WC-Co. *M.Sc dissertation*, University of the Witwatersrand, Johannesburg

Shing, T.L., Eric, R.H. and Luyckx, S. (2002). Ruthenium as an Eta-Phase Inhibitor in WC-Co. *Powder Metallurgy, Substrate Structure and Properties*, 92-99

Shing, T.L., Luyckx, S., Northrop, I.T., and Wolff, I., (2001). The Effect of Ruthenium

additions on the hardness, toughness and grain size of WC-Co. *International Journal of Refractory Metals and Hard Materials,* 19, 41-44

Shiyanovskaya, I., Ratajczak, H., Baran, J. and Marchewka, M. (1995). Fourier Transform Raman study of electrochromic crystalline hydrate films $W0_3.1/3(H_2O)$. *Journal of Molecular Structure*, 348, 99-102

Spriggs, G. E. (1995). A History of Fine Grained Hardmetal. *International Journal of Metals and hard materials*, 13, 241-255

Srivastava, M., Selvi, V. E., Grips, V.K.W. and Rajam, K.S. (2006). Corrosion resistance and microstructure of electrodeposited nickel–cobalt alloy coatings. *Surface and Coatings Technology*, 201, 3051–3060

Sutthiruangwong, S. and Mori, G. (2003). Corrosion properties of Co-based cemented carbides in acidic solutions. *International Journal of Refractory Metals & Hard Materials*, 21, 135–145

Sutthiruangwong, S., Mori, G. and Kosters, R. (2005). Passivity and Pseudopassivity of cemented carbides. *International Journal of Refractory Metals & Hard Materials*, 23, 129–136

Technical trends (2004). The graded hard edge of genuine milling advance. *Metal Powder report,* 5, 18-23

Tjong, S.C., Ku, J.S. and Ho, N.J. (1997). Laser surface alloying of ferritic Fe-40Cr alloy with ruthenium. *Surface and Coatings Technology*, 90, 203-209

Tomlinson, W.J. and Ayerst, N.J. (1989) Anodic polarization and corrosion of WC-Co hardmetals containing small amounts of $Cr_3C_2$ and/or VC. *Journal of Materials Science*, 24, 2348-2352

Tomlinson, W.J. and Linzell, C.R. (1988). Anodic polarization and corrosion of cemented carbide with cobalt and nickel binders. *Journal of Materials Science*, 23, 914-918

Tripathy, S. K., Christy, M., Park, N., Suh, E., Anand, S. and Yu, Y. (2008) Hydrothermal synthesis of single-crystalline nanocubes of $Co_3O_4$. *Materials Letters*, 62, 1006–1009

Trueman, A.R., Schweinsberg, D. P. and Hope, G.A. (1999). A study of the effect of cobalt additions on the corrosion of tungsten carbide/carbon steel metal matrix composites. *Corrosion Science,* 41, 1377-1389

Van der Lingen, E. and Sandenbergh, R.F. (2001). The cathodic modification behaviour of ruthenium additions to titanium in hydrochloric acid. *Corrosion*

*Science*, 577-590

Varga, K., Baradlai, P., Barnard, W.O., Myburg, G., Halmos, P. and Potgieter, J. H. (1997). Comparative study of surface properties of austenitic stainless steels in sulfuric and hydrochloric acid solutions. *Electrochimica Acta,* 42, 25-35

Wentzel, E. J. and Allen, C. (1997). The erosion-corrosion resistance of tungsten-carbide hard metals. *International Journal of Refractory Metals & Hard Materials*, 15, 81-87

Wentzel, E. J., and Allen, C. (1997). The erosion-corrosion resistance of tungsten-carbide hard metals. *International Journal of Refractory Metals & Hard Materials*, 15, 81-87

Wolff, I.M. (1999). New applications for Ruthenium. *South African Journal of Science*, 95, 539-542

Wolff, I.M., Iorio, L.E., Rumpf, T., Scheers, P.V.T. and Potgieter, J.H. (1998). Oxidation and corrosion behaviour of Fe–Cr and Fe–Cr–Al alloys with minor alloying additions. *Materials Science and Engineering,* A241, 264–276

Yang, B.Q., Wang, X.P., Zhang, H.X., Wang, Z.B. and Feng, P.X. (2008). Effect of substrate temperature variation on nanostructured WC films prepared using HFCVD technique. *Materials Letters,* 62, 1547–1550